(12)

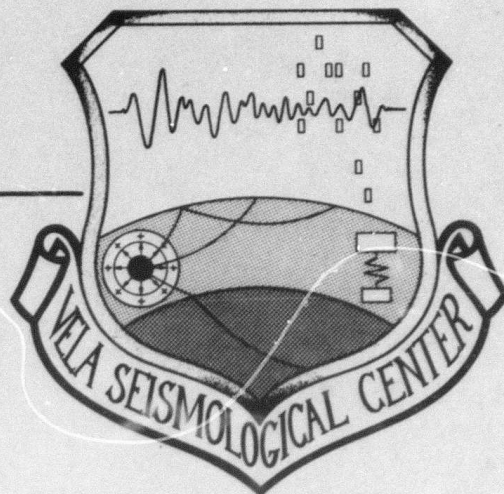**VSC-TR-82-10**

# DEFINITION OF SEISMIC SIGNAL PARAMETERS BY PARTICLE-MOTION PROCESSING

D. von Seggern and M. Marshall.

Seismic Data Analysis Center
Teledyne Geotech
314 Montgomery Street
Alexandria, Virginia 22314

**22 JAN 1982**

DTIC
ELECTE
S SEP 1 1982 D
F

**APPROVED FOR PUBLIC RELEASE; DISTRIBUTION UNLIMITED.**

(

82 08 31 001

SECURITY CLASSIFICATION OF THIS PAGE *(When Data Entered)*

| REPORT DOCUMENTATION PAGE | | READ INSTRUCTIONS BEFORE COMPLETING FORM |
|---|---|---|
| 1. REPORT NUMBER<br>VSC-TR-82-10 | 2. GOVT ACCESSION NO.<br>*AD-A118778* | 3. RECIPIENT'S CATALOG NUMBER |
| 4. TITLE *(and Subtitle)*<br><br>DEFINITION OF SEISMIC SIGNAL PARAMETERS BY PARTICLE-MOTION PROCESSING | | 5. TYPE OF REPORT & PERIOD COVERED<br>Technical |
| | | 6. PERFORMING ORG. REPORT NUMBER<br>SDAC-TR-81-19 |
| 7. AUTHOR(s)<br><br>D. H. von Seggern<br>M. E. Marshall | | 8. CONTRACT OR GRANT NUMBER(s)<br><br>F08606-79-C-0007 |
| 9. PERFORMING ORGANIZATION NAME AND ADDRESS<br><br>Teledyne Geotech<br>314 Montgomery Street<br>Alexandria, Virginia 22314 | | 10. PROGRAM ELEMENT, PROJECT, TASK AREA & WORK UNIT NUMBERS<br><br>VT/0709/B/PMP |
| 11. CONTROLLING OFFICE NAME AND ADDRESS<br>VELA Seismological Center<br>312 Montgomery Street<br>Alexandria, Virginia 22314 | | 12. REPORT DATE<br>22 January 1982 |
| | | 13. NUMBER OF PAGES<br>95 |
| 14. MONITORING AGENCY NAME & ADDRESS*(if different from Controlling Office)*<br>Defense Advanced Research Projects Agency<br>1400 Wilson Boulevard<br>Arlington, Virginia 22209 | | 15. SECURITY CLASS. *(of this report)*<br><br>Unclassified |
| | | 15a. DECLASSIFICATION/DOWNGRADING SCHEDULE |

16. DISTRIBUTION STATEMENT *(of this Report)*

APPROVED FOR PUBLIC RELEASE; DISTRIBUTION UNLIMITED.

17. DISTRIBUTION STATEMENT *(of the abstract entered in Block 20, if different from Report)*

18. SUPPLEMENTARY NOTES

19. KEY WORDS *(Continue on reverse side if necessary and identify by block number)*

Particle-Motion Processing     Estimation of Seismic Signal Parameters

Seismic Detection

Regional Seismic Phases

20. ABSTRACT *(Continue on reverse side if necessary and identify by block number)*
    Theoretical and observed particle motion of P and Lg waves indicates that a successful definition of signal parameters can be made by particle-motion algorithms. Tests on many Pn, Pg, and P phases recorded at OB2NV and RKON reveal that back azimuths can be estimated almost always to within $\pm$ 20° at S/N > 5 and quite often to this precision at S/N < 5. Incidence angles are not sufficiently resolved to reliably discriminate regional from teleseismic P waves though. Lg waves recorded at these same stations yielded better back azimuth estimates at

DD <sub>1 JAN 73</sub> **1473**    EDITION OF 1 NOV 68 IS OBSOLETE

SECURITY CLASSIFICATION OF THIS PAGE *(When Data Entered)*

equivalent S/N ratios than P waves. The azimuth estimates made by particle-motion processing showed no deterioration with increasing frequency to 10 Hz, provided S/N ratio remained high. An experiment using 3-component data at ANMO, BOCO, and BCAO resulted in only mild success for characterizing wave type and measuring the signal parameters with particle-motion processing; more complex algorithms and additional kinds of processing will be required to identify regional phases routinely.

Accession For

| | | |
|---|---|---|
| NTIS GRA&I | ☒ | |
| DTIC TAB | ☐ | |
| Unannounced | ☐ | |
| Justification | | |

By

Distribution/

Availability Codes

| Dist | Avail and/or Special |
|---|---|
| A | |

DTIC

DEFINITION OF SEISMIC SIGNAL PARAMETERS BY
PARTICLE-MOTION PROCESSING

SEISMIC DATA ANALYSIS CENTER REPORT NO.:   SDAC-TR-81-19

AFTAC Project Authorization No.:          VELA T/0709/B/PMP

Project Title:                            Seismic Data Analysis Center

ARPA Order No.:                           2551


Name of Contractor:                       TELEDYNE GEOTECH


Contract No.:                             F08606-79-C-0007

Date of Contract:                         27 October 1978

Amount of Contract:                       $2,191,475

Contract Expiration Date:                 30 September 1983

Project Manager:                          Robert R. Blandford
                                          (703) 836-3882

P. O. Box 334, Alexandria, Virginia  22313


**APPROVED FOR PUBLIC RELEASE; DISTRIBUTION UNLIMITED.**

# ABSTRACT

Theoretical and observed particle motion of P and Lg waves indicates that a successful definition of signal parameters can be made by particle-motion algorithms. Tests on many Pn, Pg, and P phases recorded at OB2NV and RKON reveal that back azimuths can be estimated almost always to within $\pm$ 20° at S/N > 5 and quite often to this precision at S/N < 5. Incidence angles are not sufficiently resolved to reliably discriminate regional from teleseismic P waves though. Lg waves recorded at these same stations yielded better back azimuth estimates at equivalent S/N ratios than P waves. The azimuth estimates made by particle-motion processing showed no deterioration with increasing frequency to 10 Hz, provided S/N ratio remained high. An experiment using 3-component data at ANMO, BOCO, and BCAO resulted in only mild success for characterizing wave type and measuring the signal parameters with particle-motion processing; more complex algorithms and additional kinds of processing will be required to identify regional phases routinely.

## TABLE OF CONTENTS

## LIST OF FIGURES

LIST OF FIGURES (Continued)

LIST OF TABLES

## PURPOSE OF STUDY

Seismic network processing for verification of possible underground
nulcear test bans will be burdened with hundreds, or even thousands, of
seismic detections per day.  Recently efforts have been made to elimin-
ate many of the human-controlled aspects of processing of seismic data,
with the goal of efficiently producing an automatic seismic event
bulletin of reasonable reliability (von Seggern, 1977; von Seggern et
al., 1978; Goncz, 1980).  These more recent studies do not include
former and present improvements in machine detection of seismic phases,
as reviewed by Blandford et al. (1981).  A truly sophisticated detection
process will seek not only to measure the time of arrival and the
amplitude of the detected signal, but should also be able to provide
additional characterizing information on the signal.  This additional
information will augment the success of any automatic phase association
algorithm such as described by Goncz (1980). Especially in the case
where a station is located within regional distances ($\Delta$ < 20°) of
active seismic zones and is recording several regional phases daily,
phase characterization will be useful for later processing stages.

This study examines the capability of identifying seismic P and Lg
phases on the basis of their particle motion and it evaluates the
accuracy of back azimuth and incidence angle estimates computed for
these phases.  The data base will be composed of three-component,
short-period recordings made at high-quality stations, such that
calibration errors can be neglected in particle-motion computations.

# THEORETICAL PARTICLE MOTION

## P Waves

Consider a harmonic wave impinging on the base of a layered media
representative of the earth's crust. For the wavelengths comprising
short-period P waves, the approximation of a slightly curved wavefront
and a spherical earth by a plane wave and plane, parallel layers will be
satisfactory. Of interest here is the vertical and horizontal motion
recorded at the surface. For high frequencies, the two components will
be in phase and have an amplitude ratio of (Bullen, 1963, p. 129)

$$\frac{A_h}{A_v} = \left( \frac{1 + 3 \tan^2 e}{2 \tan f} \right)$$

when $\gamma = 1/4$ is assumed and where e and f are the emergence angles of
the surface-reflected P and S waves, respectively, measured down from
the horizontal axis. Using $\tan \bar{e} = A_v/A_h$, Bullen derives

$$2 \cos^2 e = 3(1 - \sin \bar{e})$$

for the relation between the apparent emergence angle $\bar{e}$ of P and the
true angle e. In terms of the incidence angles, as measured from the
vertical axis this is equivalent to

$$2 \sin^2 i = 3(1 - \cos \bar{i}) \qquad (1)$$

By the law of refraction, the incidence angle at the surface is related
to the incidence angle $i_o$ at the base of the layers by

$$\frac{\sin i}{\sin i_o} = \frac{v}{v_o}$$

where v and $v_o$ are the compressional wave velocities in the surface
layer and mantle substratum respectively.

Table I shows the relations between $i_o$, $i$, and $\bar{i}$ for the Herrin 1968 velocity model. Note that the difference between $i$ and $\bar{i}$ is quite small, such that it is surely overwhelmed by measurement error due to seismic noise, inhomogeneities of elastic properties, and non-parallel layers in real observations.

The above theoretical case is not very appropriate due to the assumption of a harmonic wave, and a more interesting case is made when realistic P waveforms are assumed. Now consider a seismic pulse incident at the base of the layers which is constructed from the far-field displacement of a granite explosion as given in von Seggern and Blandford (1972). In order to propagate this to the surface, a frequency-domain method will be used. Let the surface recorded responses be given by $V(\omega)$ and $U(\omega)$ for the vertical and horizontal seismograms. Then

$$V(\omega) = RV(\omega) \cdot S(\omega) \cdot A(\omega) \cdot I(\omega)$$
$$U(\omega) = RU(\omega) \cdot S(\omega) \cdot A(\omega) \cdot I(\omega)$$

where RV and RU are the transfer functions from Haskell (1962) which produce the vertical and horizontal surface motion, respectively, for a unit amplitude delta-function impulse arriving at angle $i$ at the base of the layers, $S(\omega)$ is the von Seggern and Blandford far-field displacement spectrum, $A(\omega)$ is the attenuation operation $\exp -\pi ft*$, and $I(\omega)$ is the instrument response. By inverse transformation, the radial and vertical components of motion were synthesized as they would be recorded at the surface over crustal structures given in Table I at three stations, RKON, OB2NV and CPO. The synthesized components are shown in Figures 1 through 3 for angles of incidence at the crustal base of 20° and 40°. Along with the time series, a particle-motion plot of vertical versus radial recorded motion is shown. The recorded motion is not strictly rectilinear for these realistic P waves; however, the angle $\bar{i}$ given by measuring the maximum vertical and maximum radial motion and using $\tan (\bar{i}) = A_h/A_v$ agrees closely with the apparent angle predicted for

## TABLE I

### Incidence angles of P waves in a Herrin-68 velocity model and at selected stations

| | Herrin 68 Model | | | Surface $\bar{i}$ | | |
|---|---|---|---|---|---|---|
| | Crustal bottom | Surface | Surface | | | |
| $\Delta°$ | $i_0$ | $i$ | $\bar{i}$ | RKON | OB2NV | CPO |
| 10° | – | – | | | | |
| 20° | 52.9 | 36.9 | 40.2 | | | |
| 30° | 40.2 | 28.6 | 32.1 | 33.0°(31.8°)* | 31.5°(32.4°) | 17.3°(15.3°) |
| 40° | 37.1 | 26.6 | 30.0 | | | |
| 50° | 33.4 | 24.1 | 27.3 | | | |
| 60° | 29.9 | 21.7 | 24.7 | | | |
| 70° | 26.7 | 19.5 | 22.2 | | | |
| 80° | 23.1 | 16.9 | 19.3 | | | |
| 90° | 20.0 | 14.7 | 16.8 | 17.4°(18.6°) | 16.1°(21.5°) | 9.2°(8.8°) |
| 100° | 19.6 | 14.4 | 16.5 | | | |

| Compressional Velocity | Shear Velocity | Density | Thickness (km) |
|---|---|---|---|
| **RKON** | | | |
| 6.2 | 3.6 | 2.8 | 15 |
| 7.0 | 4.0 | 3.1 | 25 |
| 8.1 | 4.7 | 3.4 | ---- |
| **OB2NV** | | | |
| 5.70 | 3.36 | 2.70 | 10.0 |
| 6.10 | 3.60 | 2.80 | 10.0 |
| 6.70 | 4.00 | 2.95 | 10.0 |
| 7.80 | 4.50 | 3.30 | ---- |
| **CPO** | | | |
| 3.24 | 1.72 | 2.25 | 0.65 |
| 5.81 | 2.94 | 2.67 | 1.27 |
| 6.10 | 3.25 | 2.80 | 10.00 |
| 6.70 | 3.90 | 3.00 | 28.00 |
| 8.00 | 4.60 | 3.40 | ----- |

* Values in parentheses are computed from synthetic seismograms of Figures 1-3 by $\tan\bar{i} = A_h/A_v$
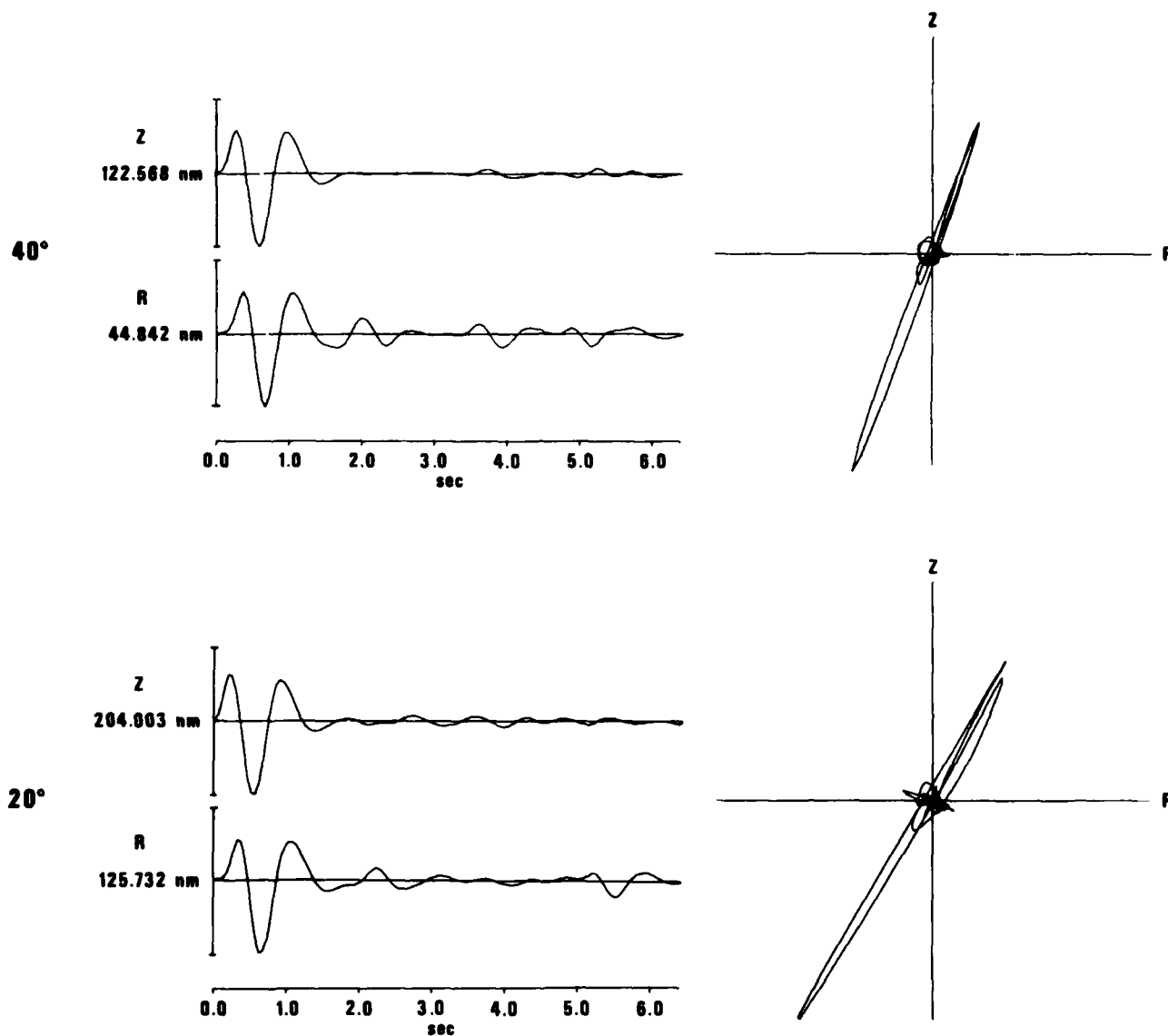
**RK-ON**

Figure 1.   Synthesized vertical and radial traces of an explosion P-wave
            at RKON.

40°

Z
124.133 nm

R
47.956 nm

20°

Z
288.878 nm

R
129.949 nm
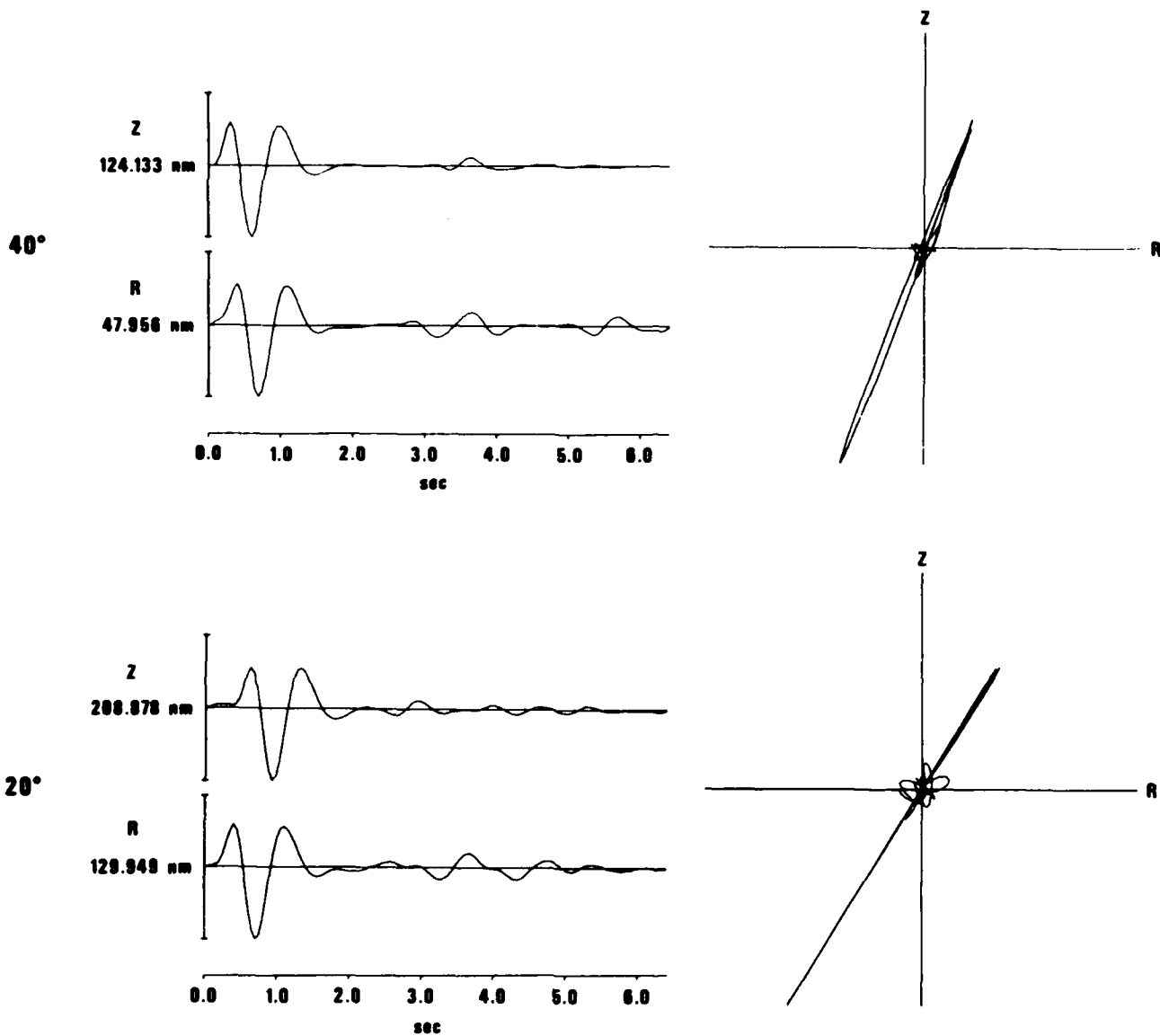
OB2NV

Figure 2.  Synthesized vertical and radial traces of an explosion P-wave at OB2NV.
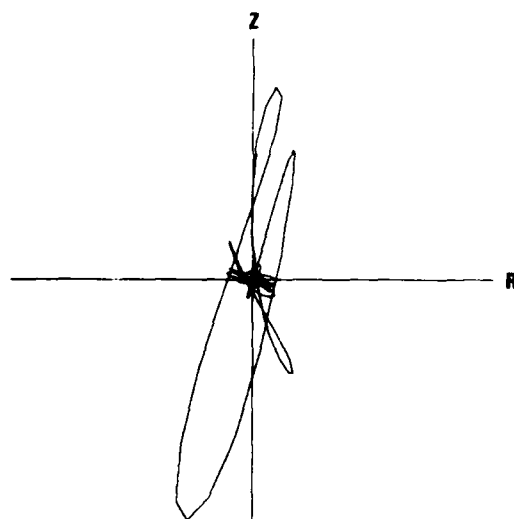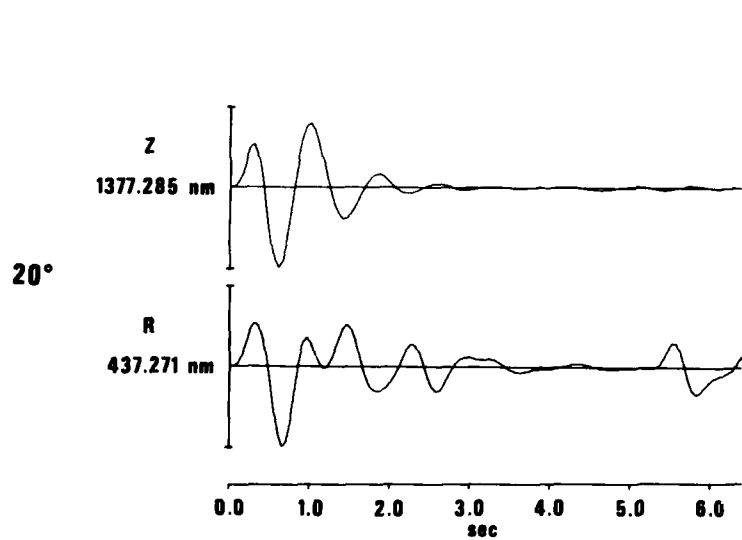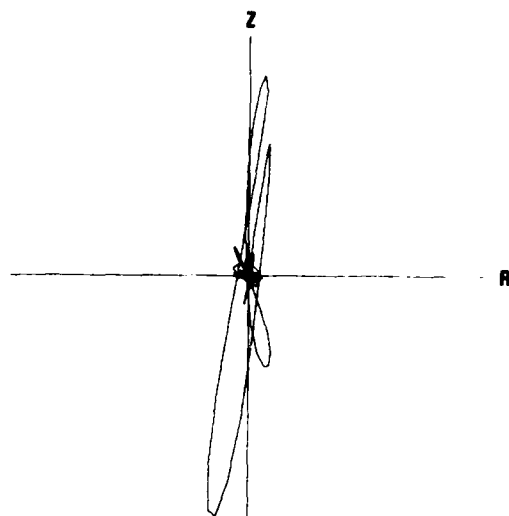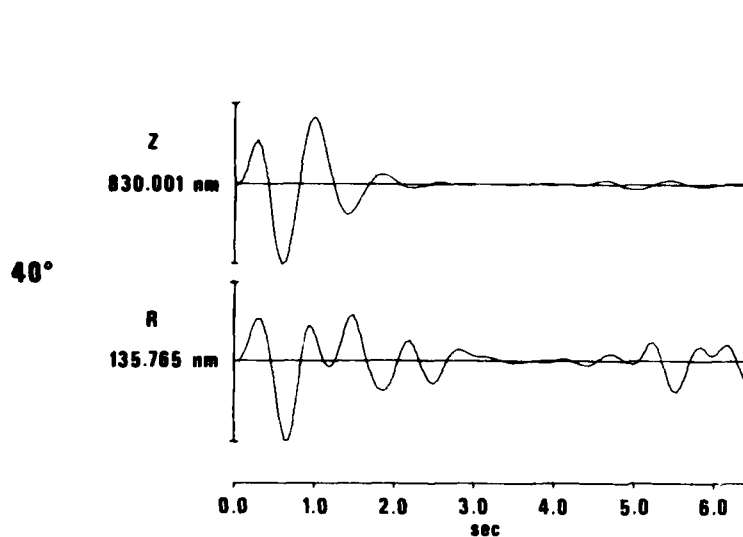
**CPO**

Figure 3. Synthesized vertical and radial·traces of an explosion P-wave at CPO.

plane harmonic waves as computed using equations 1 and 2. This comparison is shown in Table I for the three stations. Therefore the incidence angle of P waves, as measured by a particle-motion processor which assumes rectilinear motion aligned along the normal to the wavefront, provides sufficiently unbiased estimates of the actual incidence angle of the P waves.

## Lg Waves

In contrast to P waves, Lg waves will display no simple particle motion. This is because the Lg phase is a summation of numerous Rayleigh and Love modes, each having a different group-velocity curve and a different amplitude-versus-frequency response curve. In addition, Rayleigh ellipticities vary widely, even shifting to prograde from retrograde and back with increasing frequency for a given mode. Thus, even on a structure with uniform properties in parallel layers, the Lg phase defies a simple quantitative description; and the inhomogeneities of the real earth further complicate the Lg phase with scattered energy and a significant coda. In a gross sense, however, a model which parameterizes Love and Rayleigh motion according to the back azimuth may not be unsuccessful. Although the particle motion at particular instants may not fit the model, the overall motion in a wide window on Lg may fit to a sufficient degree. Thus, unlike for P waves, the optimum window length for Lg may be the longest window which encompasses visible Lg motion.

## Particle-Motion Processors

A series of related particle-motion processors has been described in Smart (1977) and Smart (1981). The basis of these processors is the assumption of a simple signal model: strictly rectilinear motion for P waves and a combination of Rayleigh and Love motion for surface waves (including Lg). The parameters of the signal model are solved for analytically using the Fourier spectral components of the raw data and are, in fact, least-squares fits of the data to the model. The signal amplitude estimates are unbiased and linear. From an examination of the

theoretical P particle motion plots in Figures 1 to 3 and the values in Table I, one concludes that an estimate of the incidence angle would not be seriously in error for high S/N ratio while back azimuth should, of course, be quite precise. However, in the presence of background noise, it is expected that incidence-angle and azimuth angle estimates will deteriorate rapidly at low S/N ratios and that the errors will be more severe for waves arriving at steep angles, as core phases do, because of the relatively small radial component of motion. The surface-wave processor should be able to estimate the Lg azimuth to an acceptable degree of accuracy, even to low S/N ratios and indeed this has been shown in Smart (1977). Because of the possibility that prograde or retrograde motion may be dominant in the Rayleigh waves for Lg, a 180° ambiguity in back azimuth exists.

# OBSERVED PARTICLE MOTION

In order to examine the recorded particle motion of regional phases, two data sets of regional recordings were assembled, one for OB2NV (Table II) and the other for RKON (Table III). A third set of teleseismic P waves was assembled for OB2NV (Table IV). All events in these sets are earthquakes. The locations of the regional events for OB2NV and RKON are shown in Figures 4 and 5 respectively. Note that many of the RKON events are actually beyond "regional" range, out to 28°. The recorded horizontal components were all rotated to the azimuth of the incoming signals and plotted. In addition, the product of the vertical and radial trace (Z*R) was formed and plotted as an aid in analyzing particle motion. This product trace has been used earlier in the study of regional recordings by Sutton et al (1967). The appearance of the Z*R trace depends on the type of wave recorded:

1) P waves will have in-phase motion on the vertical and radial components and thus give a series of all-positive peaks, with a period one-half that of the wave itself.

2) S waves will have motion 180° out of phase on the vertical and radial components and thus give the negative of the P-wave result.

3) Lg waves are a combination of numerous normal modes having Rayleigh-wave motion with prograde and retrograde ellipticity, in either case implying motion 90° out of phase between the vertical and radial, resulting in a Z*R trace which oscillates with a period one-half that of the Lg wave itself.

Some examples have been drawn from the entire set of plots and are displayed in Figures 6 through 9. In general these examples are representative of the recordings with high signal-to-noise ratios, in order to best illustrate the true particle motion during the wave trains. Figure 6 shows Pn, Pg, and P waves recorded at OB2NV. The source of each recording here and for the following similar figures can

## TABLE II

Source parameters for regional events studied at OB2NV

| Event # | Date | Origin Time | Lat.(N) | Lon.(W) | $m_b$ | Δ° to OB2NV |
|---------|------|-------------|---------|---------|-------|-------------|
| 1 | 25 Aug 76 | 07:23:59.9 | 26.6 | 109.5 | 4.3 | 12.3 |
| 2 | 26 Aug 76 | 06:43:15.8 | 50.6 | 129.4 | 4.4 | 16.4 |
| 3 | 20 Dec 76 | 17:12:41.0 | 49.1 | 129.0 | 5.1 | 15.1 |
| 4 | 16 Mar 77 | 15:46:30.6 | 50.8 | 129.6 | 4.5 | 16.6 |
| 5 | 22 Mar 77 | 08:07:14.0 | 27.4 | 111.1 | 4.4 | 10.7 |
| 7 | 04 Jul 77 | 05:28:28.9 | 24.6 | 109.0 | 4.6 | 14.0 |
| 8 | 30 May 77 | 16:16:37.9 | 33.9 | 117.9 | 2.6 | 3.6 |
| 9 | 12 Sep 77 | 06:17:42.6 | 34.2 | 117.0 | 3.2 | 3.1 |
| 10 | 12 Sep 77 | 12:14:02.3 | 34.8 | 116.8 | 3.2 | 2.5 |
| 11 | 08 Jun 77 | 13:09:07.4 | 31.0 | 109.2 | 4.6 | 8.4 |
| 12 | 30 Jul 77 | 16:35:38.1 | 36.9 | 121.5 | 3.8 | 4.4 |
| 13 | 19 Sep 76 | 11:11:42.1 | 33.5 | 116.8 | 3.3 | 3.8 |
| 14 | 09 Oct 76 | 02:09:28.1 | 33.3 | 116.2 | 3.4 | 3.9 |
| 15 | 15 Oct 76 | 01:35:31.8 | 38.0 | 122.0 | 3.4 | 4.8 |
| 16 | 15 Oct 76 | 04:01:00.5 | 33.9 | 116.6 | 2.9 | 3.4 |
| 17 | 17 Oct 76 | 05:38:11.9 | 34.4 | 118.4 | 4.3 | 3.4 |
| 18 | 20 Oct 76 | 10:39:43.9 | 35.1 | 117.2 | 3.4 | 2.3 |
| 19 | 22 Oct 76 | 23:19:13.6 | 33.5 | 116.6 | 4.5 | 3.7 |
| 20 | 23 Oct 76 | 19:24:33.2 | 36.9 | 121.5 | 3.5 | 4.4 |
| 21 | 24 Oct 76 | 02:19:52.7 | 36.9 | 121.6 | 3.8 | 4.5 |
| 22 | 01 Nov 76 | 22:22:51.1 | 44.3 | 114.9 | 3.7 | 7.1 |
| 23 | 02 Nov 76 | 02:46:05.9 | 34.1 | 117.3 | 3.3 | 3.3 |
| 24 | 11 Jun 77 | 07:37:01.7 | 32.1 | 116.2 | 4.2 | 5.1 |
| 25 | 11 Jun 77 | 14:18:20.5 | 34.4 | 118.6 | 3.1 | 3.5 |
| 26 | 27 Jul 77 | 21:51:17.5 | 37.3 | 122.1 | 3.5 | 4.8 |
| 27 | 26 Jul 77 | 21:42:16.3 | 35.9 | 120.5 | 3.7 | 3.8 |
| 28 | 26 Sep 76 | 22:44:37.2 | 39.4 | 118.1 | 3.0 | 2.7 |
| 29 | 18 Oct 76 | 02:46:16.0 | 36.8 | 121.6 | 4.4 | 4.5 |
| 30 | 18 Oct 76 | 17:26:52.6 | 32.7 | 117.9 | 4.6 | 4.8 |
| 31 | 19 Oct 76 | 00:07:01.0 | 29.6 | 113.4 | 4.6 | 7.9 |
| 32 | 11 Dec 76 | 14:15:29.6 | 25.4 | 109.7 | 4.5 | 13.0 |
| 33 | 06 Jun 77 | 09:44:23.7 | 49.1 | 129.5 | 4.5 | 15.3 |
| 34 | 12 Sep 77 | 13:59:22.3 | 35.6 | 117.5 | 3.1 | 2.0 |
| 35 | 24 Sep 76 | 14:02:17.6 | 34.1 | 118.1 | 2.2 | 3.5 |
| 36 | 27 Jul 77 | 11:10:46.7 | 36.9 | 121.5 | 3.2 | 4.4 |
| 37 | 19 Oct 76 | 01:59:10.6 | 36.0 | 114.8 | 0.0 | 1.6 |

## TABLE III

Source parameters for teleseismic events studied at OB2NV

| Event # | Date | Origin Time | Lat. | Lon. | $m_b$ | $\Delta°$ to OB2NV |
|---|---|---|---|---|---|---|
| 38 | 01 Dec 77 | 14:13:01.5 | 18.0S | 68.0W | 4.8 | 71.5 |
| 39 | 02 Dec 77 | 12:57:15.4 | 52.8N | 159.8E | 5.7 | 57.8 |
| 40 | 03 Dec 77 | 12:23:56.9 | 8.7N | 84.4W | 5.1 | 40.5 |
| 41 | 04 Dec 77 | 11:39:04.7 | 48.3N | 146.6E | 5.1 | 67.3 |
| 42 | 08 Dec 77 | 13:57:11.8 | ⸱0.4N | 149.9E | 4.8 | 64.4 |
| 43 | 13 Dec 77 | 01:14:15.7 | 17.3N | 55.0W | 5.8 | 56.8 |
| 44 | 04 Oct 77 | 13:45:11.1 | 12.0N | 59.0W | 5.2 | 56.7 |
| 45 | 07 Oct 77 | 21:19:18.2 | 57.8N | 179.8W | 4.0 | 46.1 |
| 46 | 08 Oct 77 | 03:03:54.2 | 9.3S | 74.6W | 5.5 | 60.6 |
| 47 | 13 Oct 77 | 23:16:30.0 | 12.2S | 77.9W | 5.2 | 61.0 |
| 48 | 15 Oct 77 | 07:34:31.5 | 15.6N | 98.8W | 5.0 | 26.5 |
| 49 | 16 Oct 77 | 01:59:33.7 | 47.0N | 153.8E | 5.5 | 63.8 |
| 50 | 14 Dec 77 | 08:55:52.8 | 41.9N | 147.6E | 5.2 | 70.2 |
| 51 | 17 Dec 77 | 17:27:31.3 | 52.2N | 170.0W | 5.0 | 40.1 |
| 52 | 18 Dec 77 | 06:57:34.6 | 55.1N | 160.5E | 5.1 | 56.7 |
| 53 | 19 Dec 77 | 10:52:43.9 | 51.2N | 176.5W | 5.2 | 44.1 |
| 54 | 20 Dec 77 | 08:50:40.6 | 48.5N | 152.9E | 5.8 | 63.7 |
| 55 | 16 Oct 77 | 04:25:43.0 | 59.9N | 152.5W | 4.8 | 32.4 |
| 56 | 18 Oct 77 | 07:03:59.0 | 56.0N | 150.0W | 5.2 | 29.3 |
| 57 | 21 Oct 77 | 19:09:41.0 | 53.0N | 170.0W | 5.5 | 40.0 |
| 58 | 24 Oct 77 | 05:57:05.0 | 44.0N | 39.0W | 4.7 | 56.8 |
| 59 | 29 Oct 77 | 10:41:06.4 | 20.0S | 72.7W | 4.8 | 70.3 |
| 60 | 30 Oct 77 | 00:01:50.8 | 13.6N | 90.8W | 4.9 | 32.6 |
| 61 | 24 Oct 77 | 07:09:12.0 | 55.0N | 158.0W | 5.6 | 33.3 |
| 62 | 02 Nov 77 | 05:51:31.8 | 10.6N | 85.7W | 4.7 | 38.1 |
| 63 | 02 Nov 77 | 14:47:52.0 | 10.1N | 74.8W | 4.9 | 61.1 |
| 64 | 03 Dec 77 | 12:35:44.7 | 19.6N | 69.8W | 4.6 | 43.8 |
| 65 | 04 Jan 78 | 22:52:17.1 | 9.1N | 84.4W | 5.2 | 40.1 |
| 66 | 05 Jan 78 | 03:23:16.5 | 22.0S | 127.1W | 5.6 | 60.1 |
| 67 | 22 Dec 77 | 02:57:46.8 | 10.8N | 106.9W | 4.8 | 27.7 |
| 68 | 23 Dec 77 | 11:15:45.0 | 72.3N | 10.1E | 4.8 | 62.0 |
| 69 | 04 Nov 77 | 09:53:04.3 | 51.7N | 176.1W | 5.6 | 43.8 |
| 70 | 04 Nov 77 | 12:49:33.7 | 13.4N | 90.4W | 5.2 | 33.0 |
| 71 | 05 Nov 77 | 14:44:09.2 | 51.5N | 175.8W | 5.3 | 43.7 |
| 72 | 06 Nov 77 | 02:39:35.3 | 53.4N | 159.6E | 5.5 | 57.8 |
| 73 | 08 Nov 77 | 14:59:08.3 | 47.4N | 154.3E | 5.3 | 63.3 |

## TABLE IV

Source parameters for regional events studied at RKON

| Event # | Date | Origin Time | Lat. | Lon. | $m_b$ | $\Delta^\circ$ to RKON |
|---|---|---|---|---|---|---|
| 1 | 11 Mar 78 | 23:57:45.3 | 31.9N | 114.7W | 4.7 | 24.5 |
| 2 | 12 Mar 78 | 00:30:17.4 | 32.0N | 115.0W | 4.1 | 24.5 |
| 3 | 12 Mar 78 | 18:42:24.1 | 32.0N | 114.9W | 4.7 | 24.5 |
| 4 | 09 Mar 76 | 14:00:00.1 | 37.3N | 116.4W | 6.0 | 21.0 |
| 5 | 20 Mar 76 | 00:47:27.3 | 73.2N | 69.9W | 4.5 | 24.6 |
| 6 | 25 Mar 76 | 00:41:20.5 | 35.6N | 90.5W | 4.9 | 15.4 |
| 7 | 22 Apr 76 | 04:21:39.1 | 43.6N | 127.0W | 4.2 | 23.5 |
| 8 | 26 Jul 76 | 10:45:28.2 | 45.0N | 114.2W | 4.3 | 14.9 |
| 9 | 31 Jul 76 | 22:32:10.5 | 26.2N | 110.3W | 4.8 | 27.7 |
| 10 | 10 Aug 76 | 13:54:57.5 | 45.1N | 106.6W | 3.4 | 10.4 |
| 11 | 12 Aug 76 | 06:28:59.0 | 50.6N | 123.0W | 3.8 | 18.4 |
| 12 | 02 Sep 76 | 13:36:11.0 | 48.2N | 122.8W | 4.3 | 18.9 |
| 13 | 03 Sep 76 | 04:18:16.2 | 44.0N | 106.2W | 4.8 | 10.8 |
| 14 | 13 Sep 76 | 18:54:37.1 | 36.6N | 80.8W | 3.3 | 16.9 |
| 15 | 16 Sep 76 | 10:14:39.1 | 76.1N | 108.4W | 4.6 | 25.9 |
| 16 | 25 Sep 76 | 14:06:56.0 | 35.6N | 90.5W | 3.6 | 15.4 |
| 17 | 19 Oct 76 | 07:24:34.6 | 44.8N | 110.7W | 5.3 | 12.9 |
| 18 | 23 Oct 76 | 20:58:18.0 | 47.8N | 69.8W | 3.8 | 15.8 |
| 19 | 27 Nov 76 | 00:24:46.1 | 44.6N | 111.1W | 3.3 | 13.2 |
| 20 | 08 Dec 76 | 14:40:59.1 | 44.8N | 110.8W | 5.5 | 13.0 |
| 21 | 11 Dec 76 | 07:05:00.4 | 38.1N | 91.1W | 4.2 | 12.8 |
| 22 | 13 Dec 76 | 08:35:54.9 | 37.8N | 90.2W | 3.5 | 13.3 |
| 23 | 19 Dec 76 | 17:10:15.6 | 44.7N | 110.8W | 4.9 | 13.0 |
| 24 | 20 Dec 76 | 01:34:16.7 | 44.8N | 110.8W | 4.4 | 12.9 |
| 25 | 13 Jan 78 | 08:25:34.0 | 52.8N | 132.0W | 4.4 | 23.5 |
| 26 | 05 Feb 78 | 16:07:09.5 | 78.4N | 107.8W | 4.9 | 28.0 |
| 27 | 23 Feb 78 | 16:59:59.9 | 36.9N | 115.9W | 5.6 | 21.1 |
| 28 | 04 Mar 78 | 19:13:33.3 | 50.3N | 11 .4W | 3.5 | 13.1 |
| 29 | 03 Jan 77 | 22:56:48.5 | 37.6N | 89.8W | 5.0 | 13.6 |
| 30 | 27 Jan 77 | 00:51:05.6 | 66.8N | 135.4W | 4.7 | 26.1 |
| 31 | 30 Sep 77 | 10:19:21.0 | 40.5N | 110.4W | 5.0 | 15.5 |
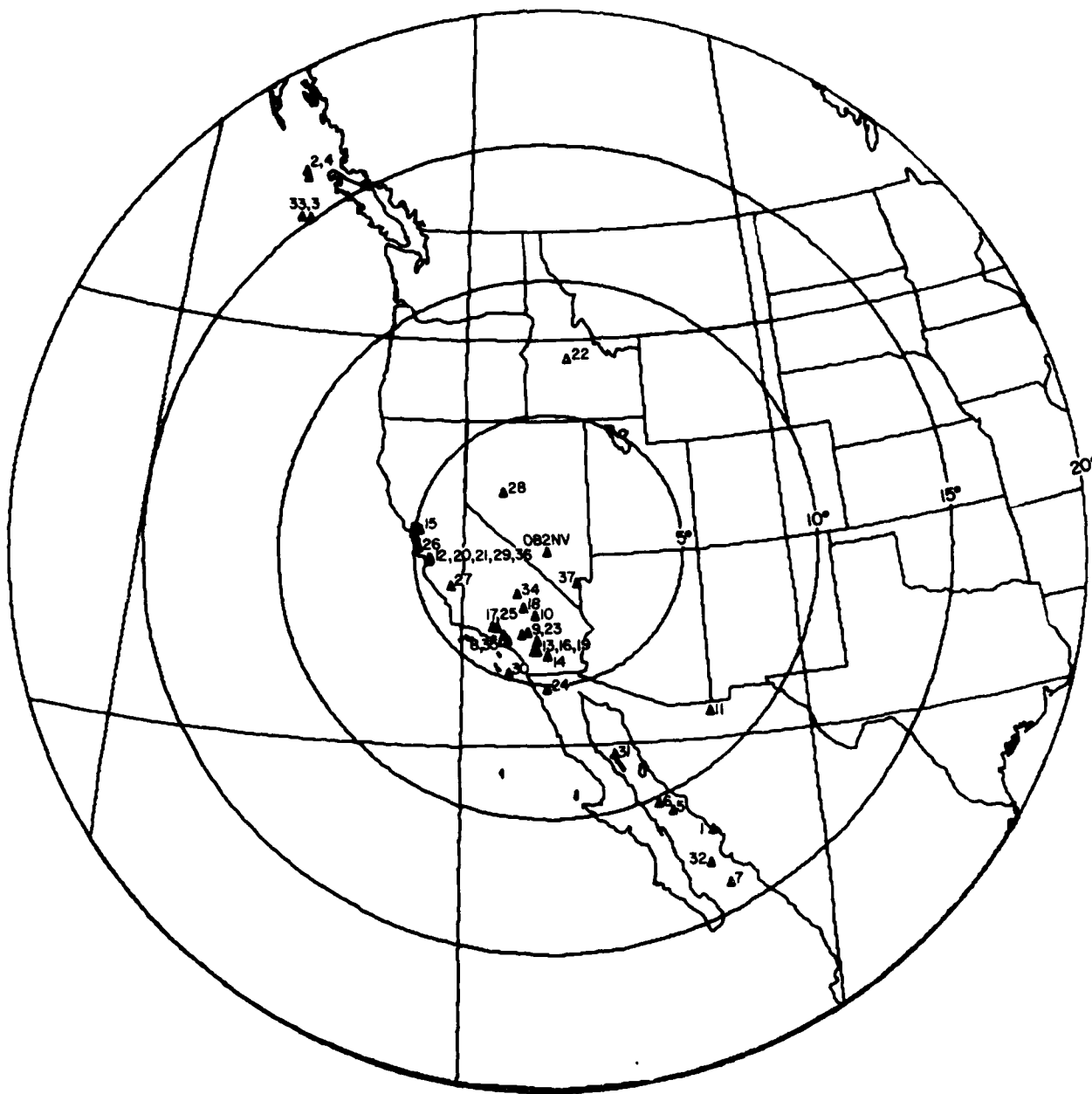
Figure 4. Events used in this study at regional distance to OB2NV.
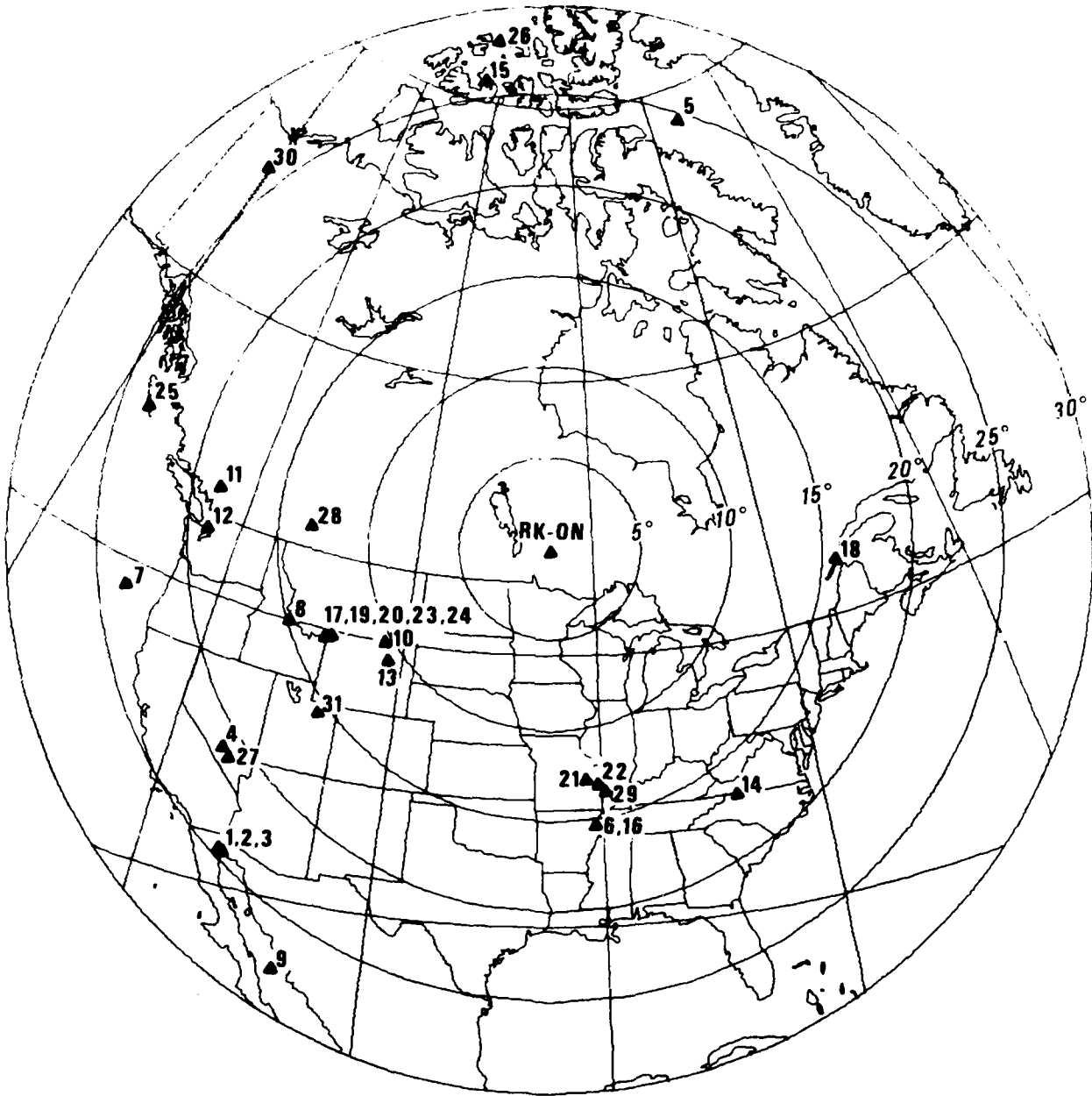
Figure 5.   Events used in this study at regional and near-regional distance
            to RKON.

EVENT 1

OB2NV

188. nm

P

380. nm

216. nm

|← 5 sec →|

Figure 6.  Particle-motion analysis for selected Pn and P waves at OB2NV.

-22-

EVENT 5

OB2NV



Figure 6 (cont.). Particle-motion analysis for selected Pn and P waves at OB2NV.

-23-

EVENT 19

OB2NV



Figure 6 (cont.). Particle-motion analysis for selected Pn and P waves at OB2NV.

-24-

EVENT 30

OB2NV



Figure 6 (cont.).   Particle-motion analvsis for selected Pn and P waves
at OB2NV.

EVENT 37

OB2NV



Figure 6 (cont.). Particle-motion analysis for selected Pn and P waves at OB2NV.

-26-

EVENT 1

RK-ON



Figure 7.    Particle-motion analysis for selected P waves at RKON.

EVENT 3

RK-ON

63.7 nm

P

59.9 nm

27.2 nm

|← 5 sec →|

Figure 7 (cont.).   Particle-motion analysis for selected P waves at RKON.

-28-

EVENT 4

RK-ON



Figure 7 (cont.). Particle-motion analysis for selected P waves at RKON.

EVENT 6

RK-ON



Figure 7 (cont.). Particle-motion analysis for selected P waves at RKON.
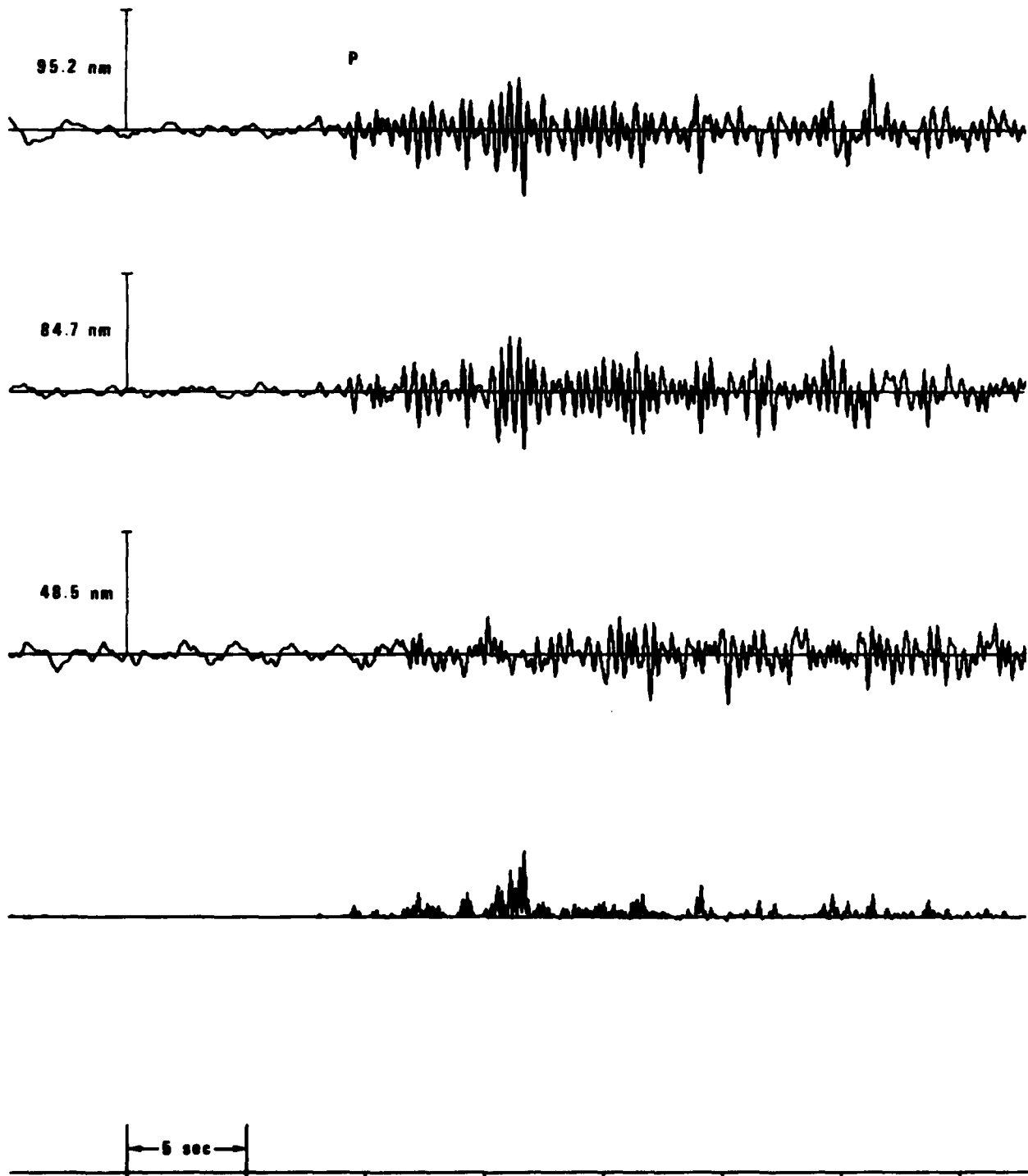
EVENT 13

RK-ON

95.2 nm

P

84.7 nm

48.5 nm

5 sec

Figure 7 (cont.). Particle-motion analysis for selected P waves at RKON.

-31-

Figure 8. Particle-motion analysis for selected Lg waves at OB2NV.

EVENT 11

OB2NV
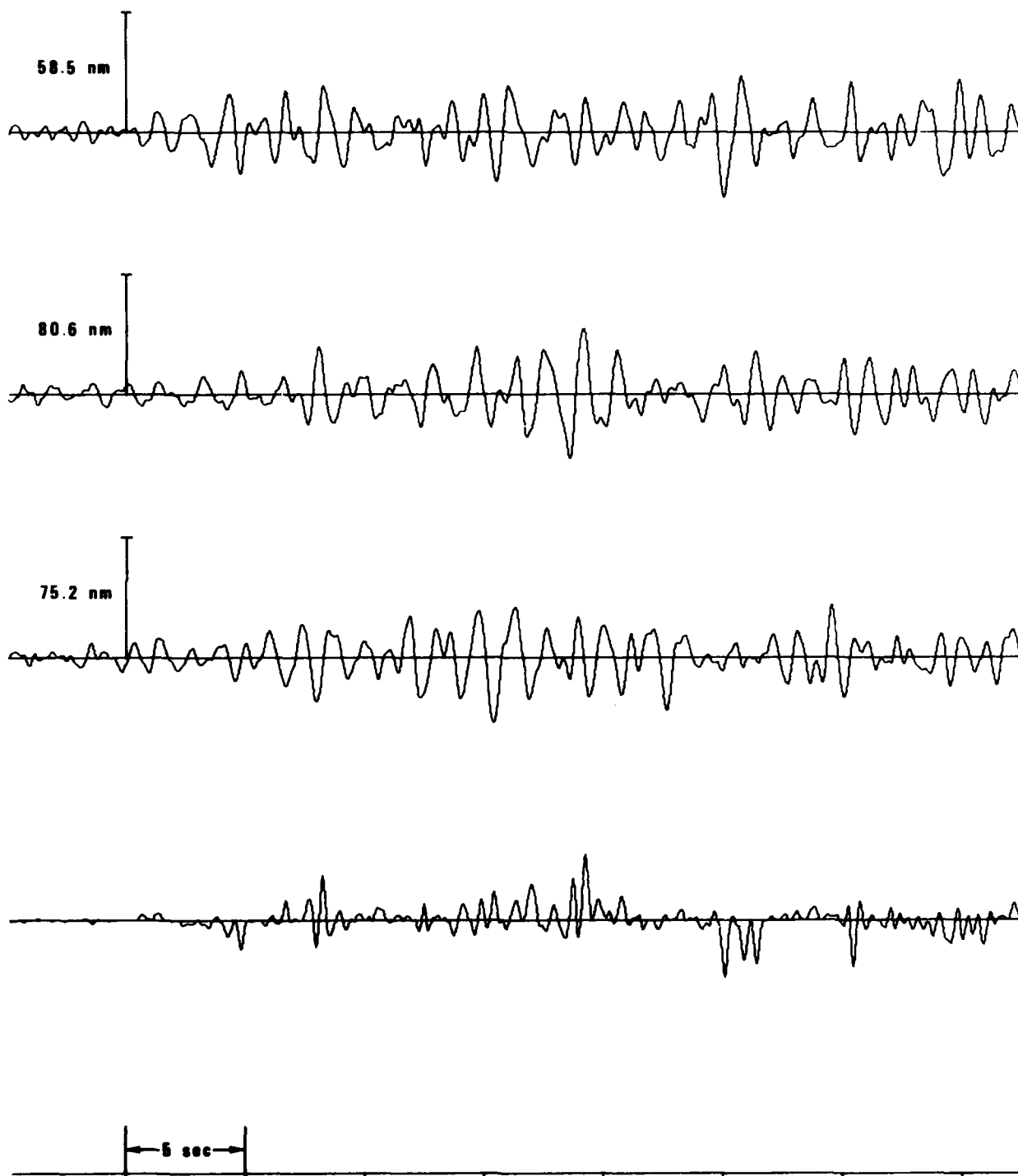


58.5 nm

80.6 nm

75.2 nm

|←— 5 sec —→|

Figure 8 (cont.).  Particle-motion analysis for selected Lg waves at OB2NV.

EVENT 24
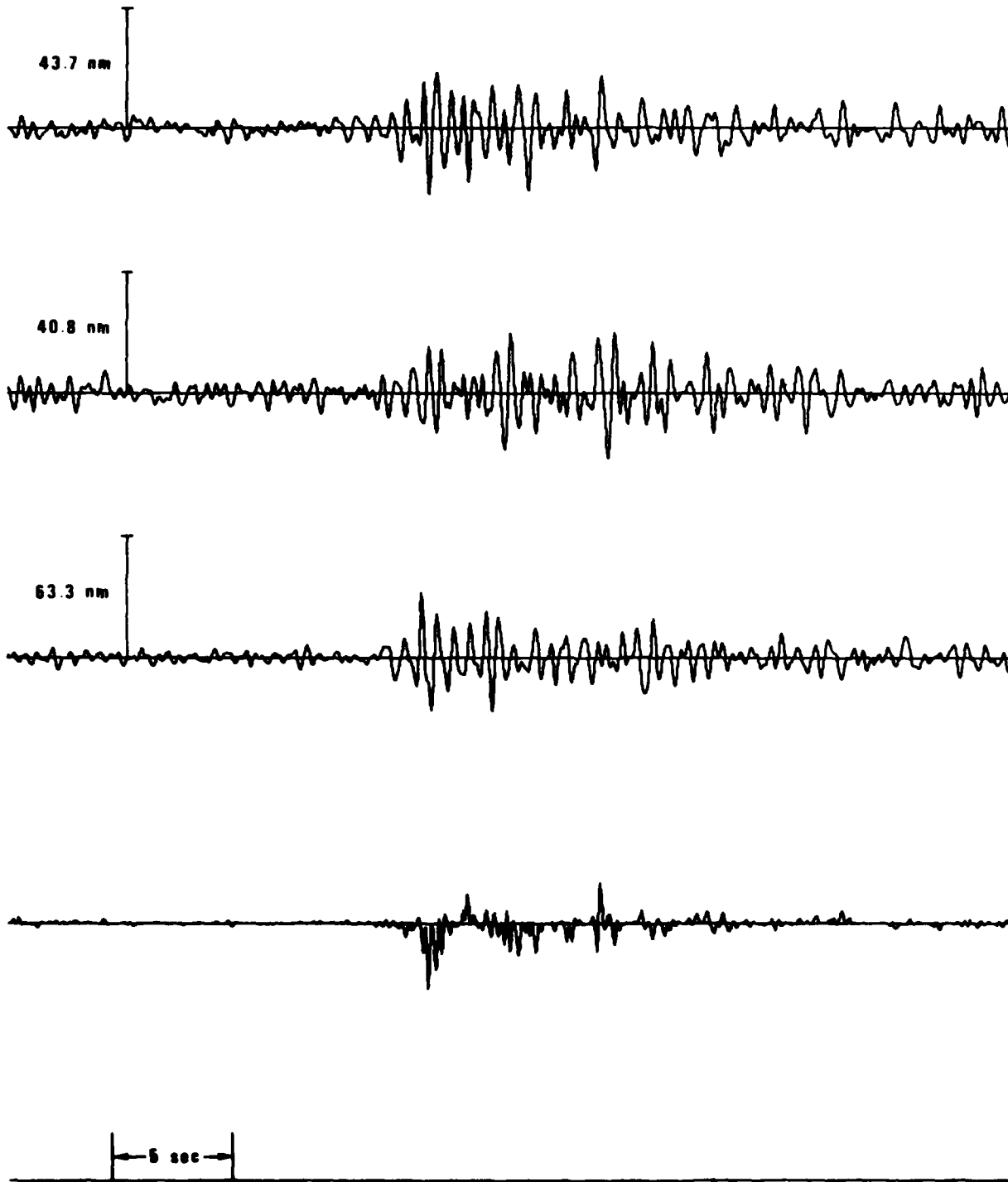
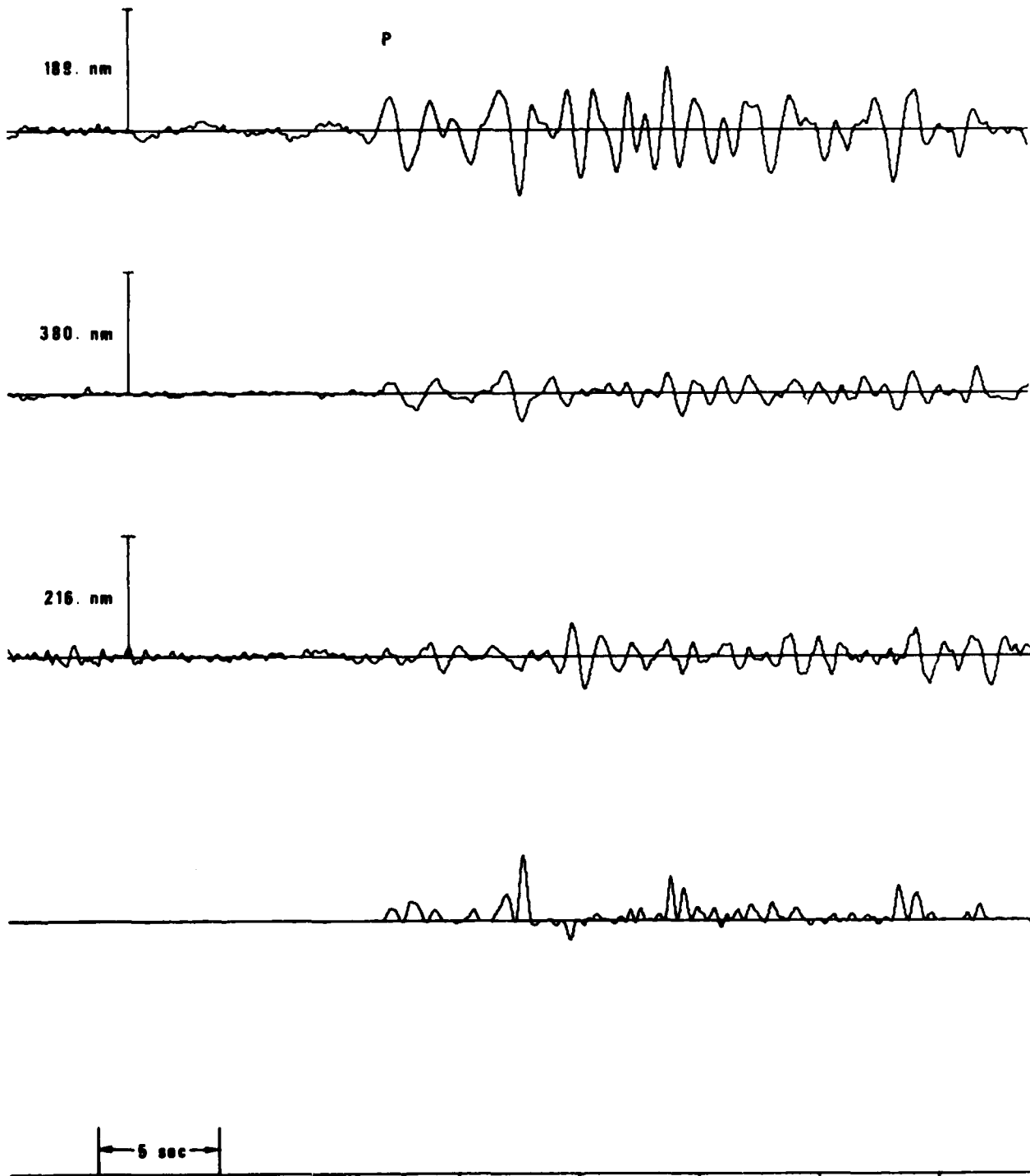OB2NV



43.7 nm

40.8 nm

63.3 nm

|—5 sec—|

Figure 8 (cont.). Particle-motion analysis for selected Lg waves at OB2NV.

-34-

EVENT 28

OB2NV



Figure 8 (cont.).   Particle-motion analysis for selected Lg waves at OB2NV.

EVENT 34

OB2NV



**82.6 nm**

**62.9 nm**

**99.0 nm**

|—5 sec—|
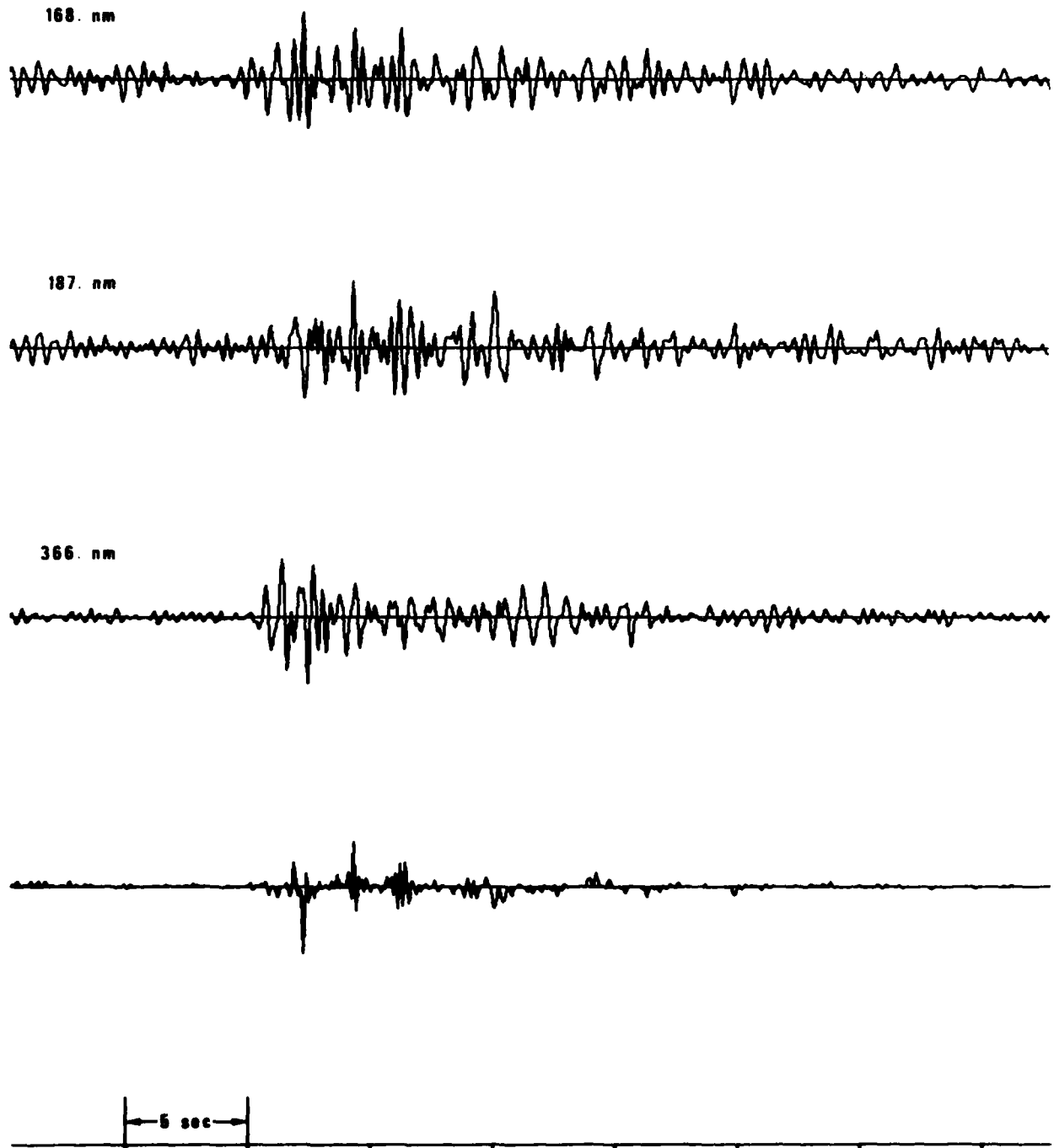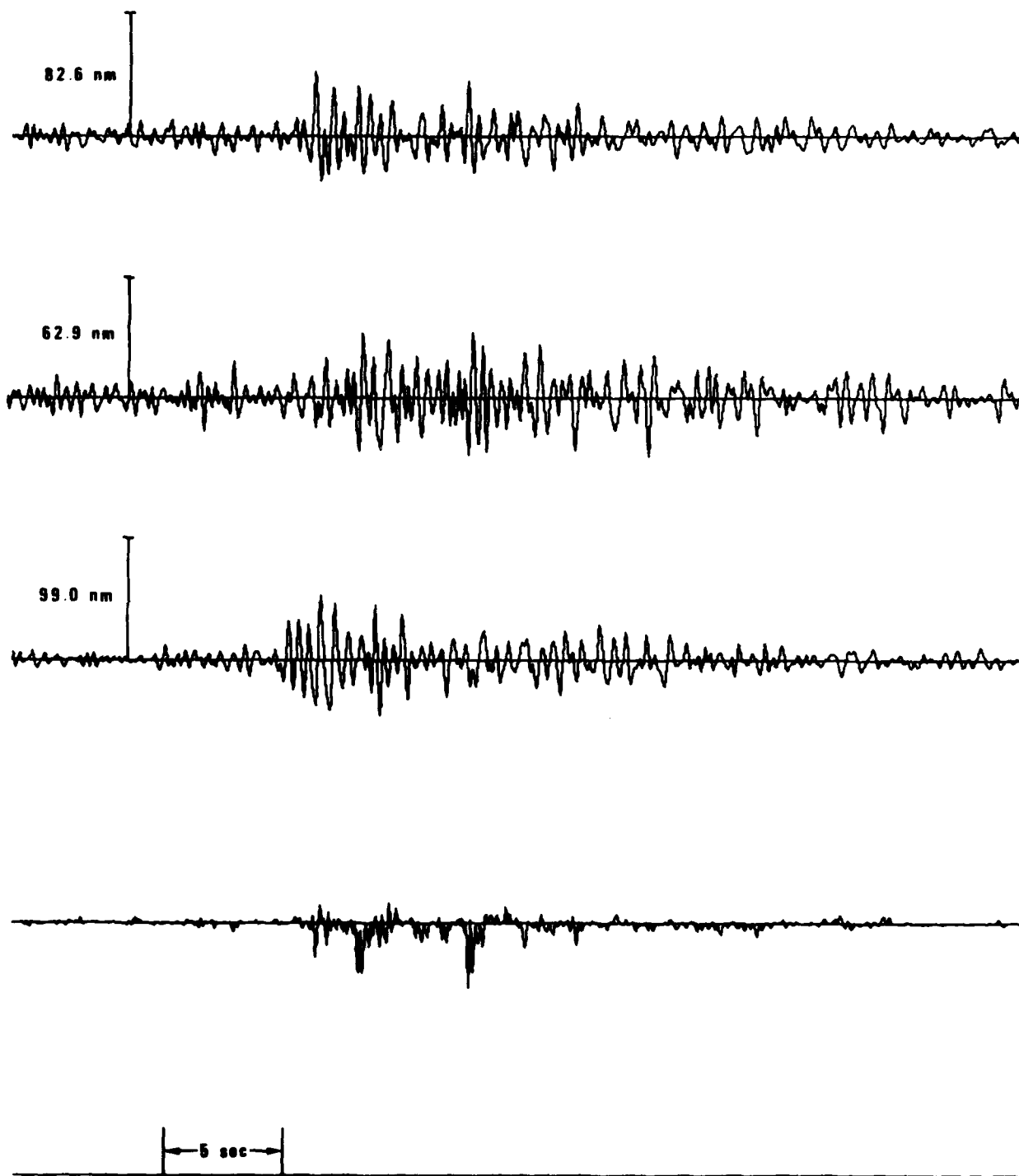
Figure 8 (cont.). Particle-motion analysis for selected Lg waves at OB2NV.

EVENT 6

RK-ON
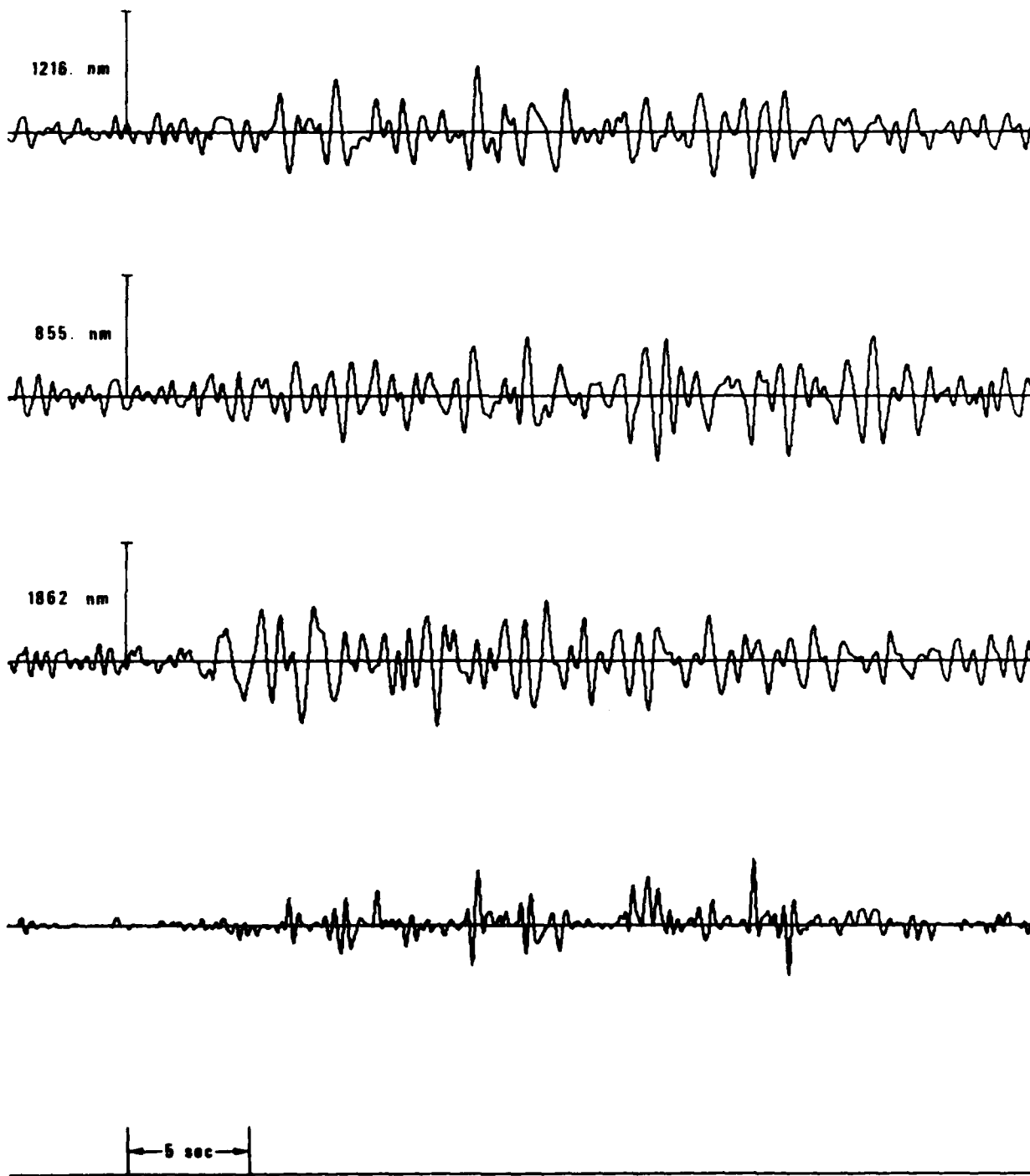


Figure 9. Particle-motion analysis for selected Lg waves at RKON.
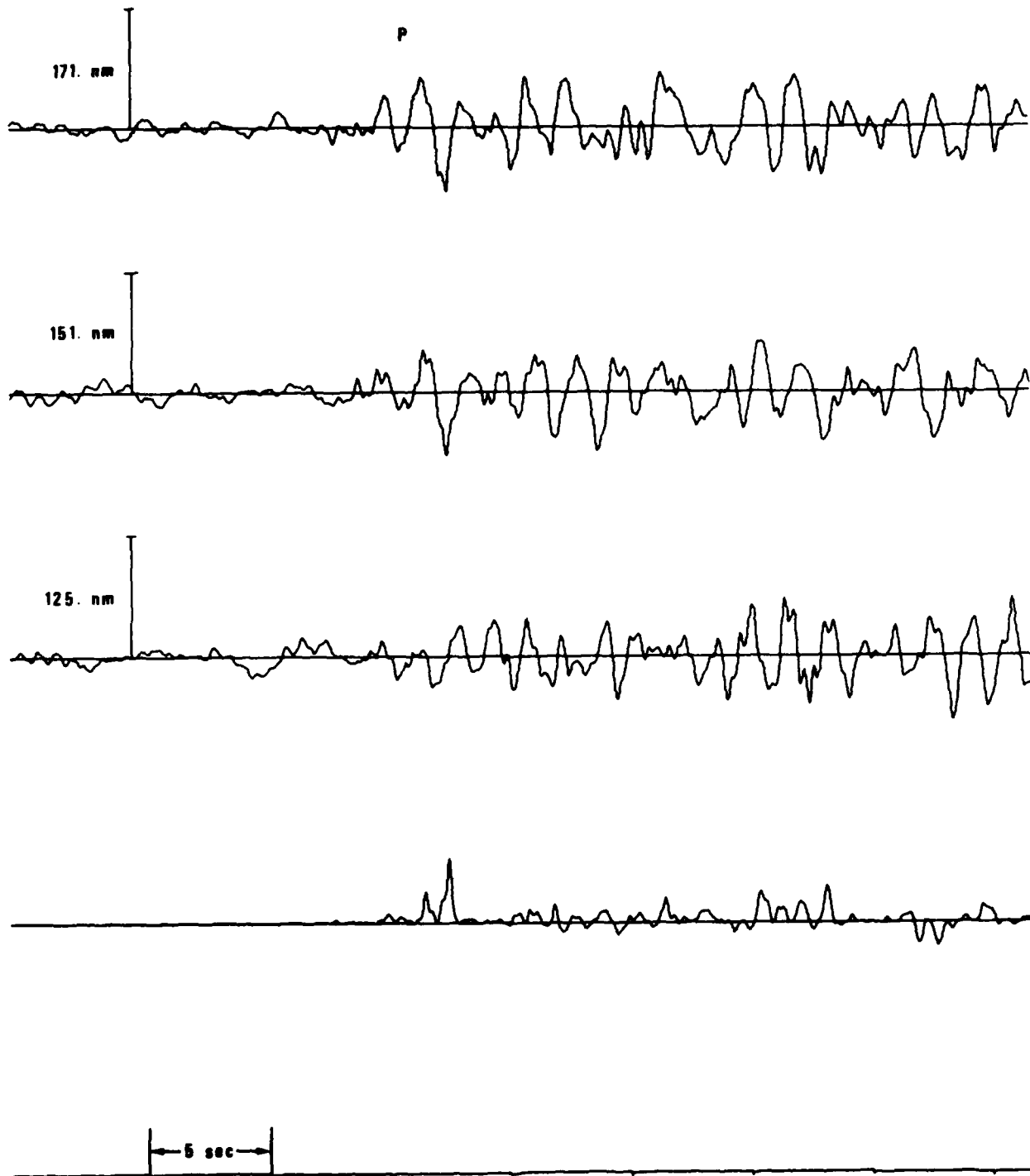
EVENT 8

RK-ON

60.2 nm

50.0 nm

98.0 nm

5 sec
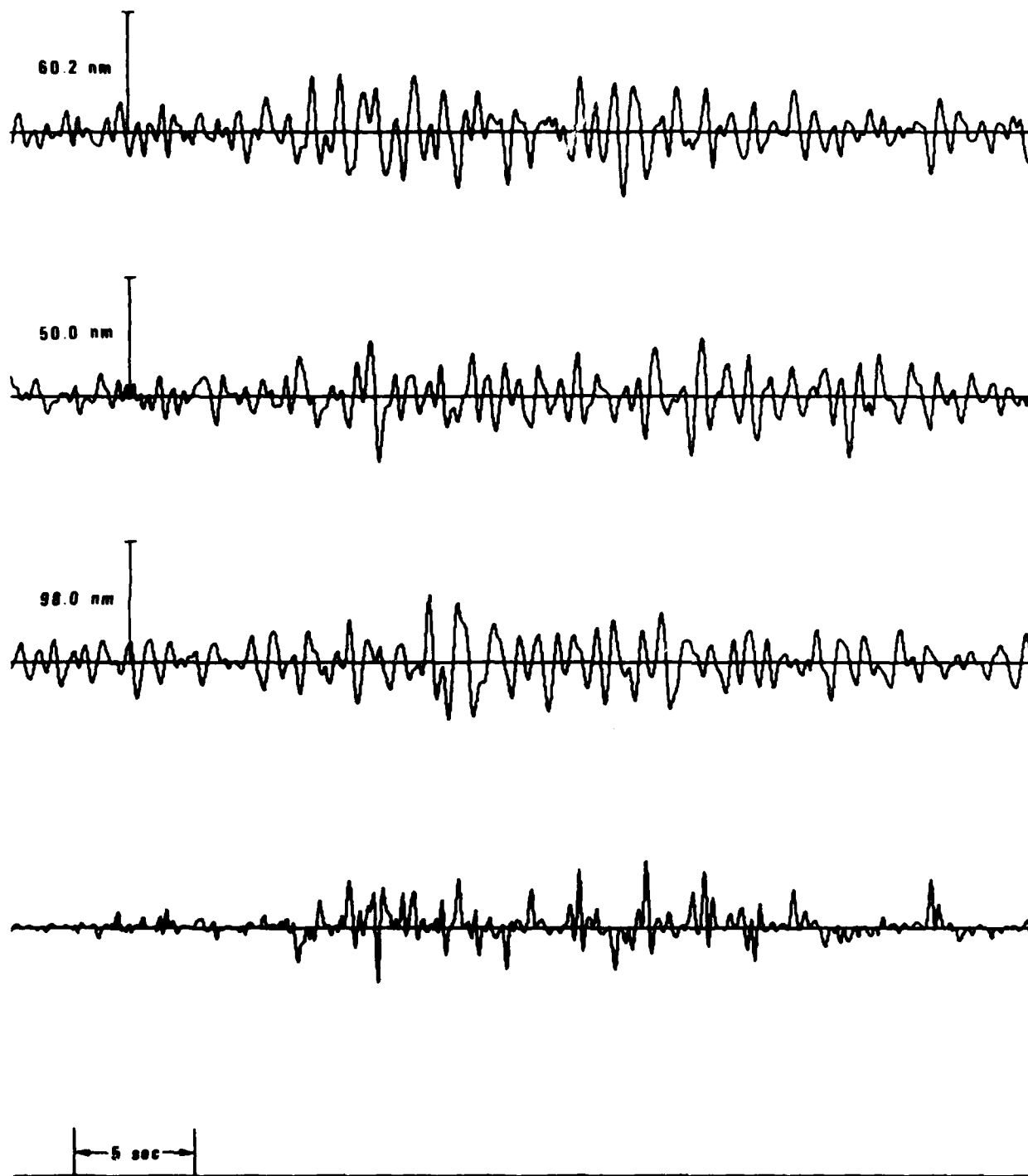
Figure 9 (cont.).  Particle-motion analysis for selected Lg waves at RKON.

EVENT 13

RK-ON



Figure 9 (cont.). Particle-motion analysis for selected Lg waves at RKON.

-39-
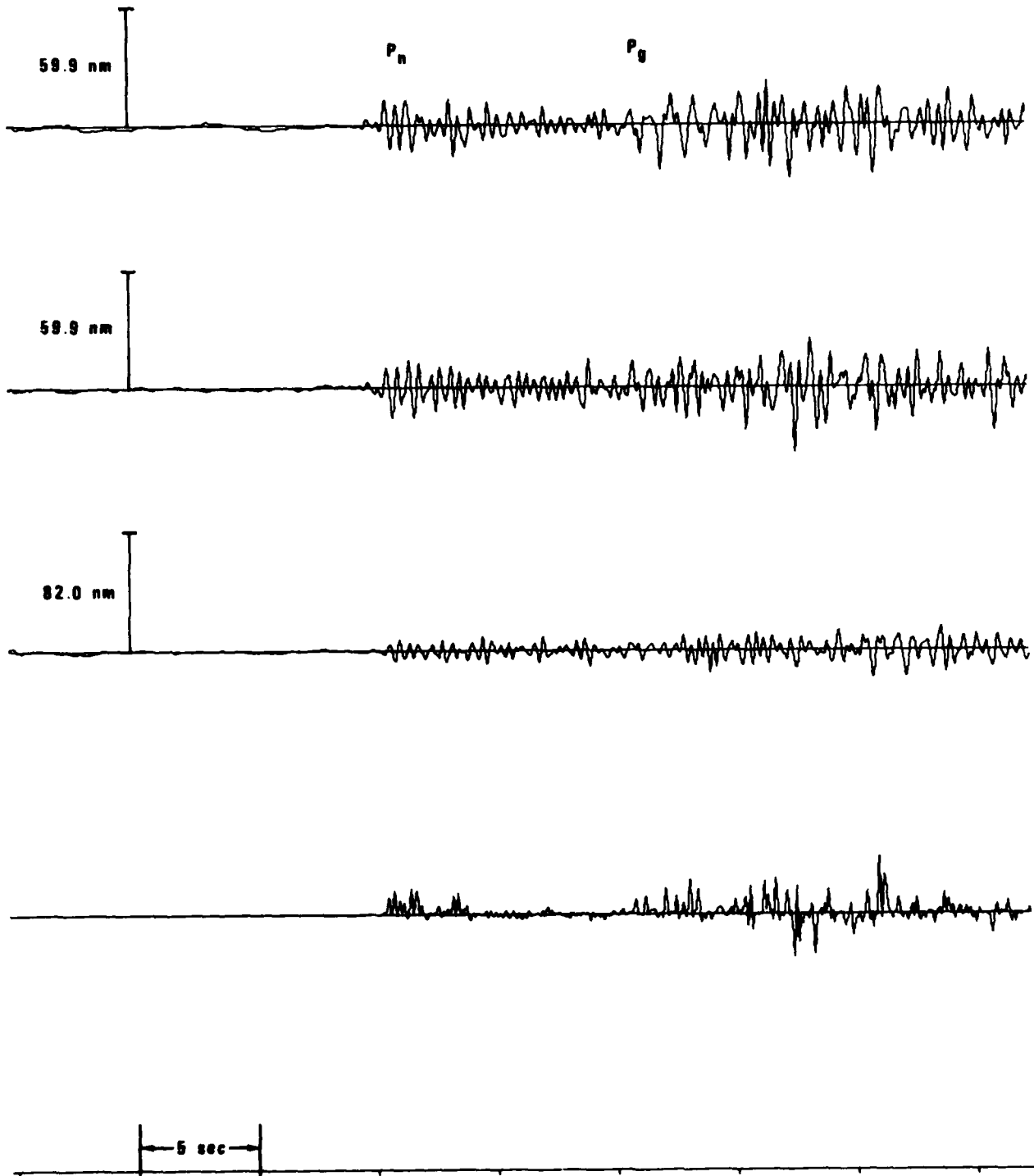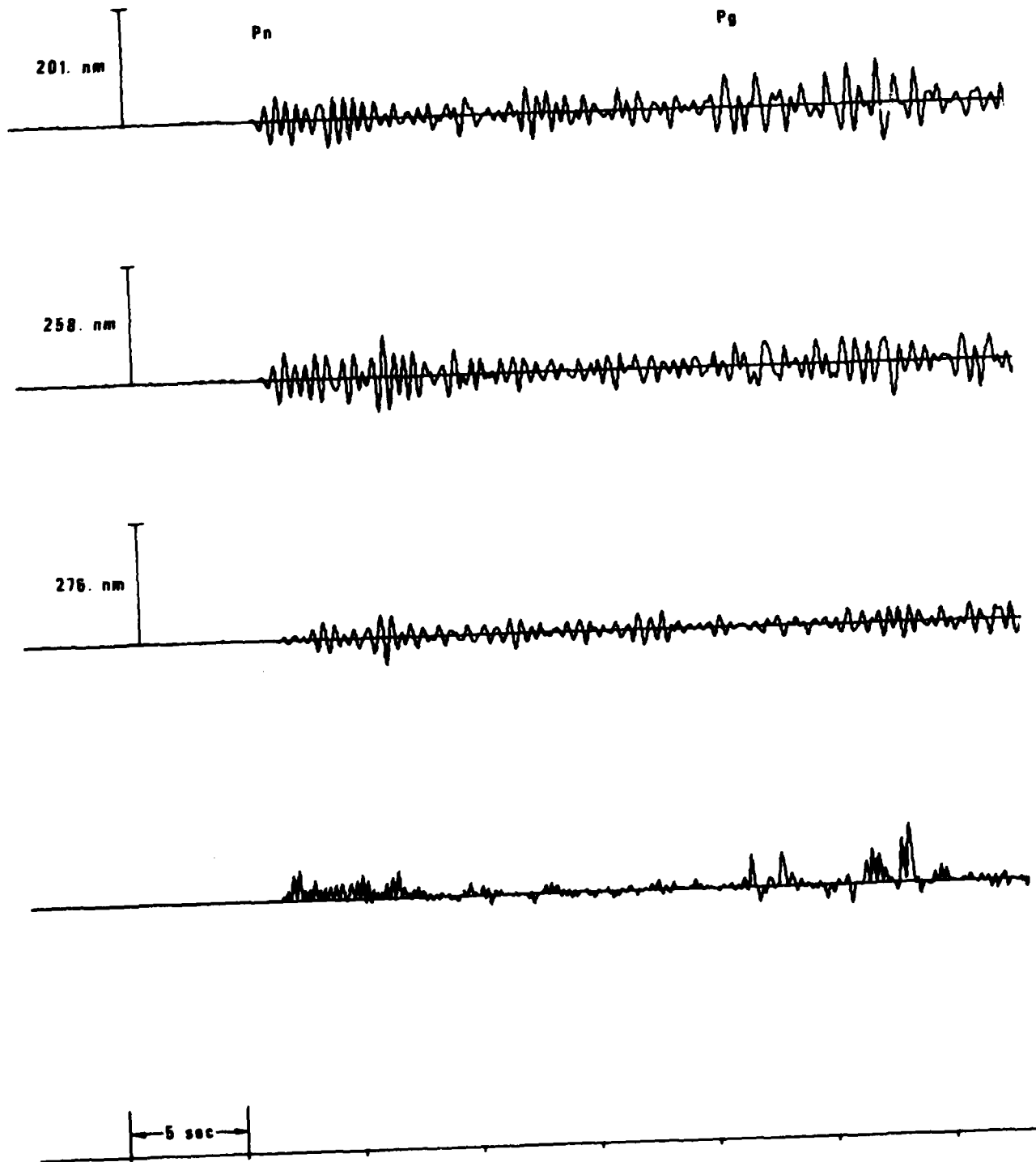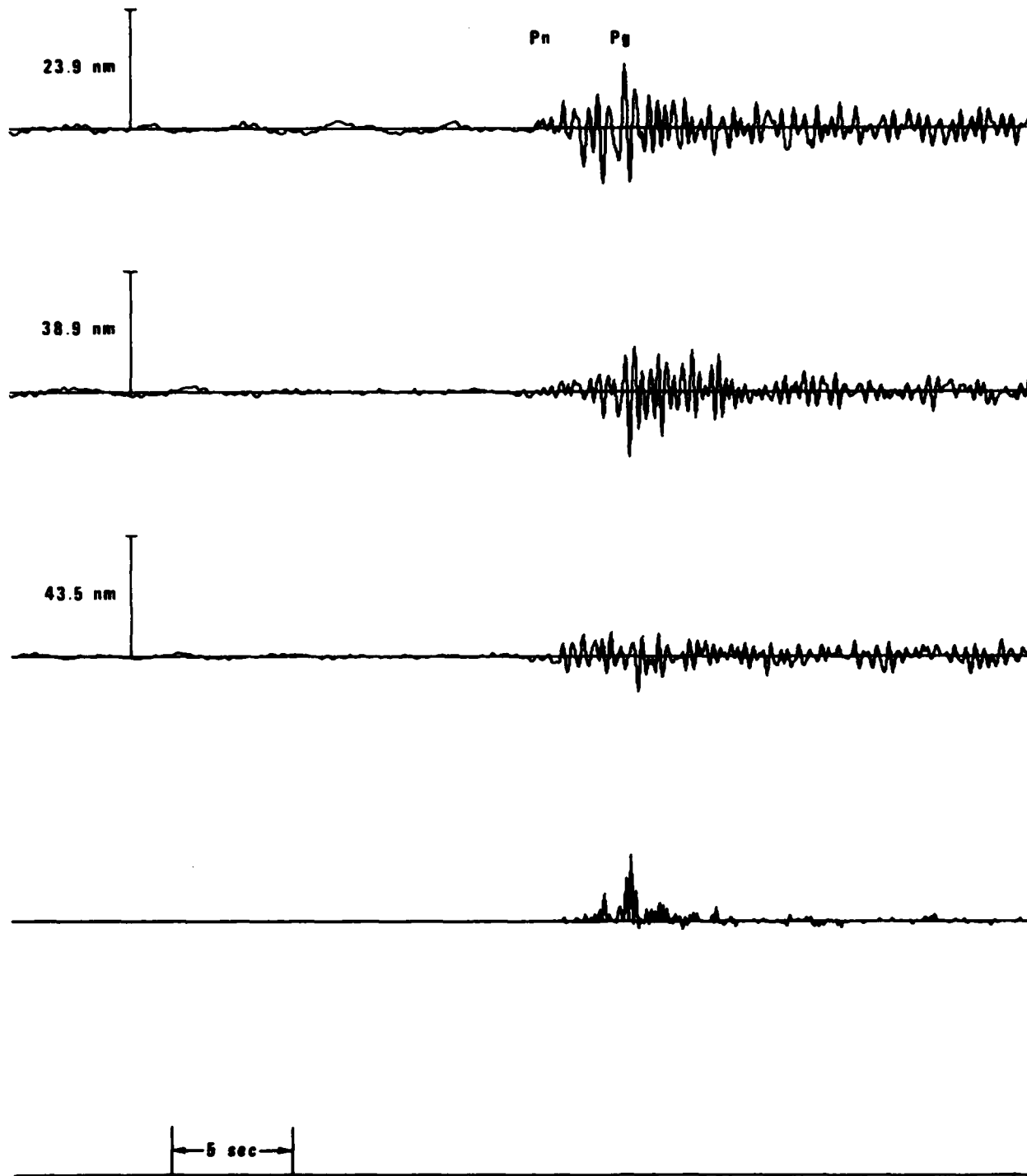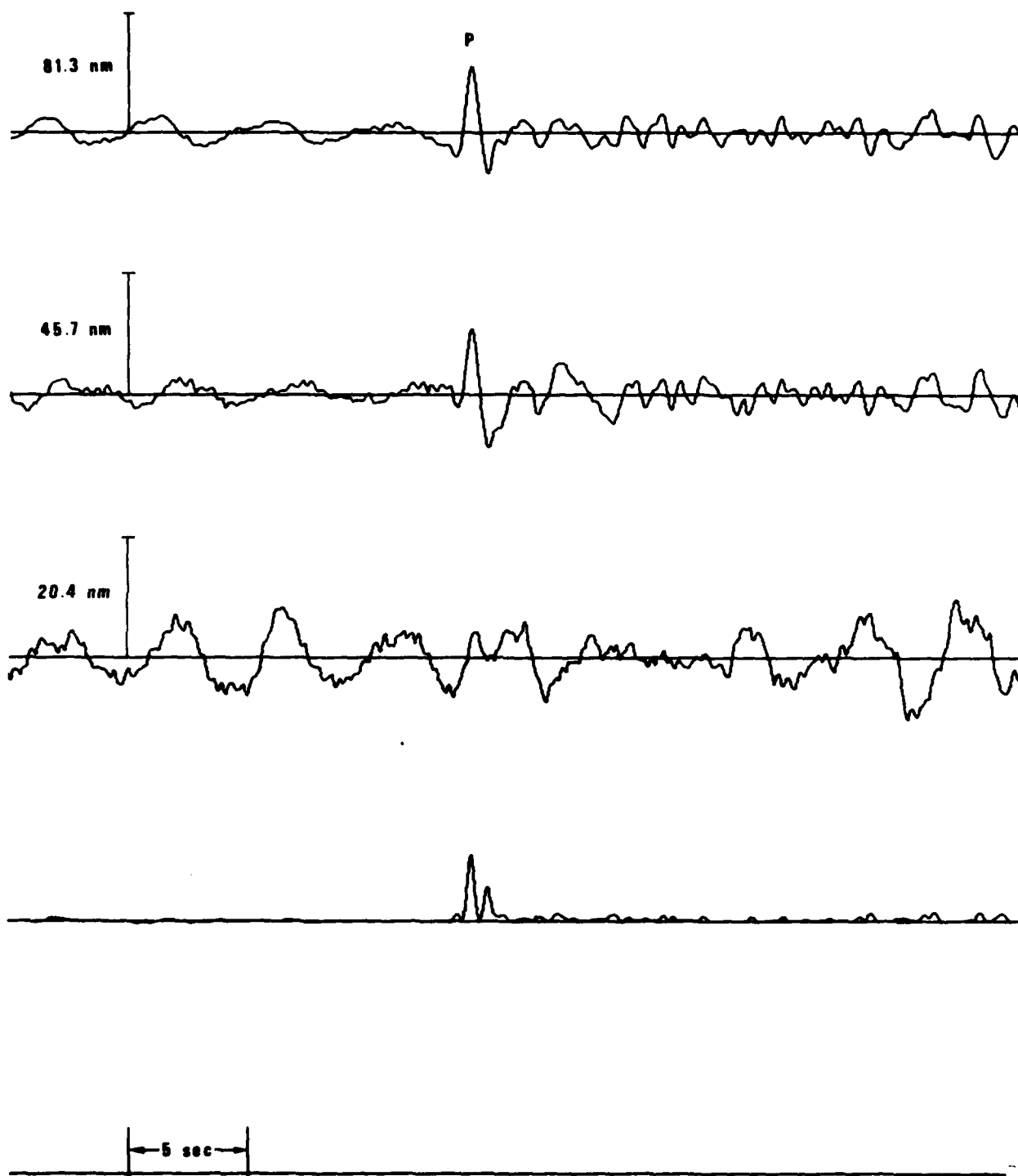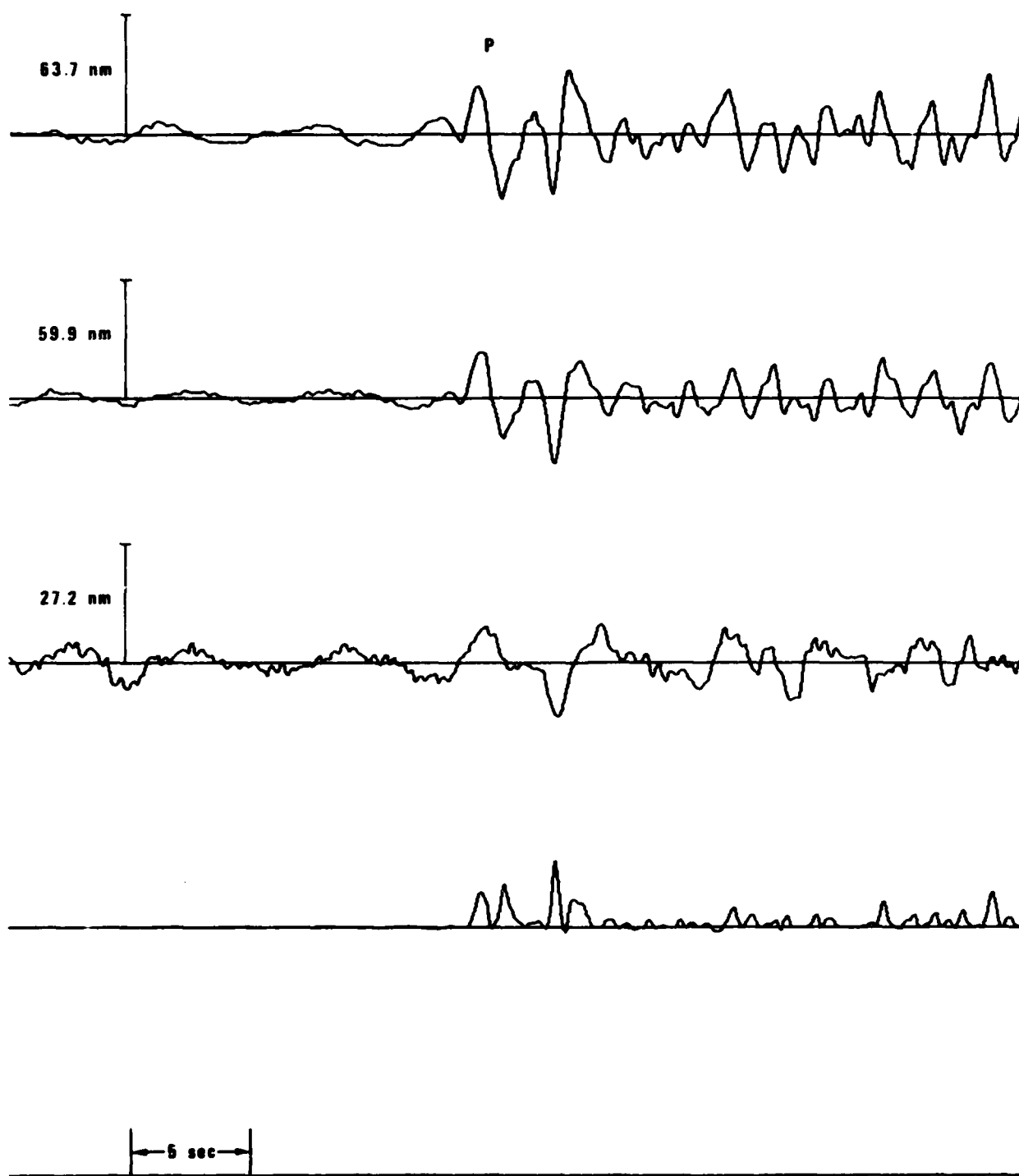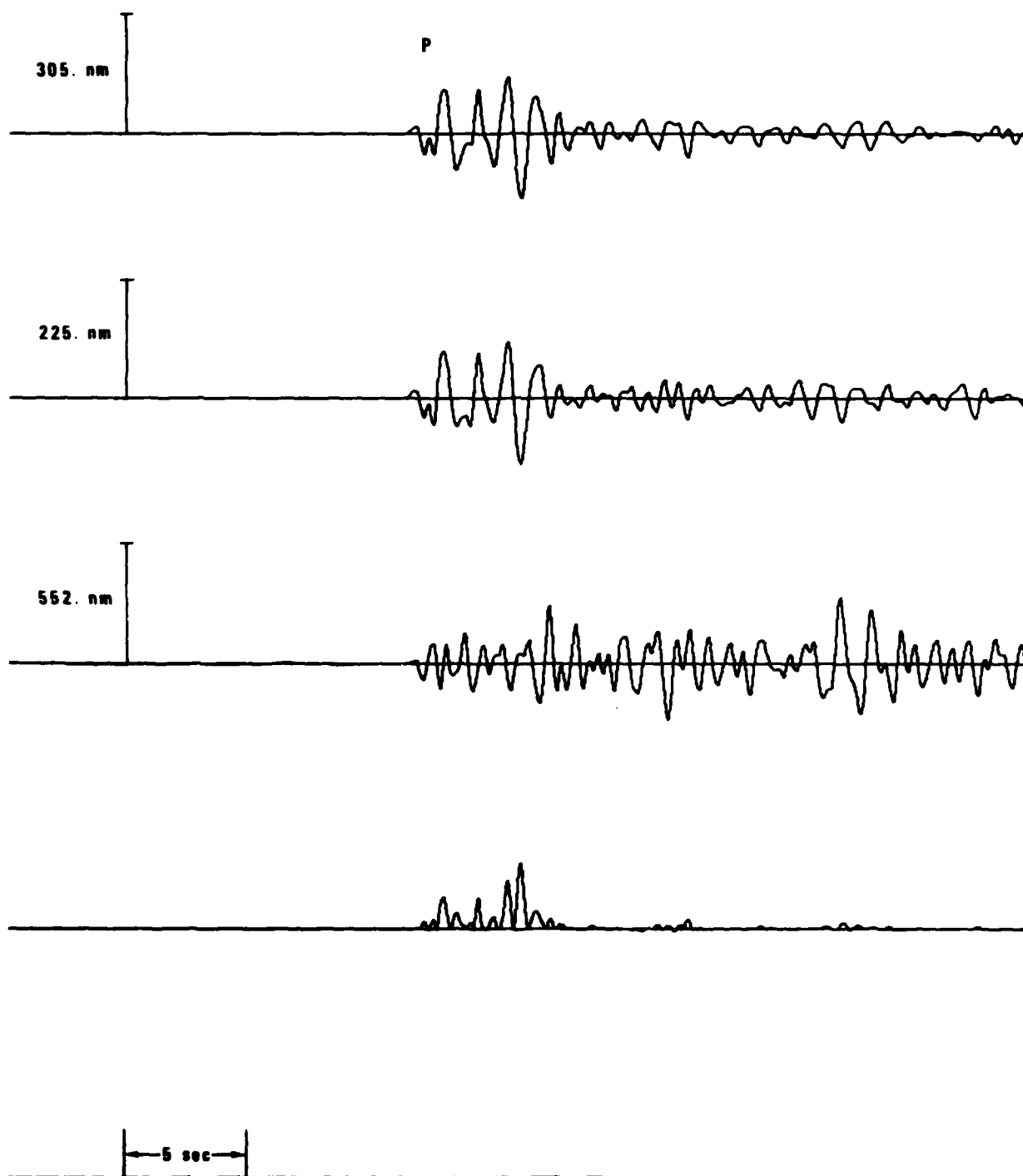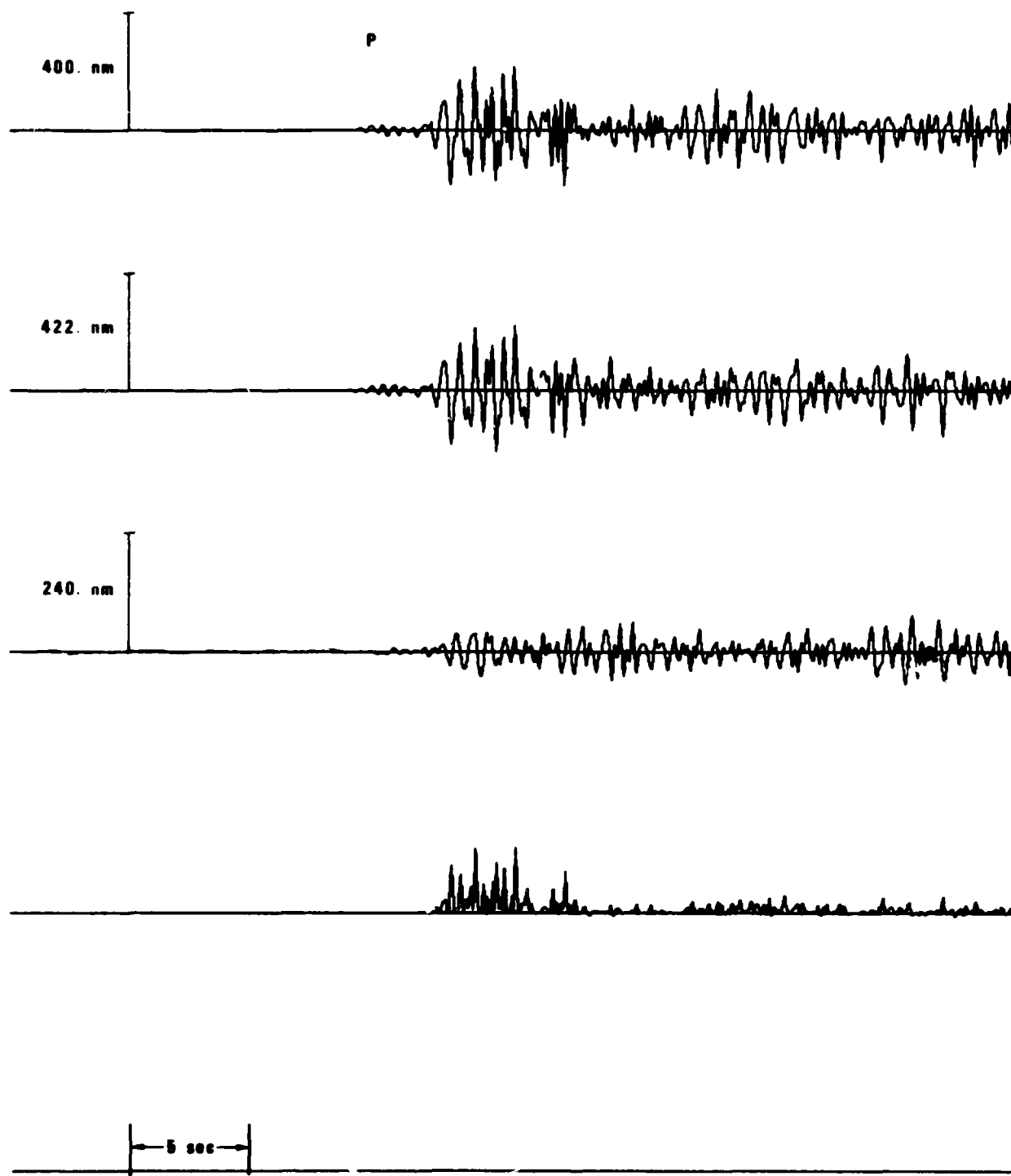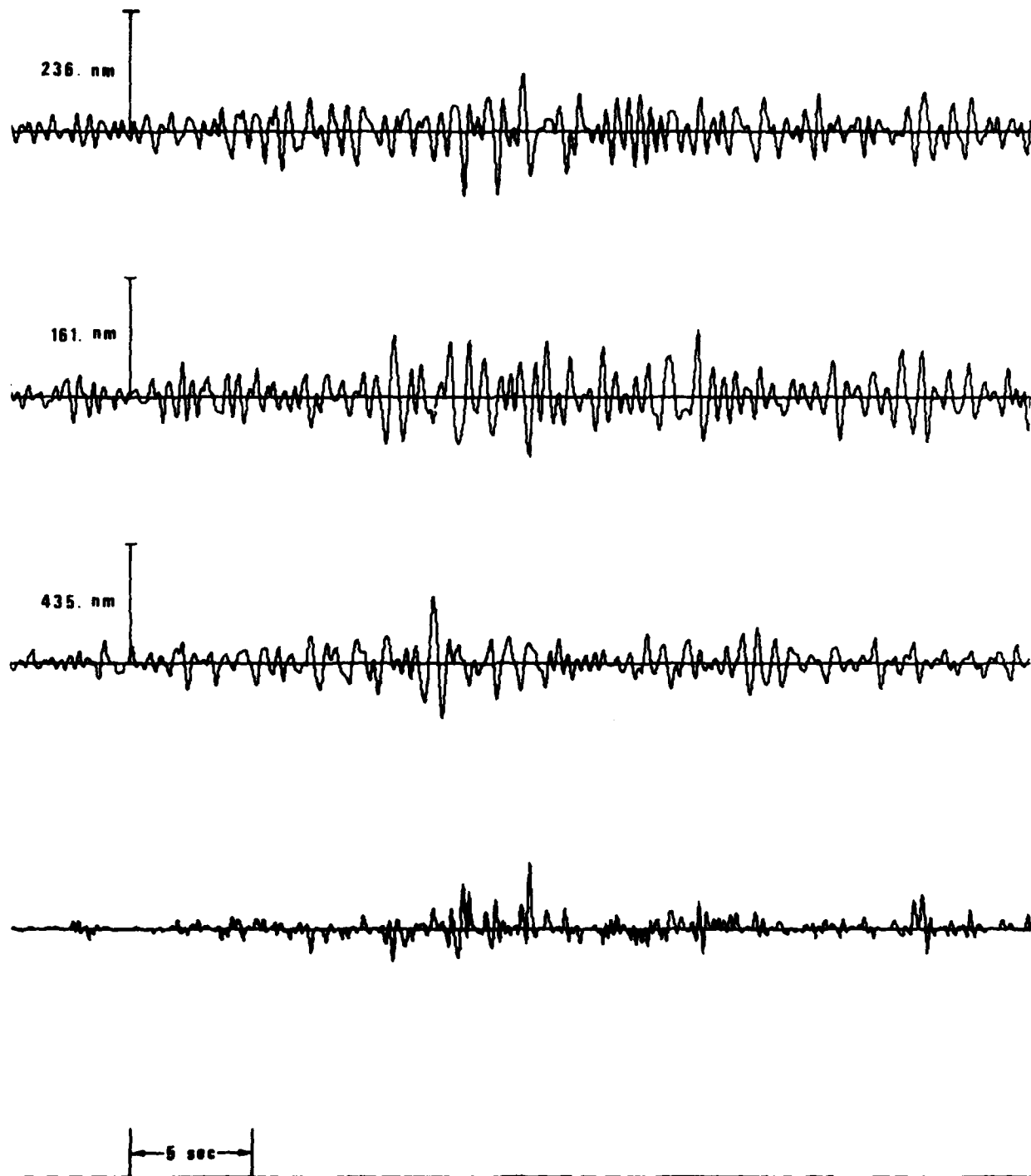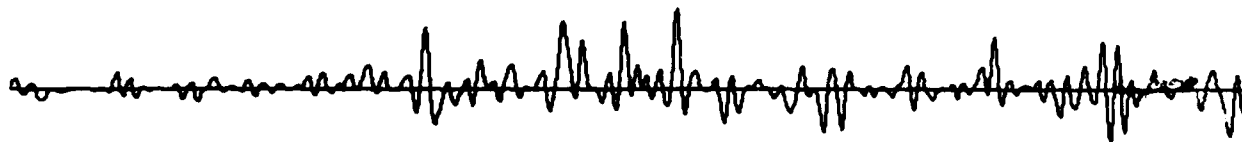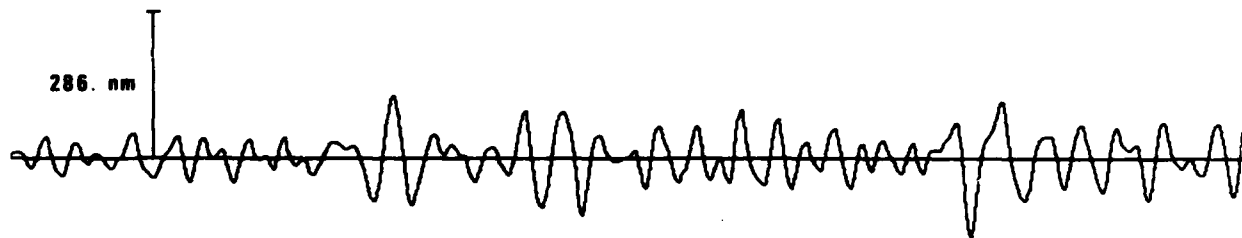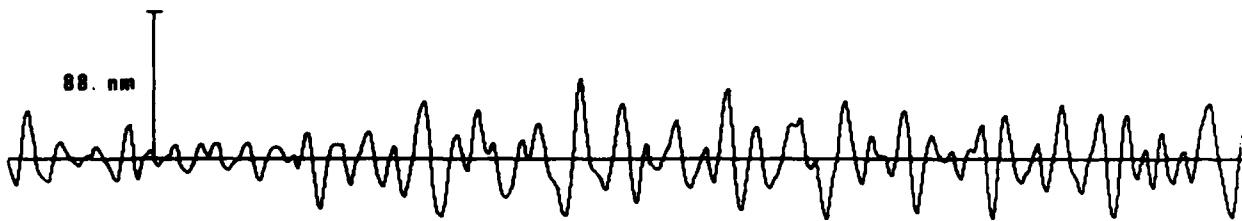
Figure 9 (cont.).   Particle-motion analysis for selected Lg waves at RKON.

EVENT 17

RK-ON



Figure 9 (cont.).   Particle-motion analysis for selected Lg waves at RKON.

-41-
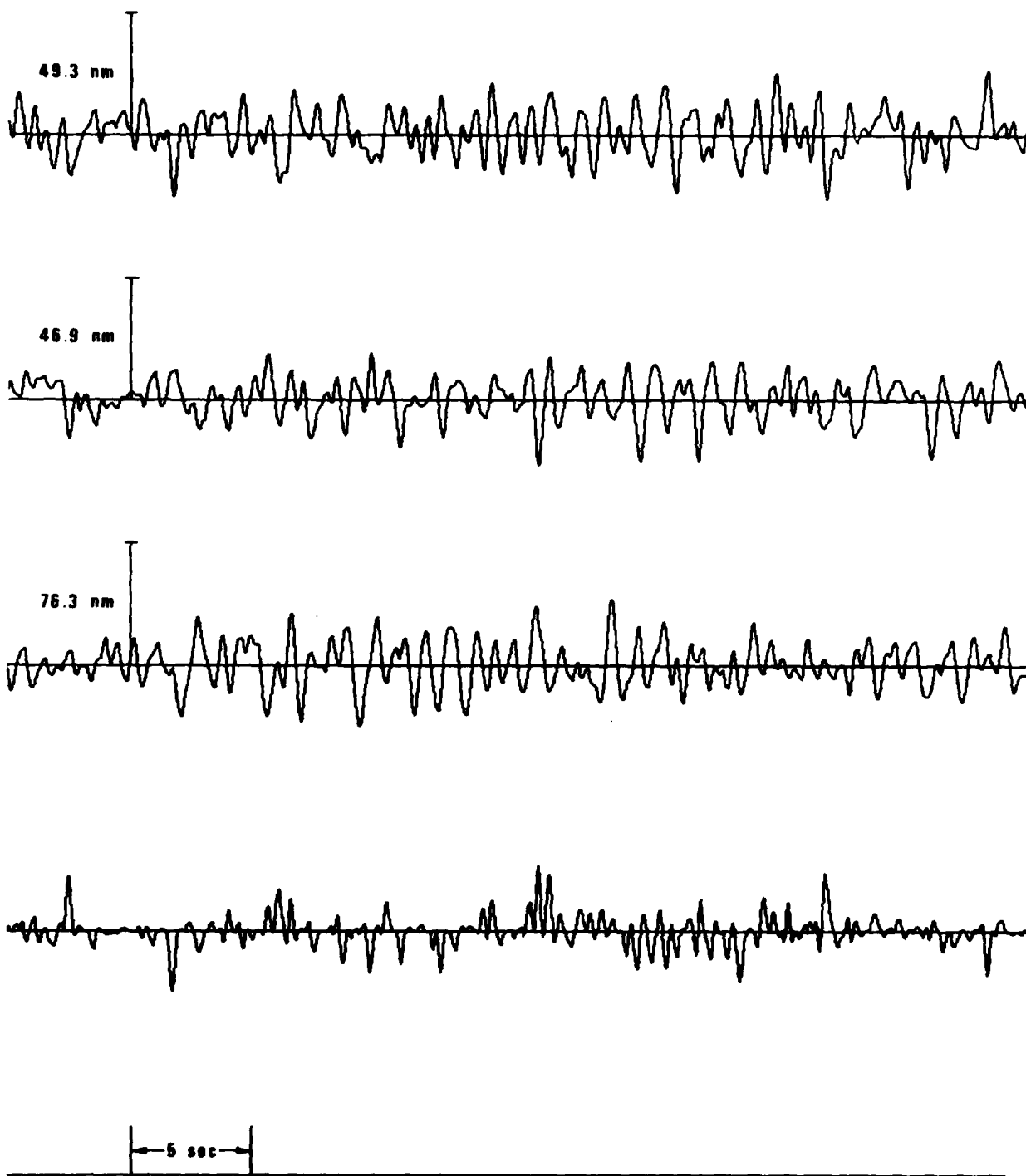
be found in Table II, III and IV by using the event number at the top of
the figures.  Figure 8 shows typical Lg recordings at OB2NV.  Figures 7
and 9 show P and Lg waves from RKON.

Examination of all the regional (1.6° < Δ < 16.6°) OB2NV signals
revealed these qualitative features:

1)  Lg is the prominent (maximum amplitude) phase out to 8.4° at
    least; however, it is an emergent phase.

2)  Pn is always weaker than Pg.

3)  Pn and Pg have true P particle motion--often for several cycles.

4)  Lg consists largely of SV-type particle motion, but sometimes
    clearly P-type.  In general Lg does not have consistent particle
    motion and is erratic, and long trains (several cycles) of
    LR-type motion are rare.

5)  The coda after Pg up to Lg has no consistent particle-motion-
    truly a scattered wave phenomenon.

6)  The transverse trace is relatively small for initial Pn and Pg
    arrivals but equal to the vertical, or somewhat larger than it,
    during Lg motion.

Examination of the RKON plots (10.4° < Δ < 28.0°) produced
generally the same inferences.  However, there were many RKON Lg signals
which had transverse motion much greater than vertical motion.  Also,
the frequency content of RKON Lg waves sometimes differed greatly
between two earthquakes at the same distance, even when the sources were
in the same region.

## SOME TESTS OF THE PARTICLE-MOTION PROCESSORS

### Earthquake P Phases Recorded at OB2NV and RKON

The signals from events as listed in Tables II, III, and IV were used to provide some baseline data on the capability of the particle-motion processors to identify and quantify regional and teleseismic signals. The results generated from this data base are reported in this section, and these results were used in devising a prototype phase-identification and phase-characterization experiment to be discussed in the following sections.

The P-wave processor amounts to a least-squares fit of the 3-component data to a model of rectilinear P-wave motion due to a plane wave, with the solution space being composed of simply back azimuth, incidence angle, and amplitude (Smart, 1981). Figures 6 and 8 suggest that only a short window should be used after the detection time, assuming it coincides with first motion. Therefore all windows were set at 1.6 sec, a duration that encloses one to three cycles of motion and effectively ignores any coda arrivals. (It was actually confirmed by tests with 3.2 and 6.4 sec windows that 1.6 sec windows gave the best results.) Furthermore, the algorithm was coded to accept only that portion of the spectrum where signal exceeded noise over a contiguous band of frequencies, and in no ase were frequencies higher than 3.125 Hz used. The ratio of signal-to-noise in the frequency band used, the signal back azimuth and incidence angle, and the F-statistic given by

$$F = \frac{\text{variance (model)} - \text{variance (noise)}}{\text{variance (noise)}} \qquad (1)$$

were computed. In this case "model" is the estimated motion of the true P-wave and noise is anything in the recorded motion which remains after the "model" is subtracted. A S/N ratio was also computed as the ratio of the rms in the signal window to that in the equivalent-length window of noise just before the signal window.

The results of running this processor on the OB2NV regional Pn waves (from events in Table I) are given in Table V. Note that many Pn waves were of low S/N ratio and had, accordingly, small F values and poor estimates of signal parameters. For those signals with F > 6.0, the azimuth estimates have an average absolute error of 20°. The emergence angle of Pn within a Herrin-68 earth model is 48°, and the estimated emergence angles in Table V generally fall below this value, indicative of lower velocities in the upper crust beneath OB2NV than the 6.00-6.75 km/sec crust of the Herrin-68 model.

Table VI is similar to Table V, except Pg waves at OB2NV are represented here. Parameters identical to those for the Pn waves were used in processing the Pg waves. The Pg wave on some regional recordings at OB2NV could not be reliably timed and some regional recordings were beyond Pg range, and so Table VI has fewer entries than Table V. Here again, the S/N ratio represents only the actual frequency band used in the processor and, being based on the noise just preceding Pg in time, greatly underestimates the actual Pg amplitude. Note that azimuth errors are often large, with unacceptable estimates of azimuth occurring even when the F statistic is large (events 9 and 16).

Table VII presents the results for the teleseismic P waves recorded at OB2NV from the events in Table III. In general the back azimuth estimates are good; considering only those with F > 6.0, there is a mean absolute error of 13° in the back azimuth estimate. Except for one signal (event #67), even those cases with F < 6.0 show good azimuth estimates, in contrast to the often erratic results for OB2NV Pn waves where F > 6.0 in Table V.

Table VII shows that the incidence angle estimates for teleseismic P all are below 30°, except for the one signal (event #67) which also had an unsatisfactory azimuth estimate. The true incidence angles are computed for the Herrin-68 velocity model, as done for the previous tables. Figure 10 is a plot of estimated versus true incidence angles for all the Pn and P phases at OB2NV. For high S/N ratios, a distinct

## TABLE V

P-wave particle motion processor results for OB2NV Pn phases

| Event # | Incidence Angle | | Back Azimuth | | # of Spectral Points Used | F Statistic | S/N Ratio |
|---|---|---|---|---|---|---|---|
| | true | est. | true | est. | | | |
| 1 | 48 | 30 | 150 | 170 | 5 | 17.8 | 5.7 |
| 2 | 48 | 33 | 329 | 335 | 5 | 4.0 | 2.5 |
| 3 | 48 | 37 | 326 | 332 | 5 | 3.7 | 6.5 |
| 4 | 48 | 39 | 329 | 342 | 4 | 10.4 | 2.9 |
| 5 | 48 | 34 | 155 | 189 | 3 | 13.8 | 5.4 |
| 7 | 48 | 27 | 152 | 161 | 5 | 33.4 | 4.0 |
| 8 | 48 | 48 | 205 | 173 | 4 | 2.8 | 4.7 |
| 9 | 48 | 18 | 195 | 346 | 3 | 4.6 | 1.9 |
| 10 | 48 | 48 | 192 | 192 | 4 | 5.3 | 3.6 |
| 11 | 48 | 37 | 136 | 95 | 3 | 7.7 | 3.5 |
| 12 | 48 | 40 | 267 | 262 | 5 | 2.6 | 2.0 |
| 13 | 48 | 48 | 189 | 197 | 4 | 9.0 | 2.9 |
| 14 | 48 | 45 | 182 | 201 | 5 | 7.9 | 7.9 |
| 15 | 48 | 32 | 281 | 37 | 3 | 1.2 | 2.8 |
| 16 | 48 | 52 | 188 | 100 | 2 | 2.3 | 2.2 |
| 17 | 48 | 42 | 215 | 227 | 4 | 6.0 | 5.1 |
| 18 | 48 | 50 | 204 | 206 | 4 | 15.1 | 18.6 |
| 19 | 48 | 43 | 187 | 195 | 5 | 9.0 | 14.7 |
| 20 | 48 | 53 | 267 | 36 | 4 | 1.0 | 2.1 |
| 21 | 48 | 17 | 267 | 326 | 5 | 7.1 | 1.5 |
| 22 | 48 | 31 | 7 | 157 | 3 | 1.5 | 3.2 |
| 23 | 48 | 38 | 198 | 207 | 5 | 6.2 | 4.7 |
| 24 | 48 | 22 | 181 | 164 | 4 | 1.7 | 3.5 |
| 25 | 48 | 38 | 217 | 209 | 5 | 2.1 | 5.6 |
| 26 | 48 | 43 | 273 | 162 | 3 | 1.9 | 2.6 |
| 27 | 48 | 67 | 251 | 186 | 4 | 1.8 | 2.1 |
| 28 | 48 | 28 | 324 | 320 | 5 | 2.5 | 2.9 |
| 29 | 48 | 41 | 266 | 292 | 1 | 1.5 | 2.3 |
| 30 | 48 | 54 | 199 | 203 | 5 | 29.2 | 28.7 |
| 32 | 48 | 64 | 154 | 214 | 2 | 12.0 | 1.6 |
| 33 | 48 | 28 | 325 | 334 | 3 | 3.6 | 3.0 |
| 34 | 48 | 39 | 216 | 216 | 4 | 5.0 | 4.1 |
| 35 | 48 | 14 | 209 | 317 | 1 | 0.3 | 4.0 |
| 37 | 48 | 61 | 140 | 194 | 4 | 2.5 | 17.2 |

## TABLE VI

P-wave particle motion processor results for OB2NV Pg phases

| Event # | Incidence Angle | | Back Azimuth | | # of Spectral Points Used | F Statistic | S/N Ratio |
|---|---|---|---|---|---|---|---|
| | true | est. | true | est. | | | |
| 8 | 63 | 48 | 205 | 209 | 2 | 2.2 | 3.3 |
| 9 | 63 | 81 | 195 | 267 | 1 | 18.8 | 2.2 |
| 10 | 63 | 52 | 192 | 191 | 3 | 11.6 | 2.7 |
| 34 | 63 | 50 | 216 | 243 | 4 | 1.6 | 2.5 |
| 12 | 63 | 35 | 267 | 248 | 5 | 1.5 | 1.7 |
| 14 | 63 | 44 | 182 | 194 | 5 | 3.8 | 3.4 |
| 15 | 63 | 51 | 281 | 255 | 3 | 2.5 | 1.2 |
| 16 | 63 | 5 | 188 | 47 | 4 | 11.4 | 3.5 |
| 35 | 63 | 20 | 209 | 142 | 5 | 4.1 | 1.2 |
| 18 | 63 | 30 | 204 | 130 | 3 | 1.0 | 2.4 |
| 19 | 63 | 32 | 187 | 191 | 4 | 2.5 | 2.3 |
| 20 | 63 | 78 | 267 | 296 | 2 | 2.4 | 2.1 |
| 21 | 63 | 45 | 267 | 287 | 4 | 2.6 | 2.0 |
| 23 | 63 | 27 | 198 | 202 | 2 | 1.3 | 1.9 |
| 24 | 63 | 31 | 181 | 194 | 3 | 9.7 | 3.1 |
| 36 | 63 | 47 | 267 | 275 | 4 | 2.8 | 2.2 |
| 27 | 63 | 59 | 251 | 250 | 3 | 4.3 | 2.4 |
| 28 | 63 | 40 | 324 | 352 | 4 | 2.4 | 3.2 |
| 29 | 63 | 61 | 266 | 284 | 3 | 2.4 | 2.0 |
| 30 | 63 | 15 | 199 | 297 | 3 | 1.3 | 2.2 |
| 11 | 63 | 84 | 136 | 319 | 1 | 3.3 | 1.2 |
| 31 | 63 | 21 | 165 | 153 | 3 | 4.5 | 3.1 |

## TABLE VII

P-wave particle motion processor results for OB2NV P phases

| Event # | Incidence Angle | | Back Azimuth | | # of Spectral | F | S/N |
|---------|------|------|------|------|-------------|-----------|-------|
| | true | est. | true | est. | Points Used | Statistic | Ratio |
| 38 | 19 | 15 | 132 | 132 | 5 | 30.6 | 5.8 |
| 39 | 22 | 12 | 315 | 298 | 5 | 4.7 | 2.5 |
| 40 | 27 | 19 | 127 | 135 | 5 | 58.1 | 7.2 |
| 41 | 20 | 8 | 314 | 3 | 5 | 26.2 | 13.6 |
| 42 | 21 | 4 | 315 | 346 | 3 | 11.0 | 8.1 |
| 43 | 22 | 23 | 93 | 84 | 5 | 272.6 | 16.9 |
| 44 | 22 | 11 | 101 | 87 | 5 | 2.6 | 1.7 |
| 45 | 25 | 14 | 318 | 294 | 5 | 6.0 | 4.7 |
| 46 | 22 | 16 | 116 | 150 | 5 | 104.6 | 156.2 |
| 47 | 22 | 12 | 136 | 136 | 4 | 36.0 | 5.5 |
| 48 | 29 | 20 | 140 | 147 | 5 | 30.0 | 19.5 |
| 49 | 21 | 13 | 310 | 301 | 5 | 31.1 | 2.2 |
| 50 | 19 | 11 | 308 | 304 | 5 | 102.4 | 11.9 |
| 51 | 27 | 20 | 310 | 318 | 5 | 24.6 | 18.6 |
| 52 | 22 | 20 | 317 | 278 | 5 | 9.9 | 2.6 |
| 53 | 26 | 22 | 308 | 305 | 4 | 18.9 | 4.7 |
| 54 | 21 | 12 | 312 | 295 | 5 | 31.4 | 28.2 |
| 55 | 28 | 18 | 326 | 319 | 5 | 17.9 | 3.7 |
| 56 | 29 | 25 | 320 | 329 | 5 | 11.5 | 9.4 |
| 57 | 27 | 18 | 311 | 302 | 5 | 21.7 | 57.8 |
| 58 | 22 | 28 | 57 | 35 | 3 | 30.4 | 12.7 |
| 59 | 19 | 14 | 137 | 144 | 5 | 52.3 | 5.9 |
| 60 | 28 | 19 | 130 | 155 | 5 | 10.9 | 4.9 |
| 61 | 28 | 21 | 316 | 331 | 5 | 43.4 | 2.6 |
| 62 | 27 | 20 | 126 | 124 | 5 | 38.4 | 8.1 |
| 63 | 21 | 17 | 115 | 148 | 5 | 25.5 | 17.9 |
| 64 | 26 | 21 | 101 | 100 | 5 | 136.6 | 19.1 |
| 65 | 27 | 29 | 126 | 132 | 4 | 4.8 | 2.9 |
| 66 | 22 | 24 | 192 | 207 | 3 | 93.7 | 7.3 |
| 67 | 29 | 49 | 160 | 270 | 4 | 8.8 | 1.5 |
| 68 | 21 | 21 | 16 | 23 | 5 | 33.3 | 3.4 |
| 69 | 26 | 19 | 309 | 320 | 5 | 40.3 | 13.5 |
| 70 | 28 | 17 | 129 | 146 | 5 | 21.1 | 9.2 |
| 71 | 26 | 15 | 309 | 296 | 5 | 21.1 | 9.7 |
| 72 | 22 | 16 | 315 | 297 | 4 | 5.4 | 6.9 |
| 73 | 21 | 16 | 311 | 297 | 5 | 24.6 | 9.5 |
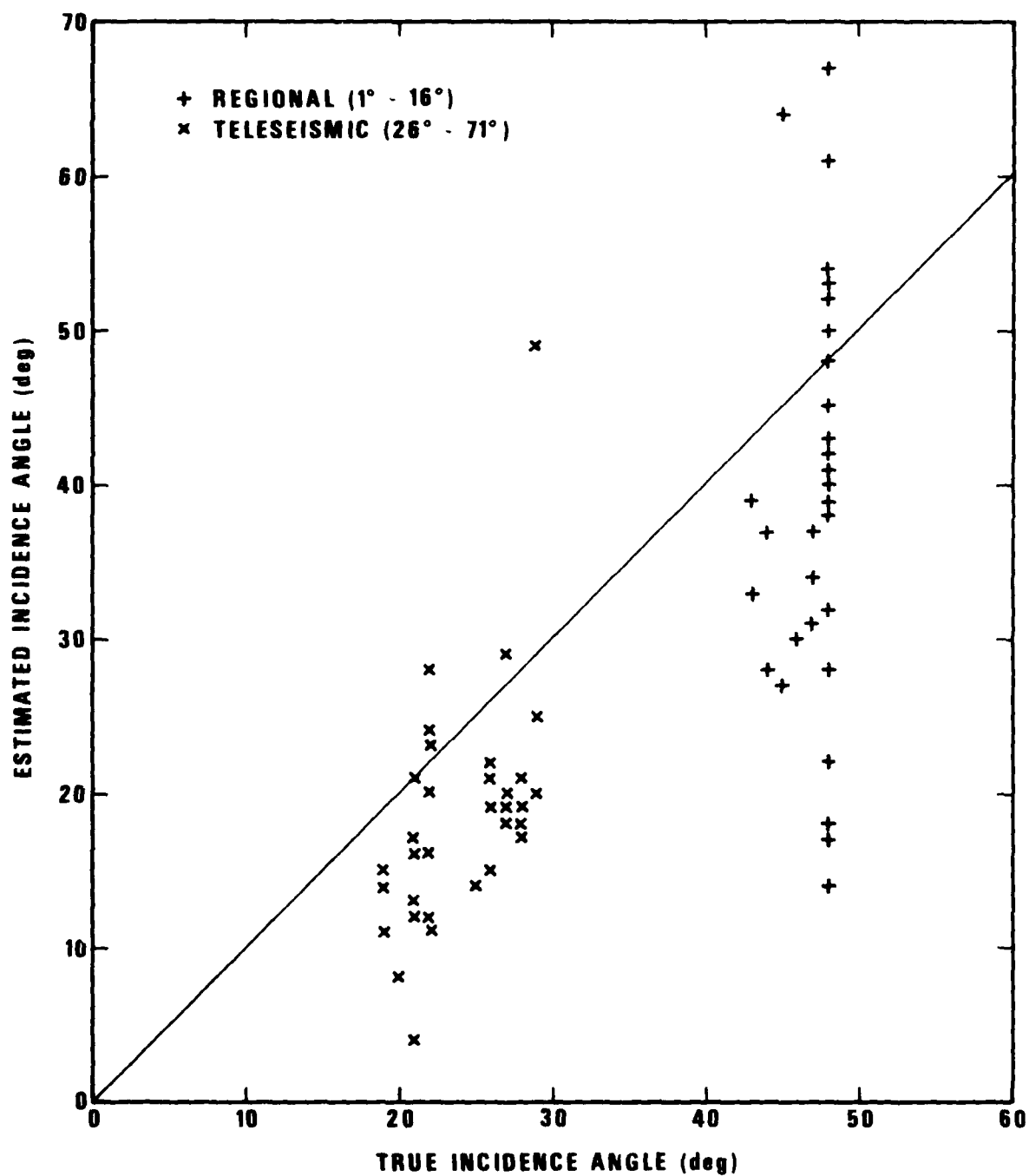
Figure 10. Estimated versus true angles of incidence for Pn and P waves recorded at OB2NV.

separation of the two groups of phases should occur on the vertical axis, but the presence of noise causes some overlap. Ignoring the high value for event #67 at 49°, one could place a decision line at an estimated angle of 30° and be reasonably confident of identifying all teleseismic signals; however, some regionals would be misidentified as teleseismic. The F statistics of the seven Pn cases with estimated angle less than 30° are 33.4, 4.6, 7.1, 1.7, 2.5, 3.6, and 0.3; therefore a small F value is usually associated with these signals.

Table VIII presents the results for RKON Pn and P phases as listed in Table IV. Considering again only those signals with F > 6.0, the mean absolute error in the back azimuth estimate is 10°. A plot of estimated versus true incidence angles, taken from this table, is shown in Figure 11. The true angles of incidence were again computed for the Herrin-68 velocity model. The overlap between regional ( $\Delta < 16°$ ) and teleseimic ( $\Delta > 16°$ ) estimates is nearly complete, and discrimination on the basis of estimated incidence angle appears to be impossible. Points for which $F \geq 6.0$ are circled in Figure 11, and even for these good signals, the separation is unsatisfactory. It should be noted, however, that many of the RKON signals lie in the range $20° < \Delta < 30°$, which is strictly neither regional nor teleseismic.

Considerable emphasis has been placed so far on the F-statistic defined in equation (1), a measure of the goodness-of-fit of the P-wave particle-motion model to the recorded data in the first 1.6 seconds after onset, and an arbitrary value of 6.0 has been mentioned as a lower bound for accepting the processor results. The F value should reflect the S/N ratio, and the dependence of F on this ratio is illustrated in Figures 12 through 15. Recall that S/N is computed in the frequency domain using only those frequencies in a contiguous band where signal exceeded noise. The correlation of F with S/N is seen to be only weak in these figures. Even S/N > 5, which would usually be regarded as indicating a good signal, does not insure a high F value of greater than 6.0. While S/N measures signal strength in relation to a sample of noise just prior to the signal sample, the F statistic represents the relative signal and noise strengths within the signal window only and is

## TABLE VIII

P-wave particle motion processor results for RKON Pn and P phases

| Event # | Incidence Angle true | est. | Back Azimuth true | est. | # of Spectral Points Used | F Statistic | S/N Ratio |
|---|---|---|---|---|---|---|---|
| 1 | 31 | 6 | 227 | 322 | 5 | 4.6 | 1.6 |
| 2 | 31 | 40 | 228 | 244 | 5 | 18.8 | 2.9 |
| 3 | 31 | 36 | 228 | 232 | 4 | 9.3 | 3.1 |
| 4 | 36 | 37 | 239 | 233 | 5 | 40.7 | 28.3 |
| 5 | 31 | 10 | 16 | 62 | 2 | 3.9 | 4.9 |
| 6 | 48 | 45 | 170 | 154 | 3 | 5.1 | 11.0 |
| 7 | 32 | 29 | 265 | 354 | 5 | 1.7 | 3.4 |
| 8 | 48 | 43 | 255 | 243 | 4 | 6.4 | 4.9 |
| 9 | 29 | 16 | 214 | 312 | 3 | 3.1 | 2.0 |
| 10 | 48 | 42 | 241 | 235 | 3 | 10.7 | 4.7 |
| 13 | 48 | 29 | 236 | 223 | 5 | 4.1 | 2.3 |
| 15 | 30 | 43 | 352 | 340 | 4 | 12.1 | 4.9 |
| 16 | 48 | 32 | 170 | 141 | 4 | 1.8 | 2.9 |
| 17 | 48 | 39 | 249 | 204 | 3 | 2.4 | 1.2 |
| 18 | 48 | 33 | 92 | 95 | 3 | 1.3 | 1.8 |
| 19 | 48 | 53 | 249 | 223 | 4 | 1.2 | 3.0 |
| 20 | 48 | 49 | 249 | 247 | 3 | 8.0 | 2.2 |
| 21 | 48 | 32 | 171 | 178 | 3 | 3.1 | 11.8 |
| 22 | 48 | 26 | 168 | 181 | 2 | 5.1 | 6.3 |
| 23 | 48 | 35 | 249 | 213 | 2 | 2.0 | 1.5 |
| 24 | 48 | 29 | 249 | 208 | 2 | 3.7 | 1.5 |
| 25 | 32 | 37 | 290 | 285 | 5 | 8.7 | 5.2 |
| 26 | 29 | 33 | 354 | 336 | 4 | 9.7 | 7.5 |
| 27 | 36 | 36 | 237 | 241 | 5 | 62.7 | 74.2 |
| 29 | 48 | 45 | 167 | 161 | 5 | 3.1 | 11.0 |
| 30 | 30 | 8 | 323 | 294 | 3 | 1.7 | 1.6 |
| 31 | 48 | 40 | 235 | 233 | 5 | 16.0 | 8.8 |
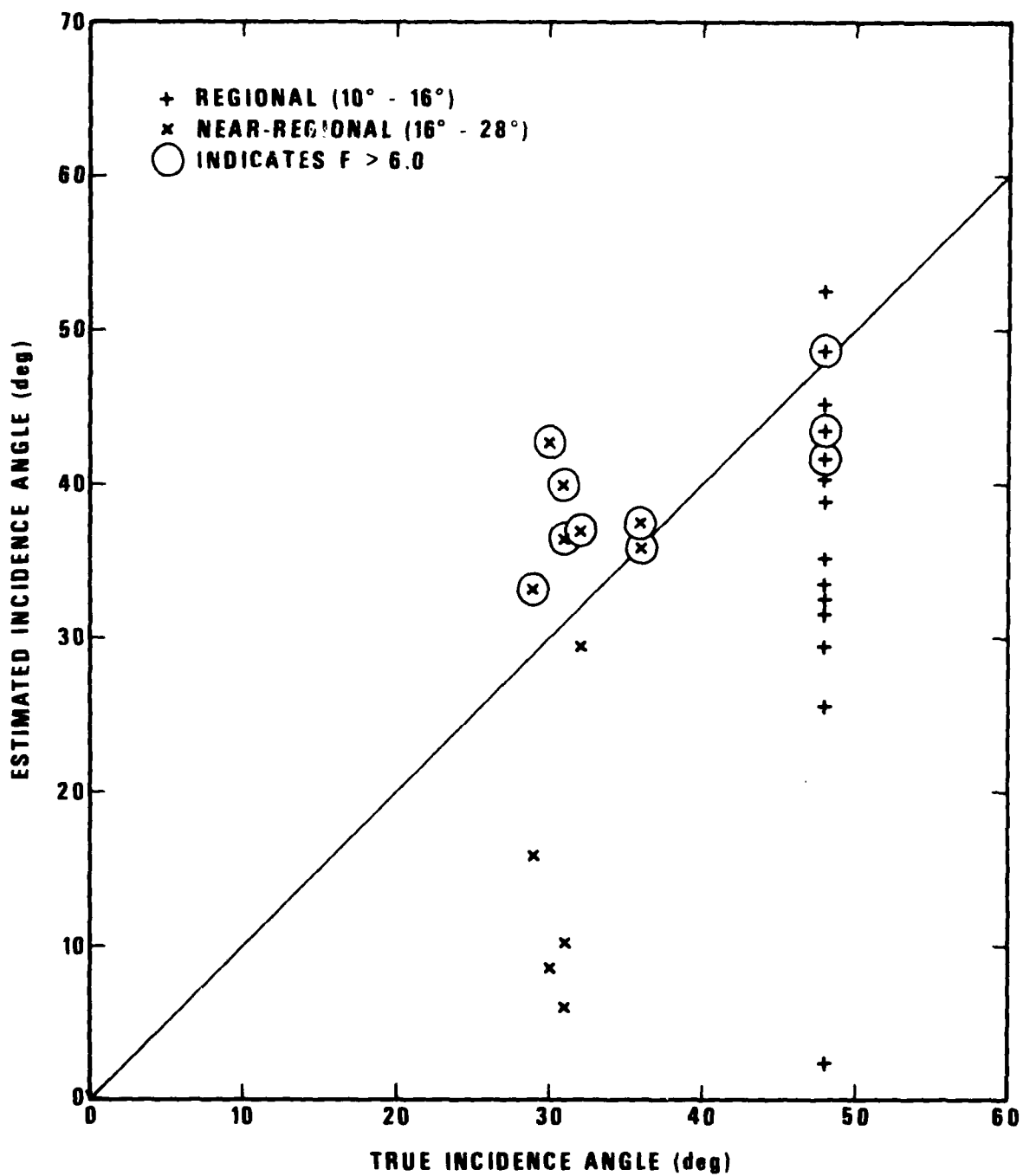
Figure 11. Estimated versus true angles of incidence for Pn and P waves recorded at RKON.
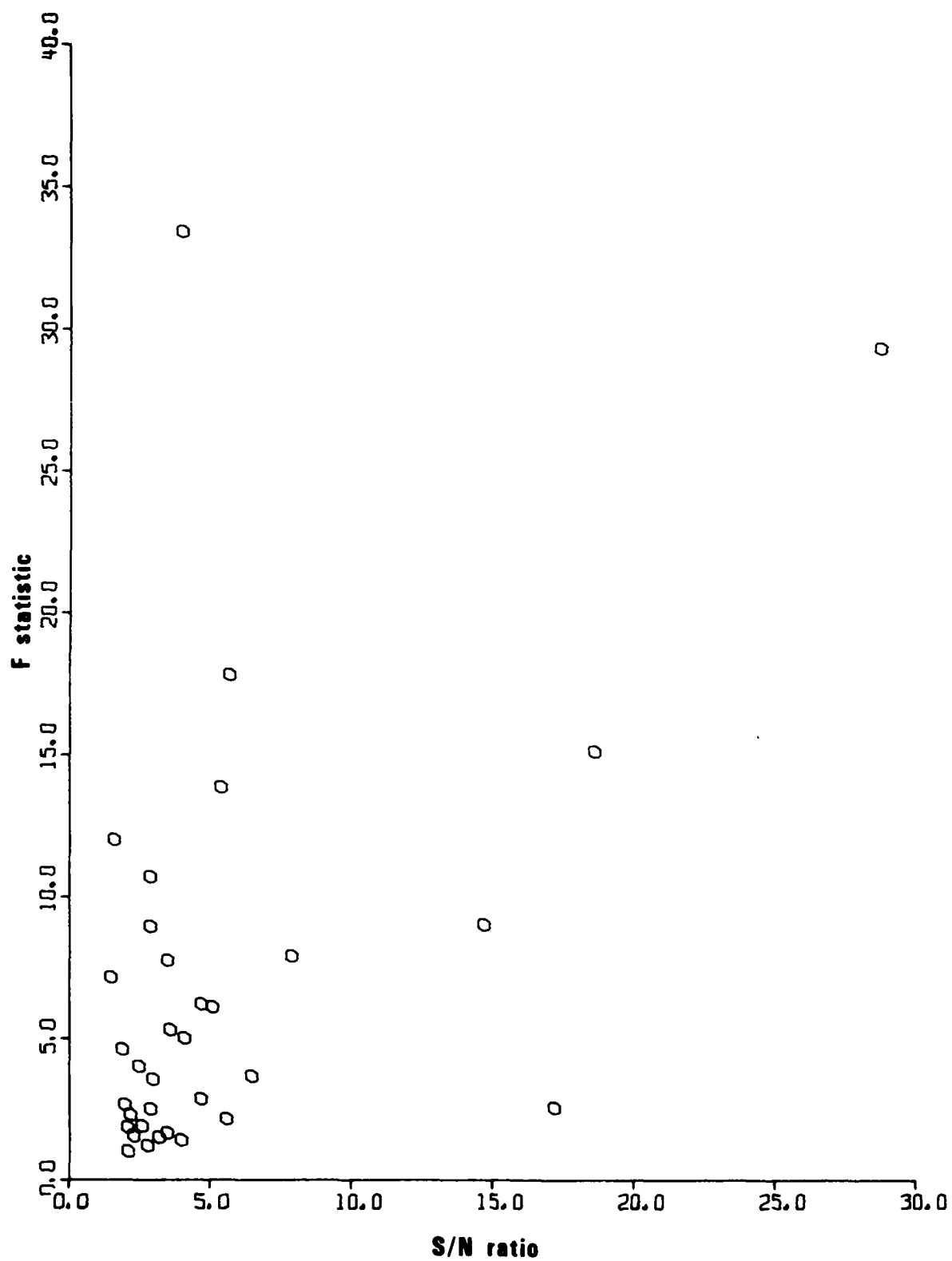
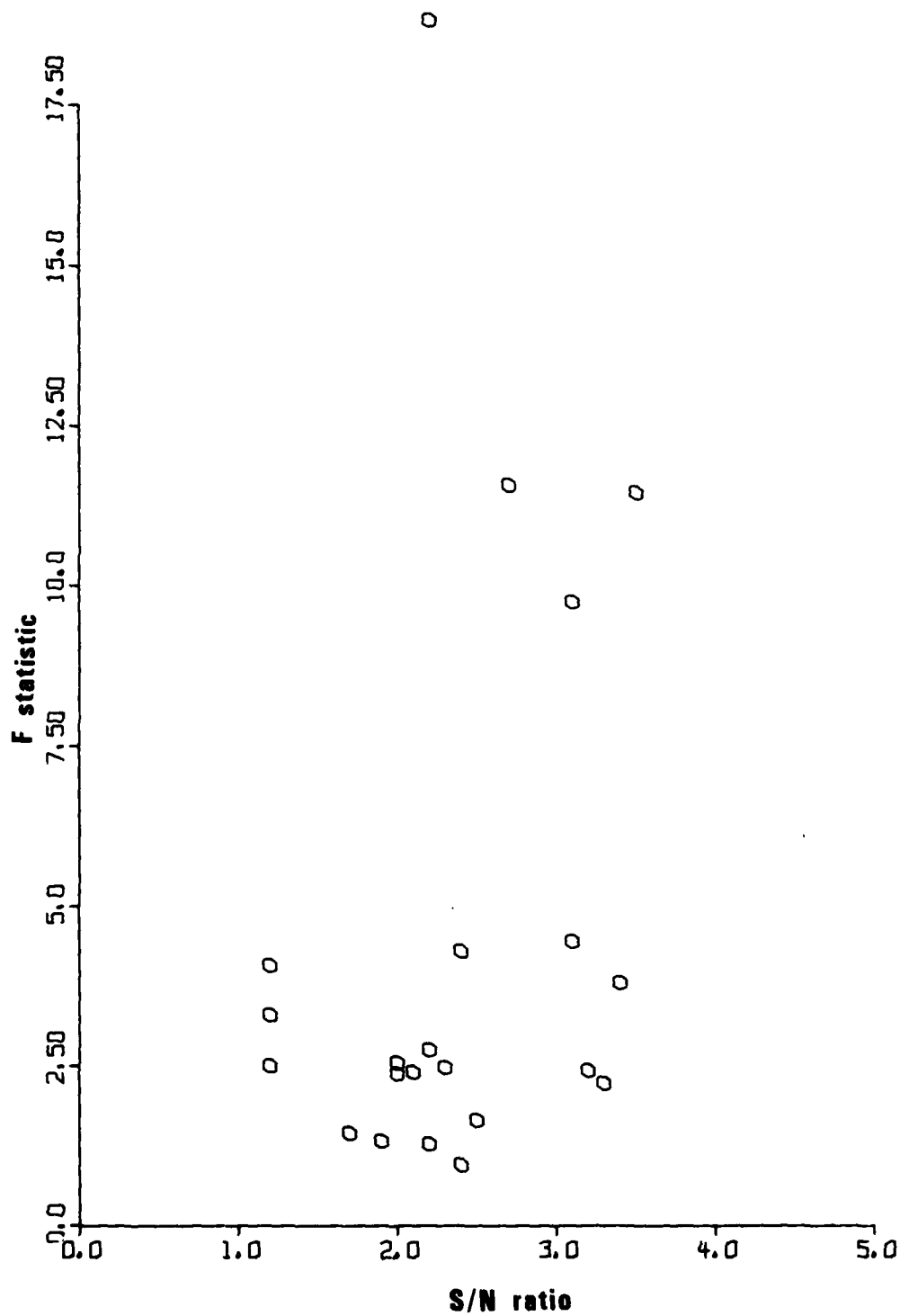Figure 12. F-statistic versus S/N ratio for OB2NV Pn waves.

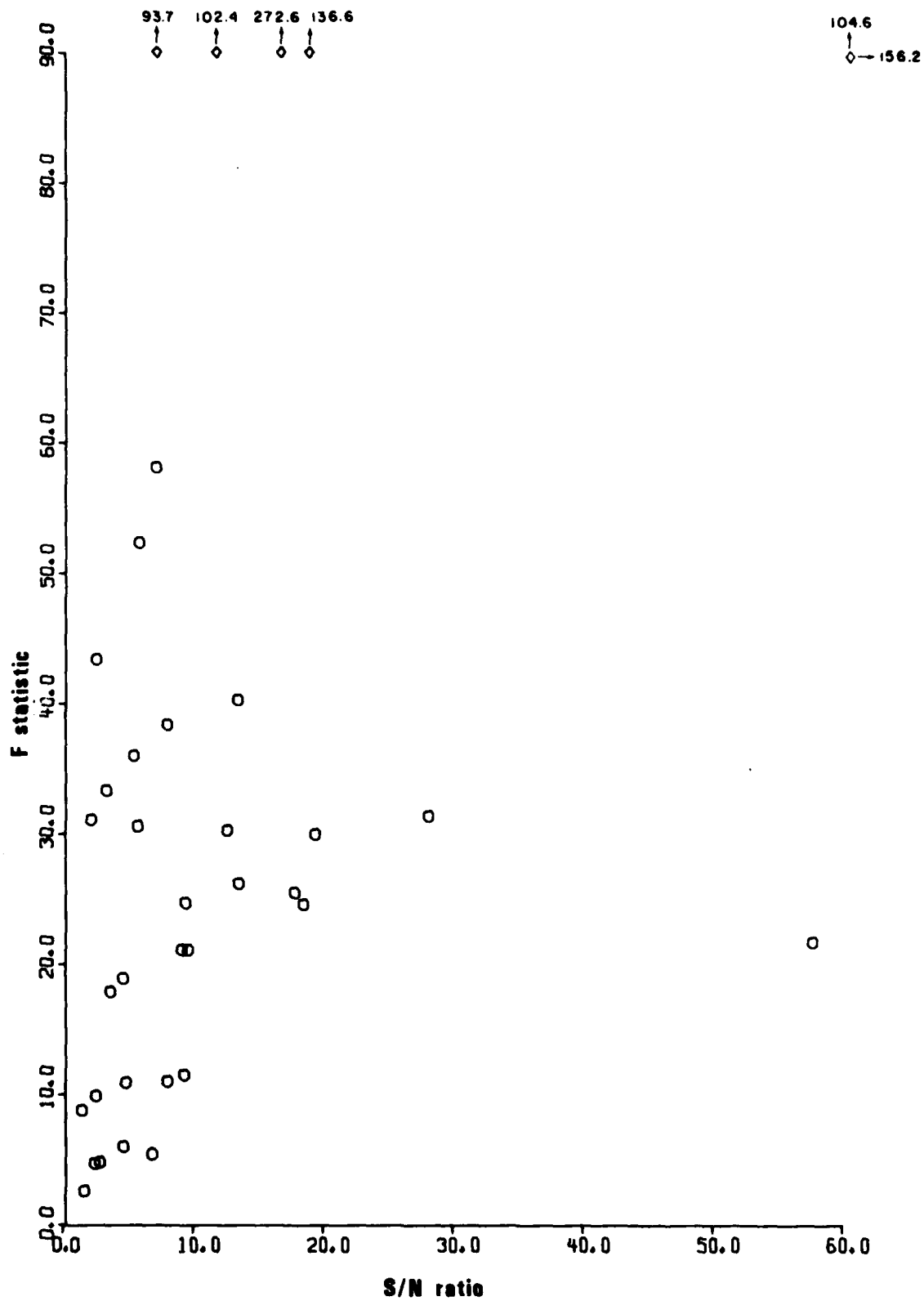Figure 13.   F-statistic versus S/N ratio for OB2NV Pg waves.

Figure 14. F-statistic versus S/N ratio for OB2NV teleseismic P waves.
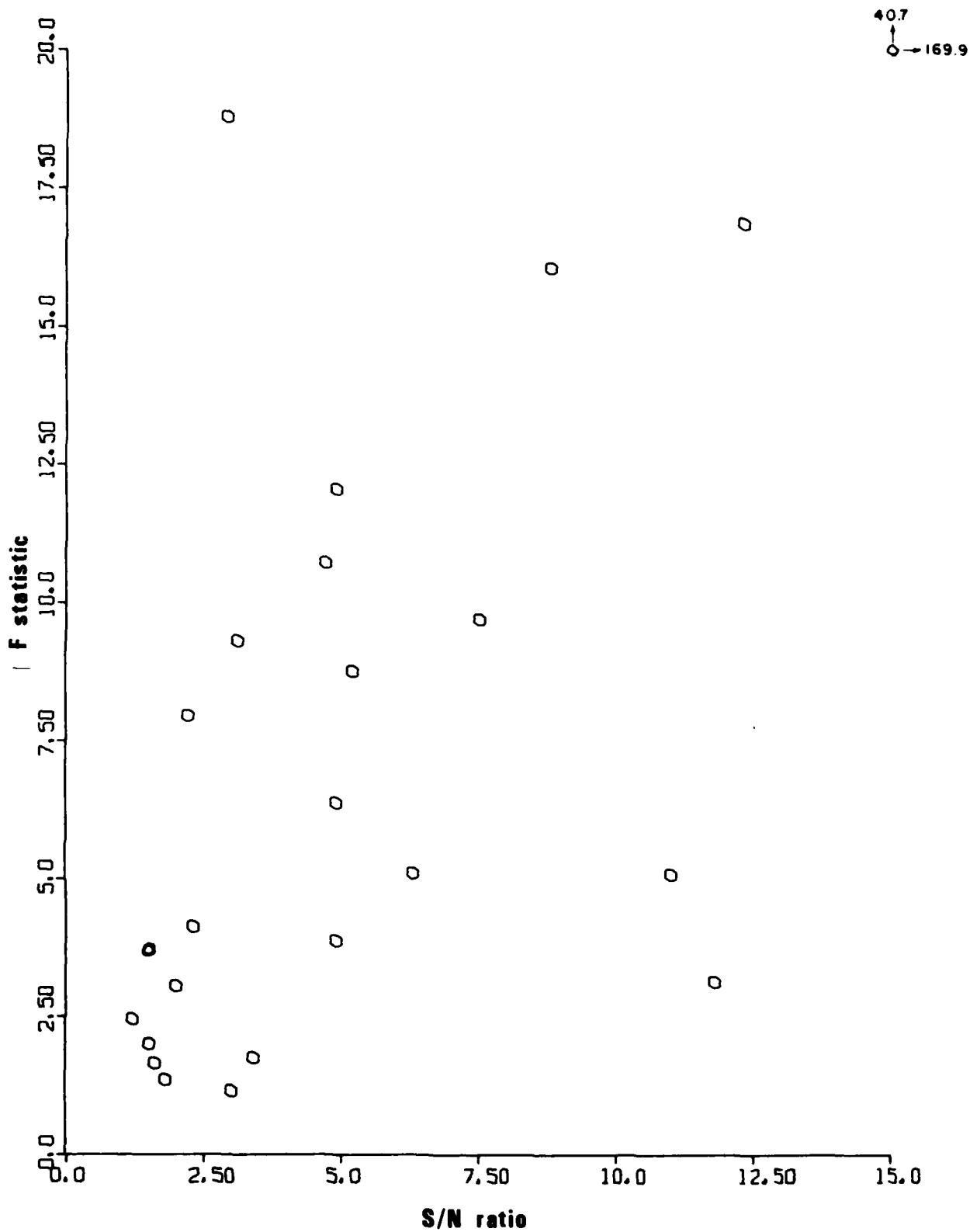
Figure 15.  F-statistic versus S/N ratio for RKON Pn and P waves.

therefore assumed to be the more appropriate indicator. In Figure 16
through 19, the back azimuth error is illustrated versus the F statistic
and versus the S/N ratios. In general, the errors decrease with
increasing F, and F values of $\geq 10.0$ usually insure an azimuth error of
less than 10°. It is not clear from these plots whether the F-statistic
or S/N ratio is a better indicator of the probable error in the
estimated azimuth.

## Earthquake Lg Phases Recorded at OB2NV and RKON

The surface-wave particle-motion processor as derived in Smart
(1981) was applied to Lg waves from the events in Tables II and IV,
except for a few events at OB2NV because the Lg window was not retrieved
when $\Delta > 10°$. For this processing, a window of 12.8 sec following the
Lg maximum vertical motion was selected. In addition to back azimuth,
the ellipticity of the Rayleigh component and a Love/Rayleigh energy
ratio were computed using a set frequency band of 0.31 to 3.83 Hz. A
set band was used for the Lg, rather than the variable band used for the
P, because S/N ratio for the emergent Lg is not computable in the sense
that it is for the P wave.

The results are given in Tables IX and X for RKON and OB2NV
respectively. In general, the back azimuth estimates are quite close to
the true ones. Taking only those cases with $F > 6.0$ at RKON and ignor-
ing events 22 and 27, there is a less than 4° mean error in back azimuth
estimation. Results at OB2NV are similar, with $F > 6.0$ insuring an
estimate close to the true back azimuth except for events 20 and 26. A
longer time window than 12.8 sec will, with proper precautions, stabi-
lize the results (Smart, 1977) and is reported on in a later section.
It was found, however, that shorter windows of 3.2 and 6.4 sec defi-
nitely gave poorer results.

Note that in Tables IX and X, the F statistics for OB2NV Lg phases
are less than those for RKON Lg phases generally. This occurs in spite
of the fact that the Lg phases processed from OB2NV have equal or better
S/N ratios on the average and therefore is most likely an indicator of

-56-

Figure 16. Azimuth error versus F-statistic and S/N ratio for OB2NV Pn wave processing.

-57-
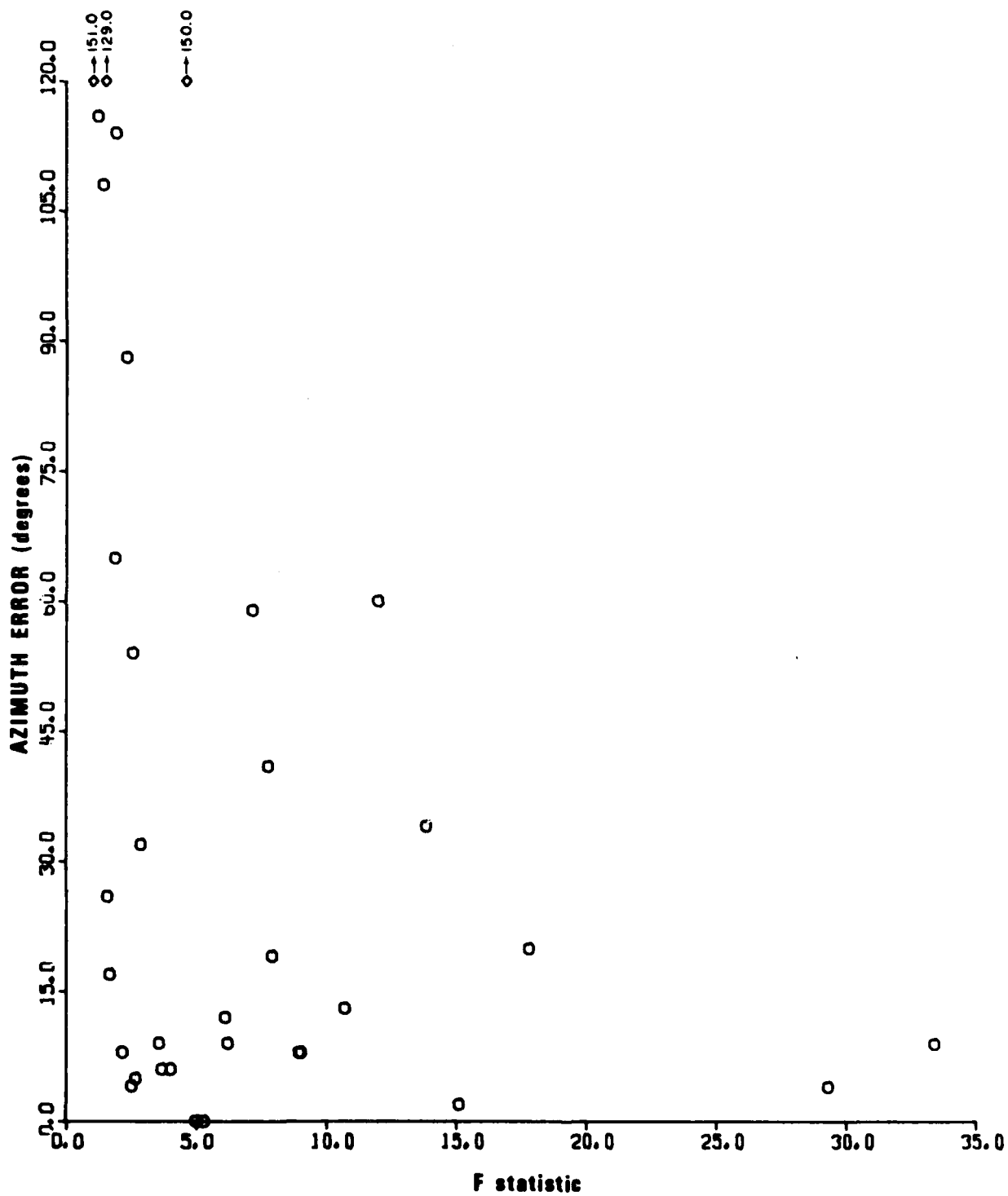
Figure 16 (cont.).   Azimuth error versus F-statistic and S/N ratio for OB2NV
Pn wave processing.

-58-
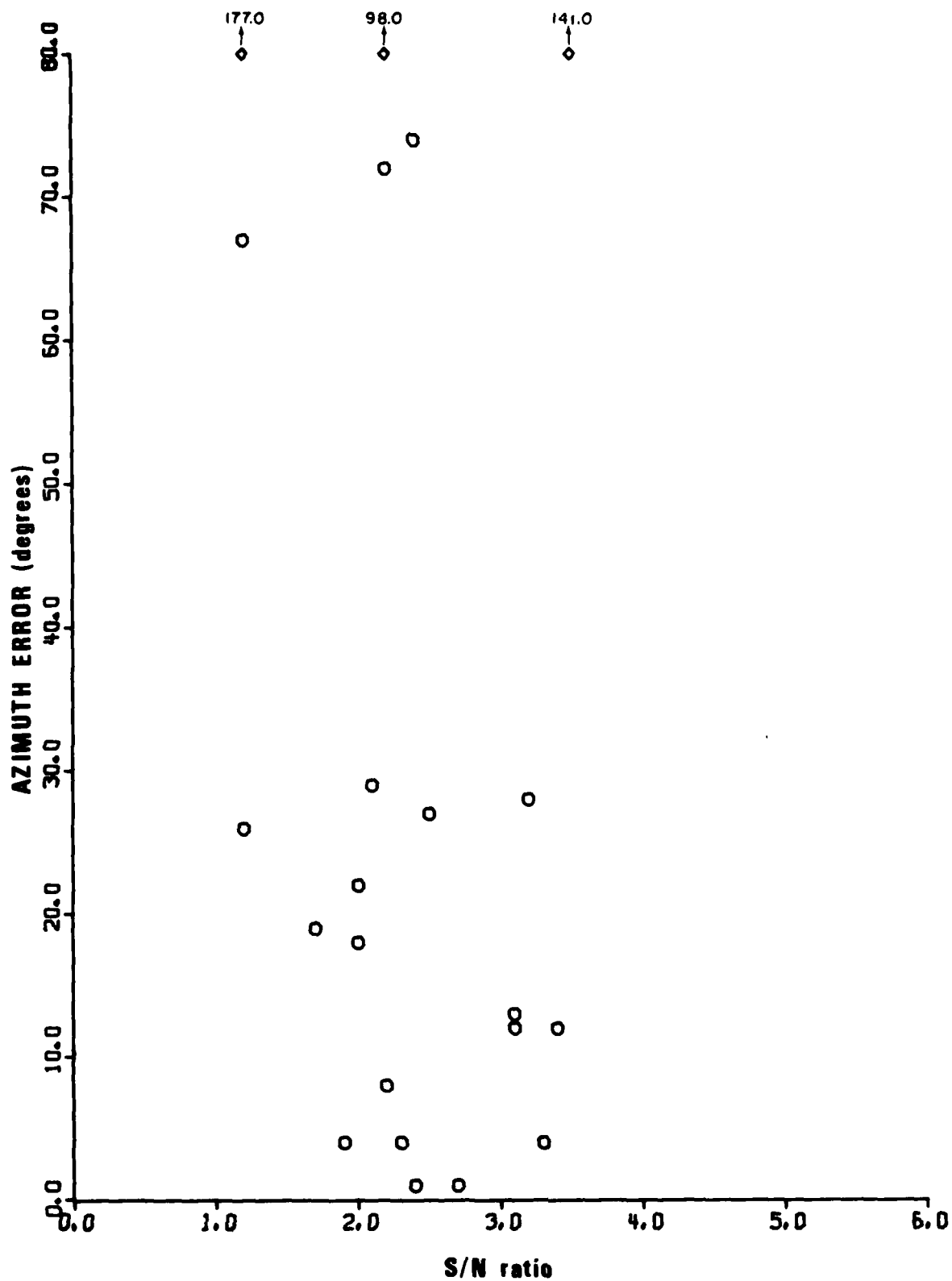
Figure 17. Azimuth error versus F-statistic and S/N ratio for OB2NV Pg wave processing.
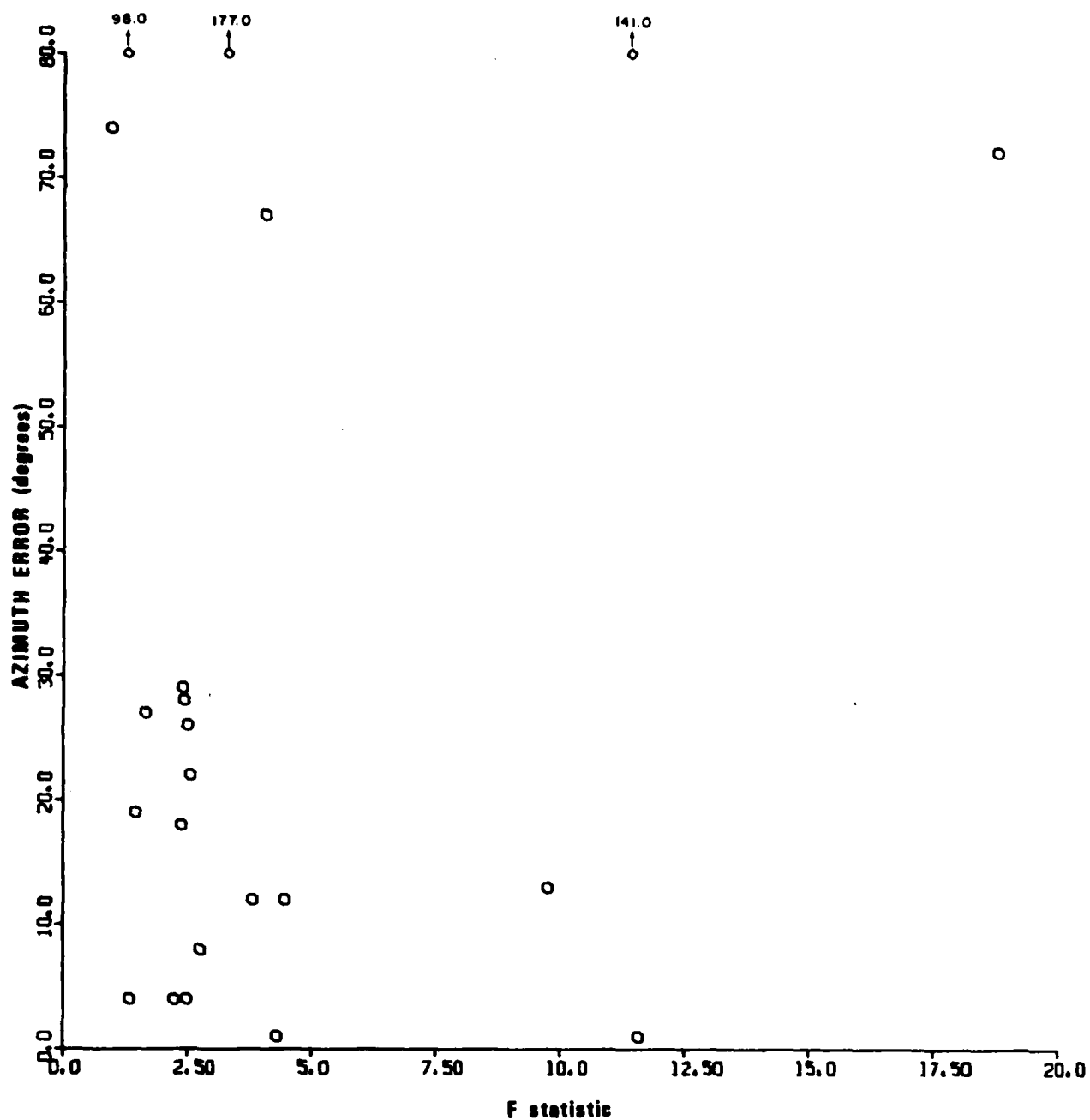
Figure 17 (cont.). Azimuth error versus F-statistic and S/N ratio for OB2NV
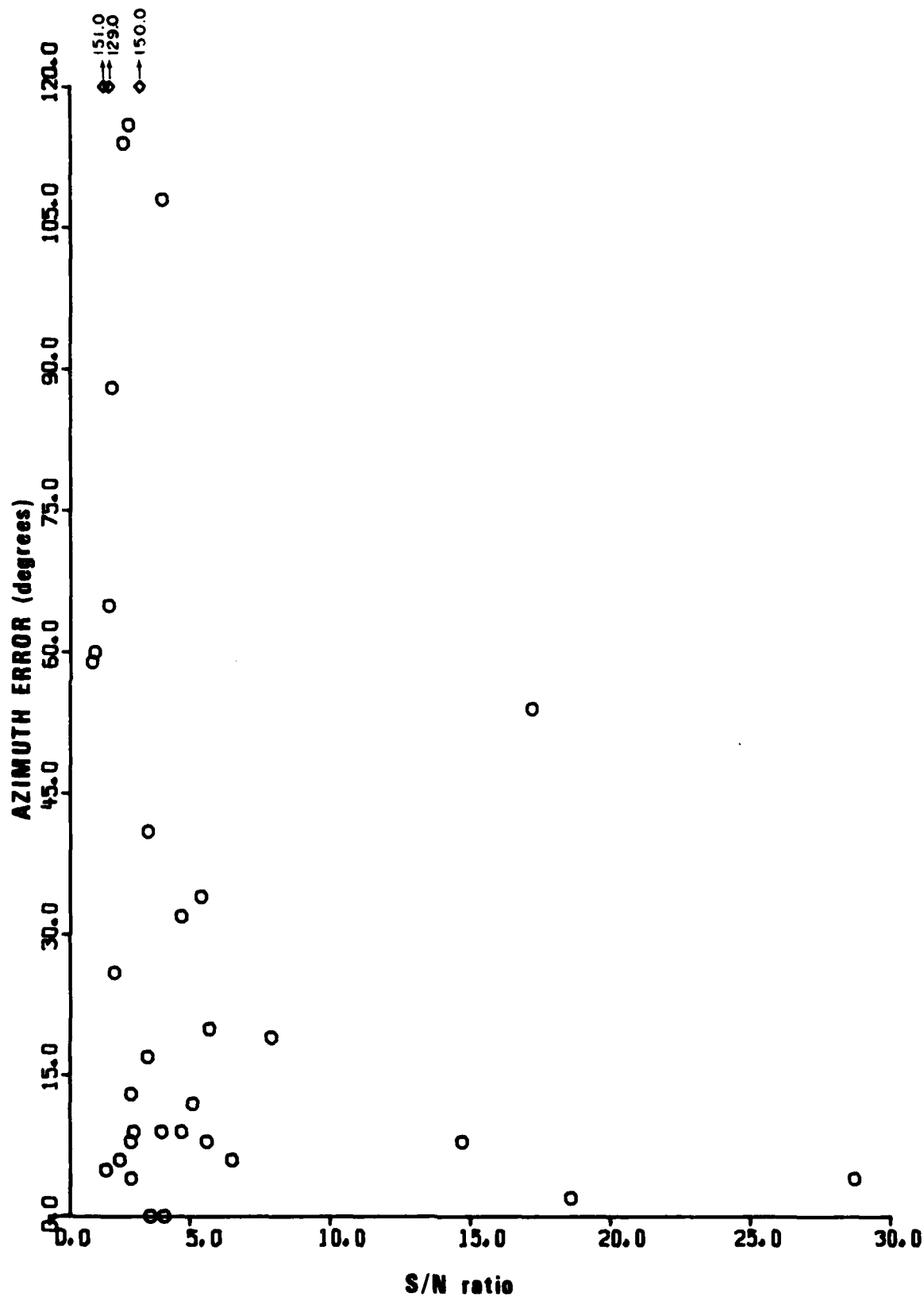Pg wave processing.
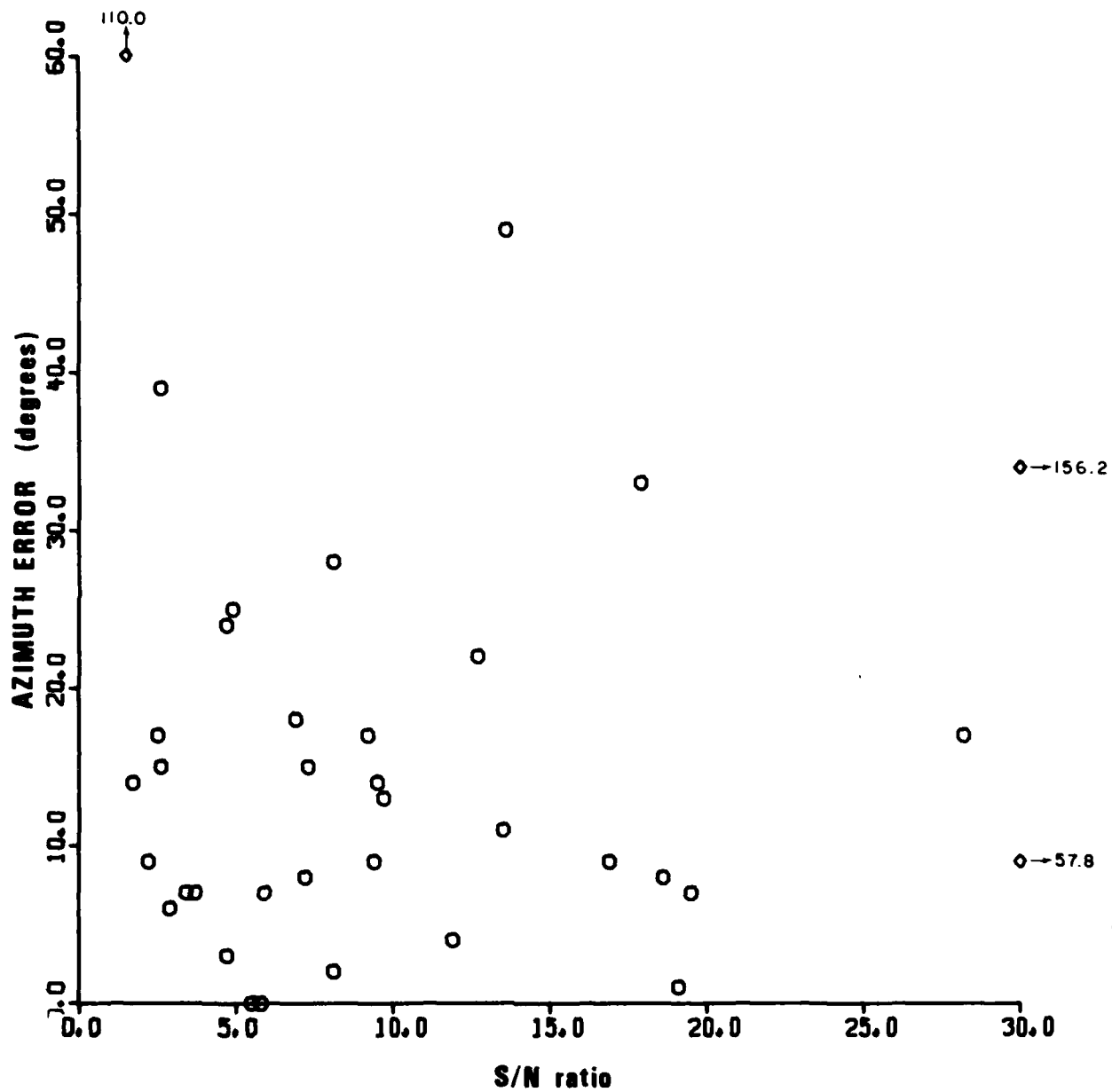
Figure 18.  Azimuth error versus F-statistic and S/N ratio for OB2NV P wave
processing.
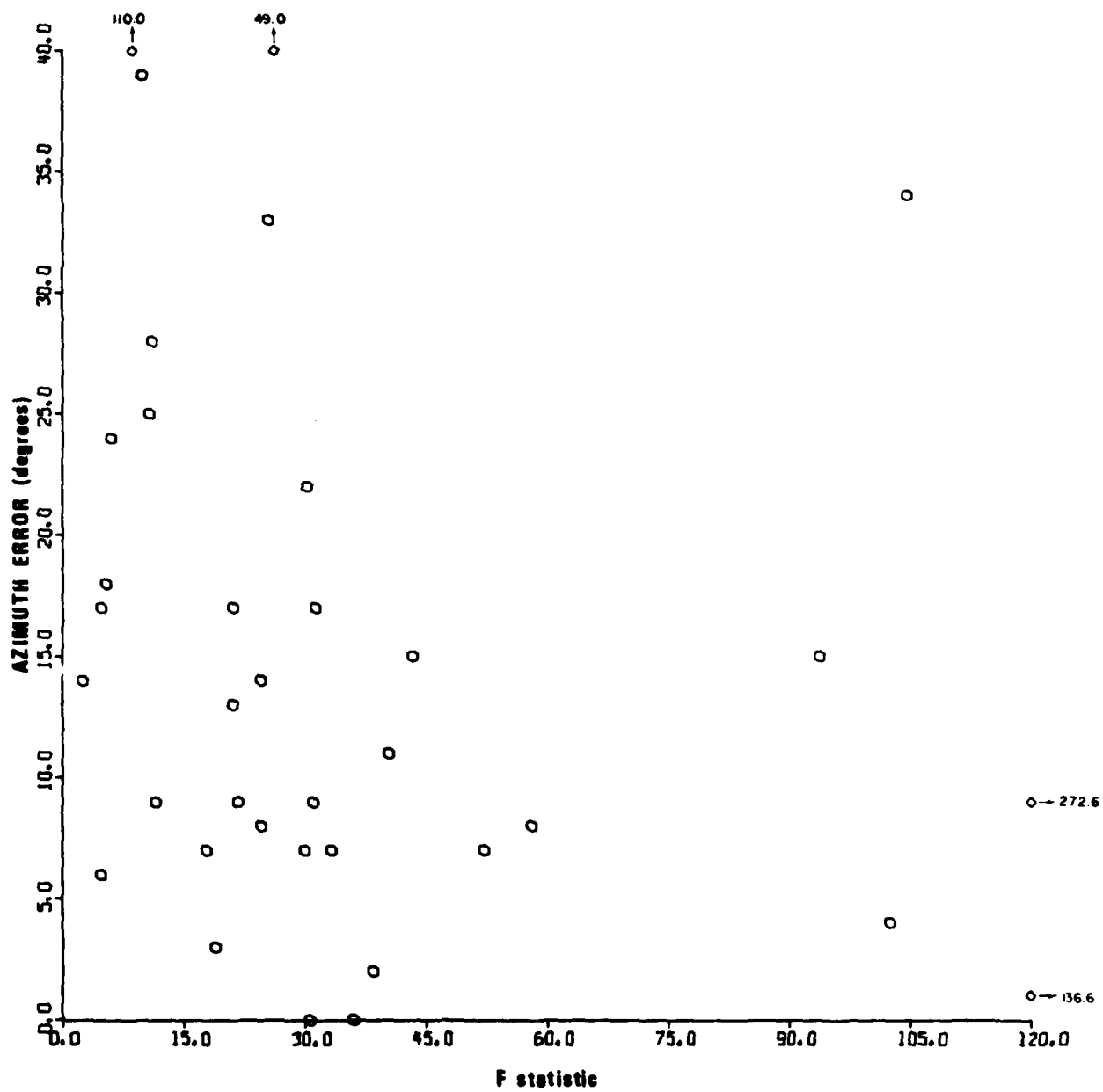
Figure 18. (cont.). Azimuth error versus F-statistic and S/N ratio for OB2NV
P wave processing.

Figure 19. Azimuth error versus F-statistic and S/N ratio for RKON Pn and P wave processing.
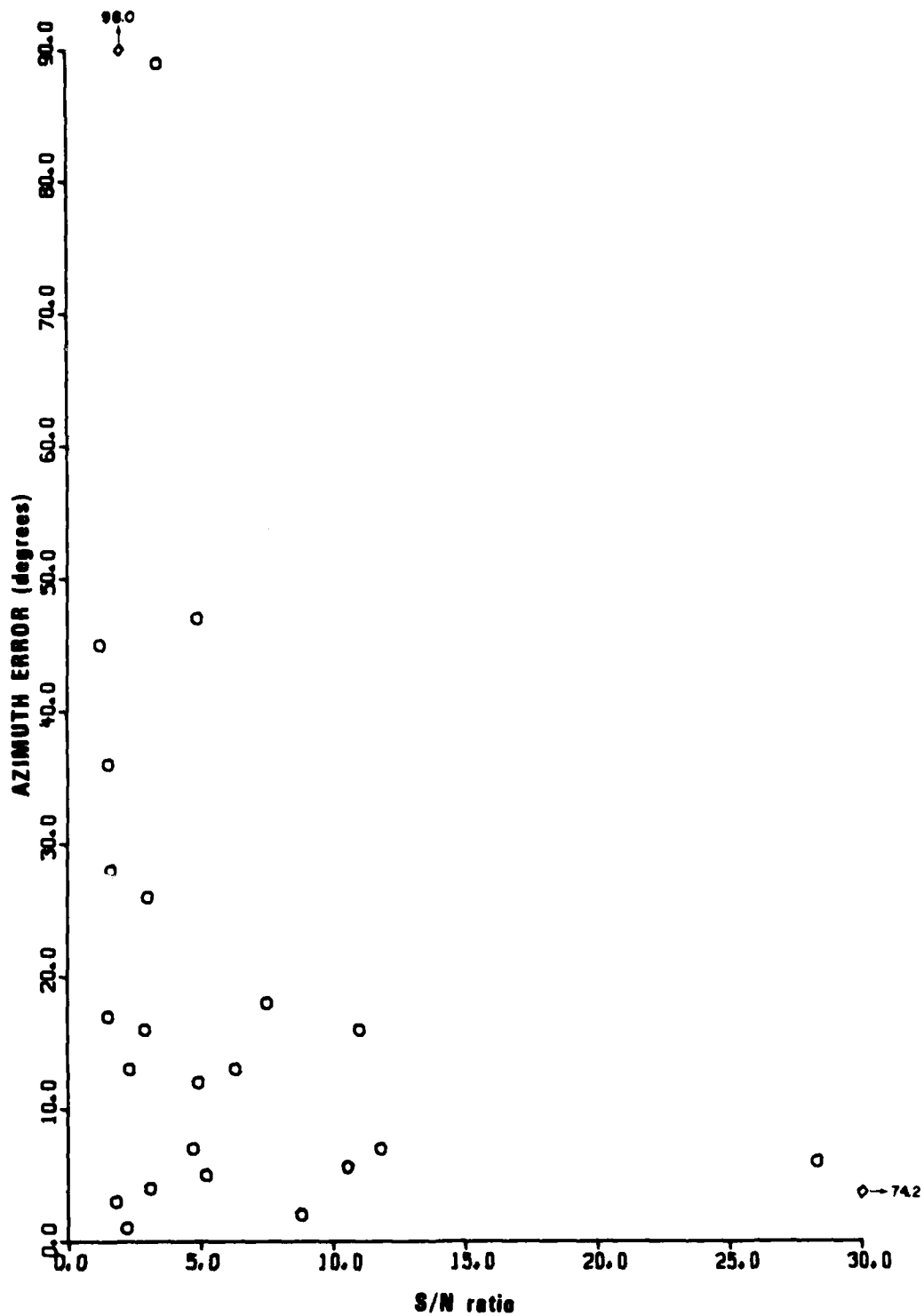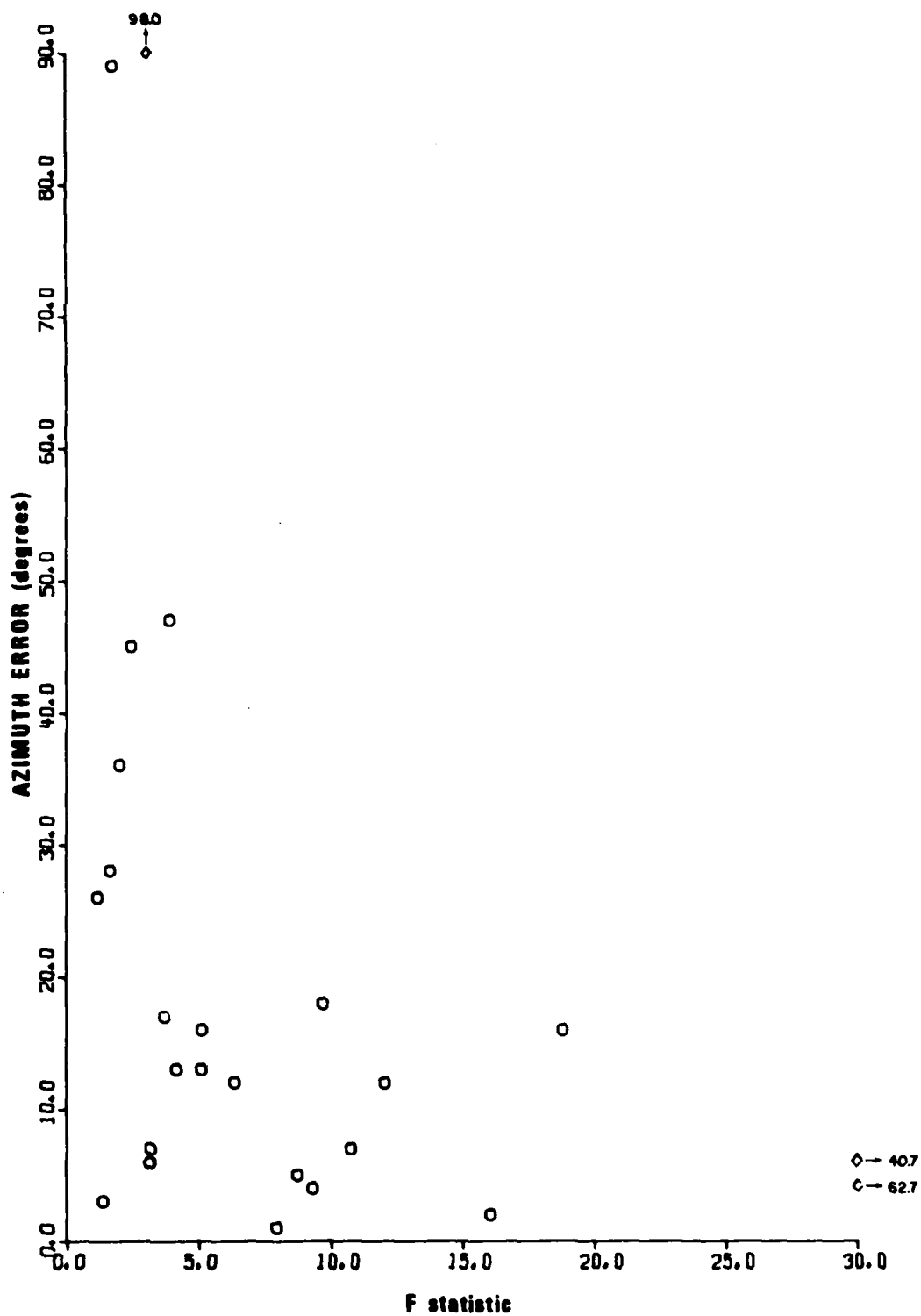
Figure 19 (cont.).  Azimuth error versus F-statistic and S/N ratio for RKON
Pn and P wave processing.

## TABLE IX

Surface-wave particle motion processor results for RKON Lg phases

| Event # | Back Azimuth true | Back Azimuth est. | Ellipticity | LO/LR Ratio | F Statistic |
|---|---|---|---|---|---|
| 1 | 227 | 225 | .64 | 1.53 | 6.9 |
| 2 | 228 | 162 | .06 | .99 | 3.6 |
| 3 | 228 | 221 | .82 | 2.80 | 8.2 |
| 5 | 16 | 18 | .52 | 1.65 | 14.3 |
| 6 | 170 | 169 | .51 | 2.03 | 22.2 |
| 7 | 265 | 130 | .48 | .89 | 4.0 |
| 8 | 255 | 263 | .24 | 1.66 | 8.2 |
| 9 | 214 | 220 | .52 | 1.30 | 21.4 |
| 10 | 241 | 243 | .82 | 2.27 | 9.3 |
| 11 | 281 | 281 | .20 | 1.52 | 5.2 |
| 12 | 273 | 39 | .20 | .85 | 3.9 |
| 13 | 236 | 241 | .39 | 2.00 | 10.3 |
| 14 | 142 | 131 | .45 | .97 | 4.0 |
| 15 | 352 | 355 | .58 | 2.05 | 31.3 |
| 16 | 170 | 161 | .33 | 1.24 | 8.9 |
| 17 | 249 | 82* | .22 | 1.32 | 5.5 |
| 18 | 92 | 93 | .81 | 2.62 | 31.7 |
| 19 | 249 | 240 | .26 | 1.16 | 4.8 |
| 20 | 249 | 255 | .25 | 1.50 | 11.5 |
| 21 | 171 | 171 | .59 | 1.06 | 4.4 |
| 22 | 168 | 120 | .93 | 1.46 | 6.2 |
| 23 | 249 | 245 | .24 | 1.12 | 5.4 |
| 24 | 249 | 249 | .32 | 1.64 | 13.8 |
| 25 | 290 | 295 | .14 | 1.46 | 16.7 |
| 26 | 354 | 356 | .52 | 1.89 | 55.3 |
| 27 | 237 | 182 | .78 | 1.03 | 7.5 |
| 28 | 276 | 110* | .53 | 1.18 | 5.8 |
| 29 | 167 | 167 | .55 | 1.88 | 16.1 |
| 30 | ₃23 | 80 | 1.09 | 1.26 | 4.3 |
| 31 | 235 | 235 | .72 | 1.54 | 12.1 |

*   180° shift in estimate needed to get back azimuth

## TABLE X

Surface-wave particle motion processor results for OB2NV Lg phases

| Event # | Back Azimuth true | est. | Ellipticity | LQ/LR Ratio | F Statistic |
|---|---|---|---|---|---|
| 8 | 205 | 224 | .12 | .76 | 3.4 |
| 9 | 195 | 247 | 1.49 | 1.20 | 3.6 |
| 10 | 192 | 192 | 1.17 | 1.73 | 5.0 |
| 34 | 216 | 204 | .44 | 1.34 | 3.3 |
| 11 | 136 | 68 | 1.42 | 1.19 | 3.8 |
| 12 | 267 | 287 | .42 | .95 | 5.9 |
| 13 | 189 | 221 | 1.29 | 1.97 | 4.6 |
| 14 | 182 | 191 | 1.84 | 2.69 | 4.2 |
| 15 | 281 | 286 | .32 | 1.20 | 5.3 |
| 16 | 188 | 200 | 1.21 | 2.01 | 6.1 |
| 17 | 215 | 190 | 5.03 | 6.71 | 3.2 |
| 35 | 209 | 233 | .27 | 1.16 | 4.8 |
| 18 | 204 | 321 | .56 | 1.04 | 3.2 |
| 19 | 187 | 244 | 1.73 | 1.79 | 4.9 |
| 20 | 267 | 293 | .65 | 1.07 | 6.7 |
| 21 | 267 | 91* | .04 | 1.04 | 6.1 |
| 22 | 7 | 359 | .11 | 1.71 | 7.1 |
| 23 | 198 | 186 | 1.01 | 1.70 | 3.8 |
| 24 | 181 | 196 | .79 | 1.55 | 3.3 |
| 25 | 217 | 219 | .44 | 1.20 | 4.2 |
| 26 | 273 | 227 | .87 | 1.25 | 9.2 |
| 36 | 267 | 268 | .51 | 1.41 | 8.9 |
| 27 | 251 | 254 | .42 | 1.32 | 4.4 |
| 37 | 140 | 78 | 1.99 | 2.88 | 4.0 |
| 28 | 324 | 324 | 1.17 | 2.50 | 10.9 |
| 29 | 266 | 271 | 1.60 | 1.35 | 10.5 |
| 30 | 199 | 188 | .76 | 1.13 | 8.1 |
| 31 | 163 | 270 | .19 | .87 | 3.7 |

* 180° shift in estimate needed to get back azimuth

more strongly scattered Lg arrivals at OB2NV than at RKON, a result
compatible with knowledge of crus.al structure in the regions
surrounding these stations. Also, there is a disparity in estimated
ellipticity ratios between OB2NV and RKON. On the other hand, the
Love/Rayleigh ratios are nearly the same on the average and are in
agreement with most observations of the horizontal/vertical $L_g$ ratio
which lie in the range of one to two empirically.

The dependence of azimuth-estimate errors on the F-statistic is
shown in Figures 20 and 21 for RKON and OB2NV, respectively. Unlike
results for P waves, a high F-statistic of 10 or greater guarantees a
very accurate estimate of azimuth based on Lg motion.

Figure 20. Azimuth error versus F-statistic for RKON Lg-wave processing.

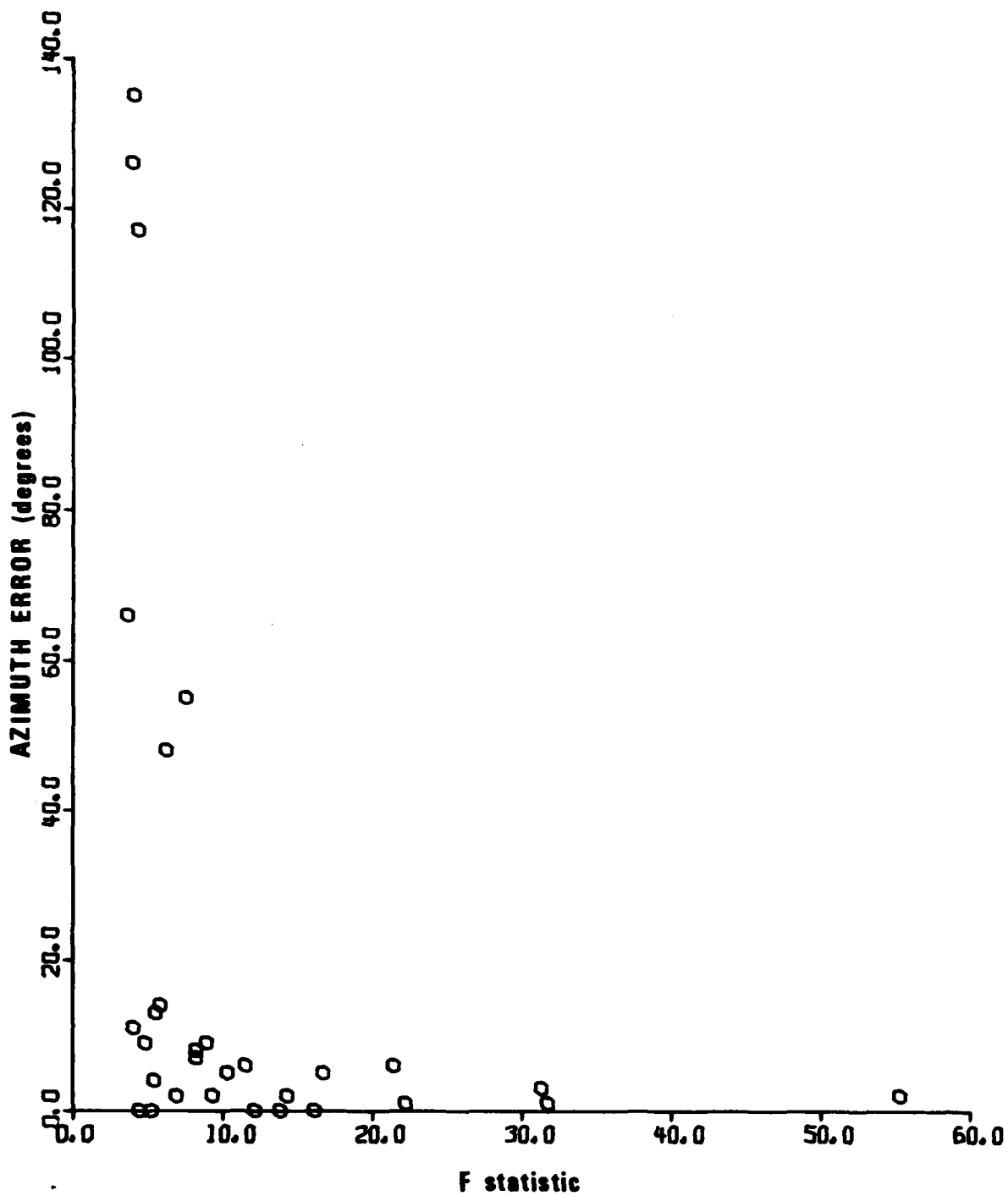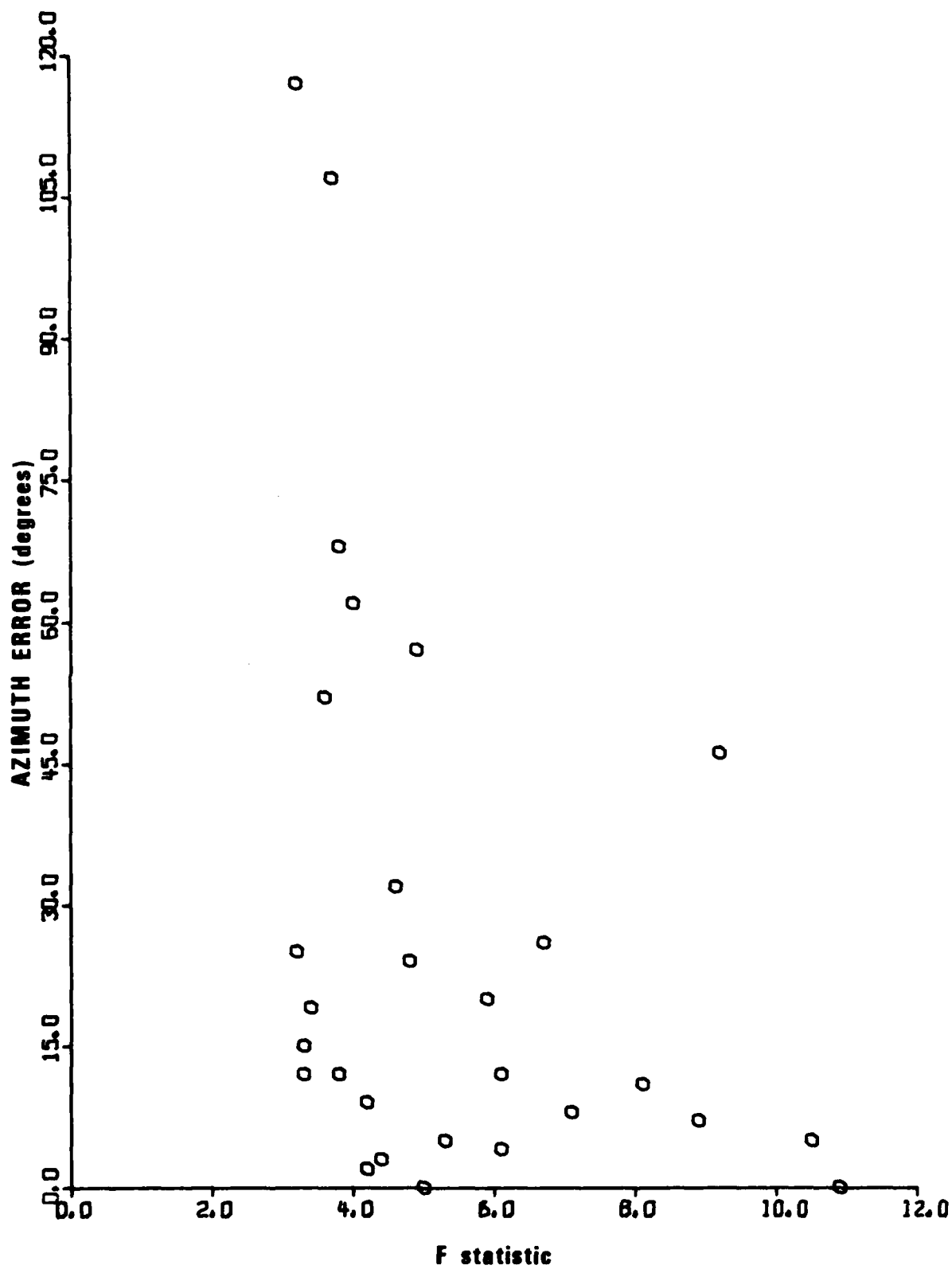Figure 21. Azimuth error versus F-statistic for OB2NV Lg-wave processing.

## Explosion P Waves Recorded at SDCS Stations

Some idea of the bias and variance of the signal parameter estimates can be obtained from a study of events with good S/N ratios from one source region. Therefore a suite of 5 Nevada Test Site explosions was selected during the time of operation of the Special Data Collection System (SDCS) installations at CPO, FNWV, HNME, RKON, and WH2YK. The entire suite of vertical-component signals is shown in Figure 22. Except for the CHIBERTA explosion, the S/N ratios can all be described as excellent. Again using the first 1.6 sec of signal, and only that portion of the frequency band where signal exceeds noise continuously, the processor gave the results listed in Table XI. Because of the relatively low S/N ratios at FNWV and WH2YK for CHIBERTA, those particular entries should be disregarded. Of the five stations, only WH2YK shows a clear bias in estimated azimuth--the signals apparently arriving eastward of the true azimuth. The incidence angle estimates are fairly consistent, with CPO showing a clear bias to an angle less than the true angle based on a Herrin-68 velocity model. This result is due to a low-velocity cap of sedimentary rock on the Cumberland Plateau (Sodbinow and Bollinger, 1978), which refracts the incoming P up at a steeper angle of incidence than the other crustal structures (see Figure 3).

The standard deviation of estimates of back azimuth for signals with good S/N ratios appears to be only a very few degrees in Table XI, on the order of roughly 3°. The standard deviation of incidence angle estimates is somewhat more.

From these results it can be seen that calibration with regard to source region and station may be necessary to more accurately estimate the location of sources of P waves using 3-component particle-motion processing. Back azimuth errors for signals with good S/N ratios are not much worse than those for typical large array estimates; but incidence angle estimates, which map to epicentral distance estimates, are much less reliable than those of large arrays (Shlien and Toksoz, 1973).

-70-

# CHIBERTA

FN-WV    20 DEC 75
29.1°

SPZ
50.10  MU

20:05:59.9

HN-ME    20 DEC 75
36.7°

SPZ
159.27  MU

20:07:07.8

RK-ON    20 DEC 75
21.1°

SPZ
853.67  MU

20:04:45.6

WH2YK    20 DEC 75
26.2°

SPZ
49.83  MU

20:05:39.3
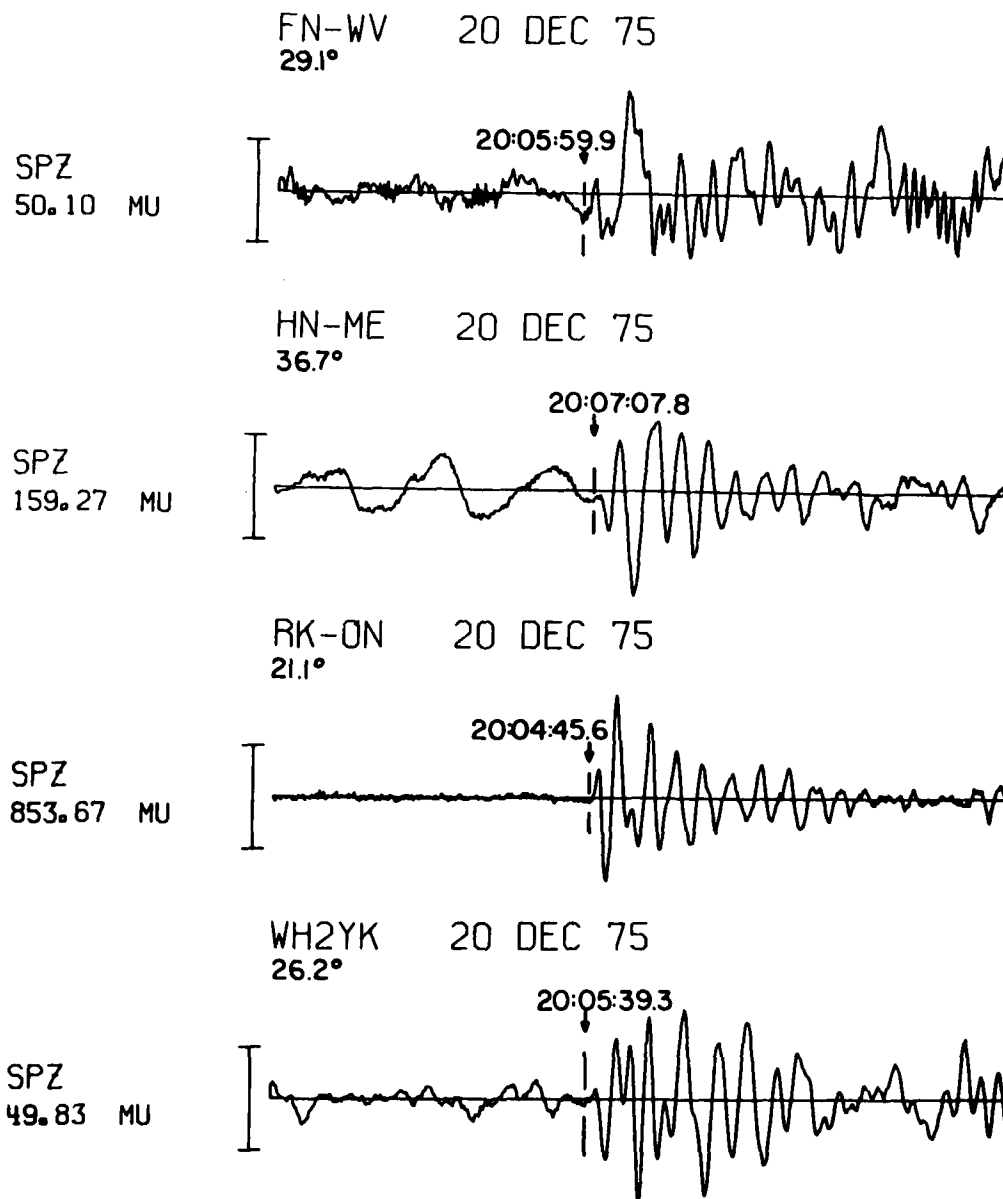
Figure 22.   P-waves at 5 SDCS stations recorded from 5 Nevada Test Site explosions.

# MUENSTERR

CPSO          3 JAN 76
24.9°
                    19:20:24.0

SPZ
1371.94  MU

FN–WV        3 JAN 76
29.1°
                    19:21:01.7

SPZ
167.13  MU
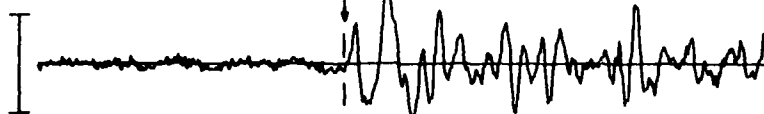
HN–ME        3 JAN 76
36.7°
                    19:22:08.9

SPZ
1106.30  MU

WH2YK        03 JAN 76
26.2°
                    19:20:37.3

SPZ
171.74  MU
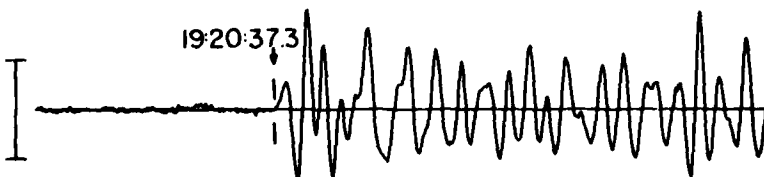
Figure 22 (cont.).    P-waves at 5 SDCS stations recorded from 5 Nevada Test Site
                      explosions.

-72-

# FONTINA

CPSO    12 FEB 76
24.9°

14:50:25.4

SPZ
1610.63 MU

FN-WV    12 FEB 76
29.1°

14:51:03.0

SPZ
242.10   MU

HN-ME    12 FEB 76
36.7°

14:52:09.9

SPZ
721.80 MU

RK-ON    12 FEB 76
21.0°

14:49:46.5

SPZ
1643.64 MU

WH2YK    12 FEB 76
26.2°

14:50:37.4

SPZ
281.00 MU
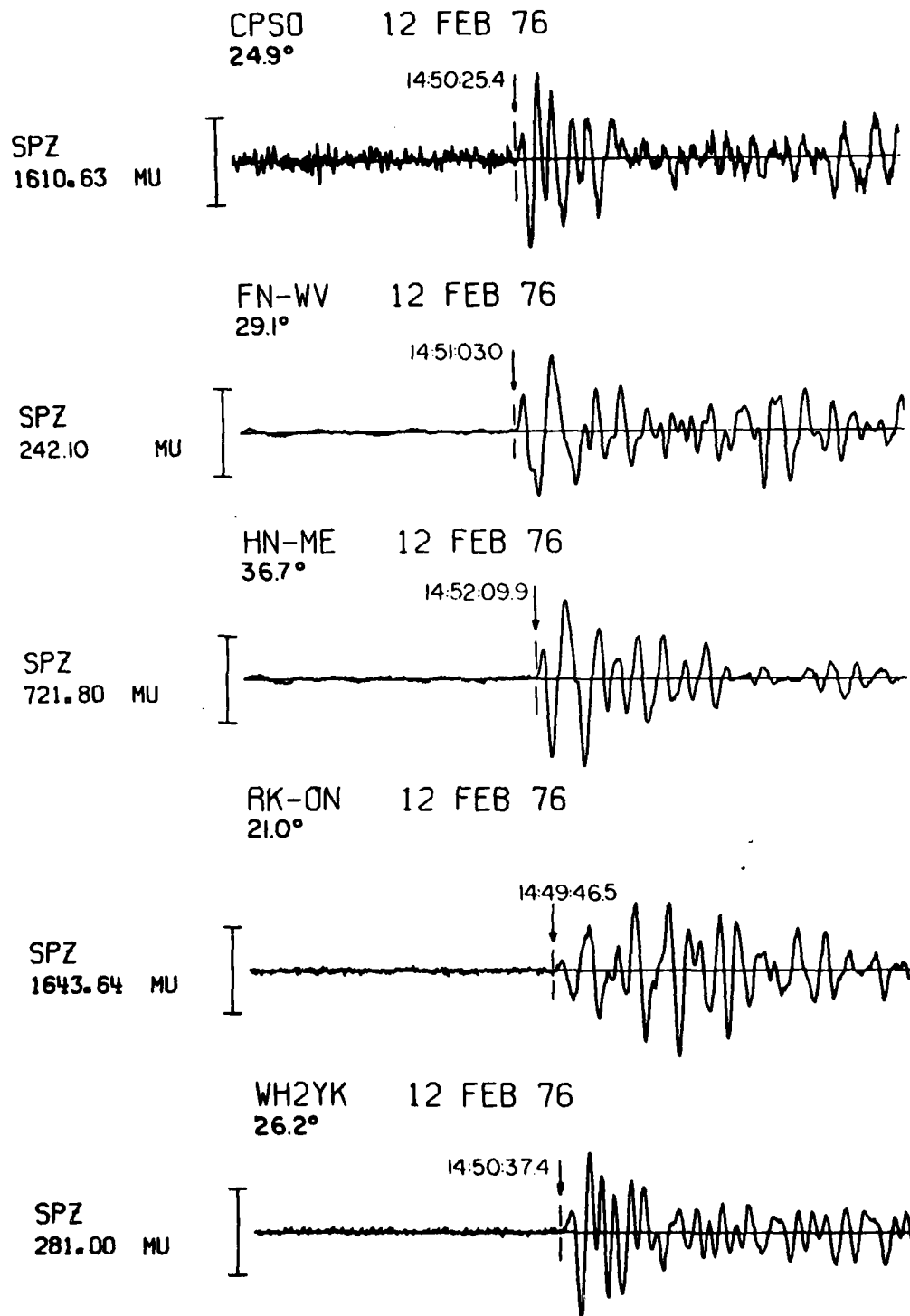
Figure 22 (cont.).    P-waves at 5 SDCS stations recorded from 5 Nevada Test Site explosions.

# KEELSON

CPSO          4 FEB 76
**24.9°**
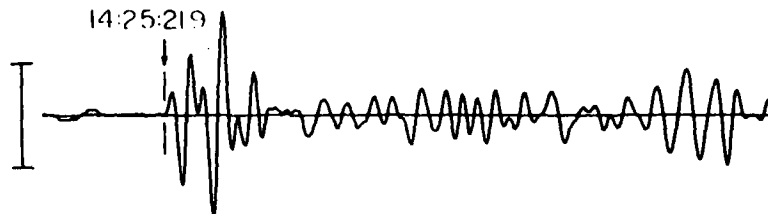
14:25:21.9

SPZ
178.00  MU

HN-ME      4 FEB 76
**36.7°**

14:27:08.1

SPZ
80.61  MU

RK-ON      04 FEB 76
**21.1°**

14:24:15.8

SPZ
610.23  MU

WH?YK      04 FEB 76
**26.2°**
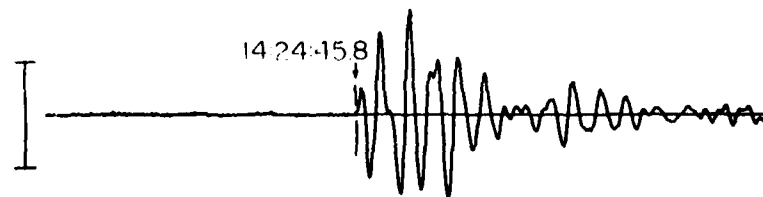
14:25:39.6

SPZ
33.06  MU
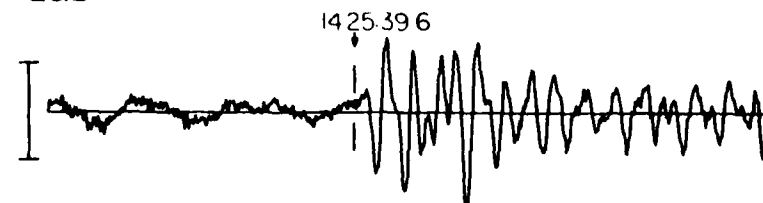
**Figure 22 (cont.).**   P-waves at 5 SDCS stations recorded from 5 Nevada Test Site
explosions.

# ESROM

CPSO    04 FEB 76
24.9°
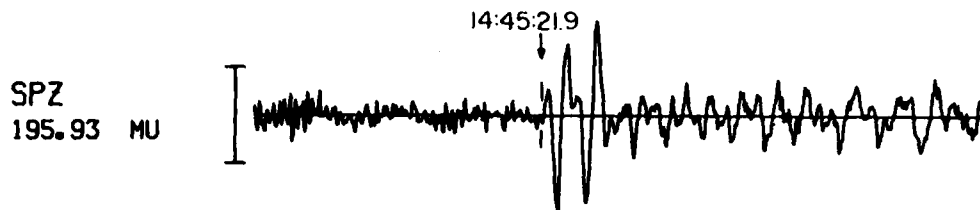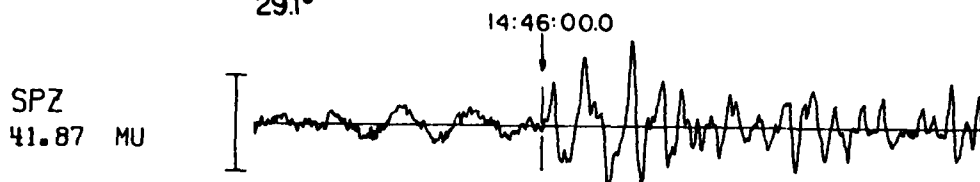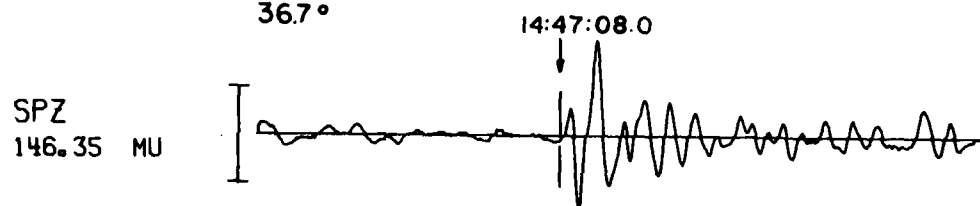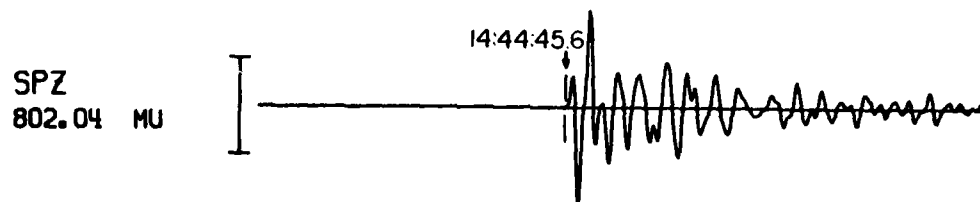
14:45:21.9

SPZ
195.93 MU

FN-WV    4 FEB 76
29.1°

14:46:00.0

SPZ
41.87 MU

HN-ME    4 FEB 76
36.7°

14:47:08.0

SPZ
146.35 MU

RK-ON    04 FEB 76
21.1°

14:44:45.6

SPZ
802.04 MU

WH2YK    4 FEB 76
26.2°

14:45:39.3

SPZ
30.36 MU
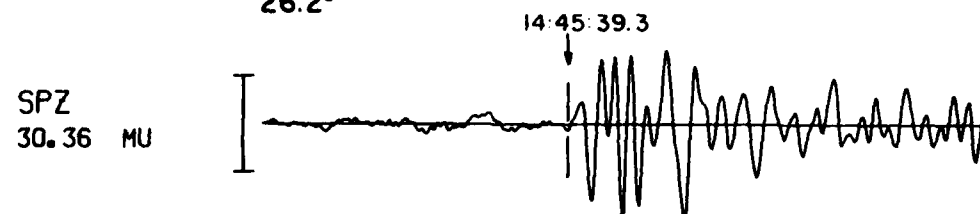
Figure 22 (cont.).    P-waves at 5 SDCS stations recorded from 5 Nevada Test Site
explosions.

## TABLE XI

P-wave particle motion processor results for Nevada Test Site
explosion P phases

### ERROR IN AZIMUTHAL ESTIMATE (deg)

|          | RK-ON | HN-ME | CPO | FN-WV | WH2YK |
|----------|-------|-------|-----|-------|-------|
| Esrom    | 0     | 6     | -1  | 6     | -5    |
| Keelson  | 0     | 3     | 1   | NA    | -2    |
| Chiberta | 3     | 5     | NA  | -53   | -21   |
| Muenster | NA    | -2    | 2   | -8    | -4    |
| Fontina  | 1     | -2    | -1  | -13   | -11   |

### ESTIMATED INCIDENCE ANGLE (deg)

|          | RK-ON | HN-ME | CPO | FN-WV | WH2YK |
|----------|-------|-------|-----|-------|-------|
| Esrom    | 35    | 31    | 13  | 37    | 31    |
| Keelson  | 35    | 41    | 12  | NA    | 23    |
| Chiberta | 40    | 32    | NA  | 11    | 29    |
| Muenster | NA    | 33    | 13  | 25    | 34    |
| Fontina  | 24    | 30    | 14  | 20    | 34    |

NA - No recording available

## Frequency Dependence of Particle-Motion

In the analysis thus far, spectra in the range from 0 to 10 Hz have been used and the exact frequency window within those limits was chosen automatically by a frequency-by-frequency S/N criterion for P waves and set to a constant band for Lg waves; however, the band with best S/N ratio may not be optimum for estimation of the signal parameters. This question is now investigated using four good P waves, two each at OB2NV and RKON, all having S/N > 2 over the entire 0-10 Hz band. The P-wave processor was programmed to use a constant bandwidth window over 5 frequency points (2.5 Hz), sliding up in frequency point by point and recomputing the azimuth and incidence angles each time. The 1.6 sec window was again used in the time domain. Figure 23 shows the errors in the azimuth estimate versus the center frequency of the window for the four P waves. The results for RKON are remarkably consistent over frequency, even to 10 Hz while the OB2NV results show some deterioration towards the highest frequencies. (The OB2NV signals were in fact somewhat weaker than the RKON ones.) Figure 24 is a plot of the F statistics versus center frequency for the same four signals. It can be seen that the RKON signal fits the P-wave model equally well over all frequencies but that the OB2NV signal fit deteriorates toward 10 Hz, probably due to decreasing S/N ratio.

It thus appears that one need not avoid any part of the spectrum in computing P-wave signal parameters with the particle-motion processor and that whatever portion of the signal spectrum lies above the noise spectrum is satisfactory in each particular case. A larger set of signals should be studied in the above manner to affirm these tentative results though.

## Use of Later Windows During P Motion

Many of the P signals in the OB2NV and RK-ON data sets are emergent in character, reaching maximum amplitude after several seconds of motion. Although S/N ratio will be increasing, it is likely that this later motion is contaminated by some signal arriving significantly off the true back azimuth. Study of the Z*R particle motion plots show that
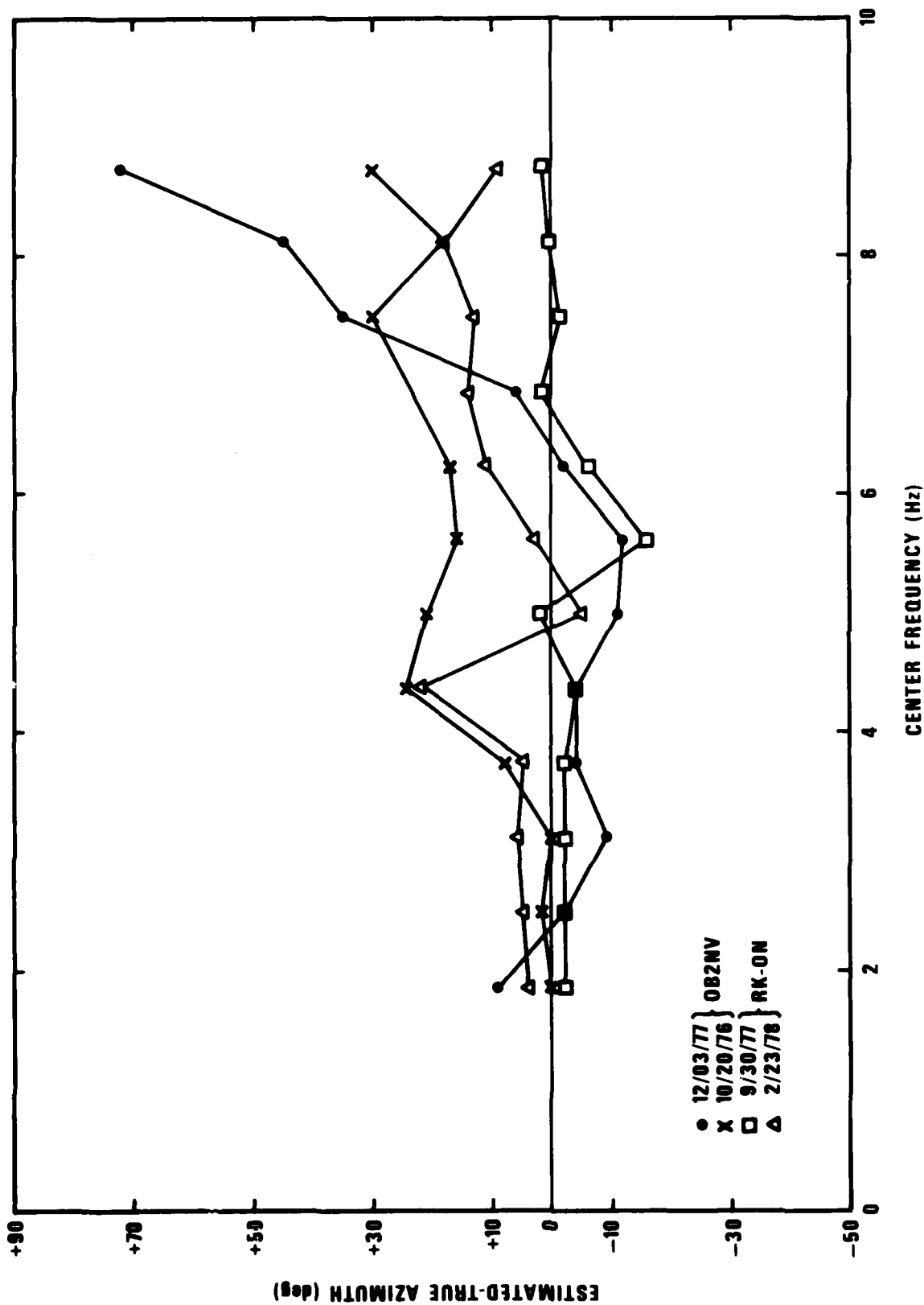
Figure 23. Error in azimuth estimate versus frequency band used for P-wave processing.
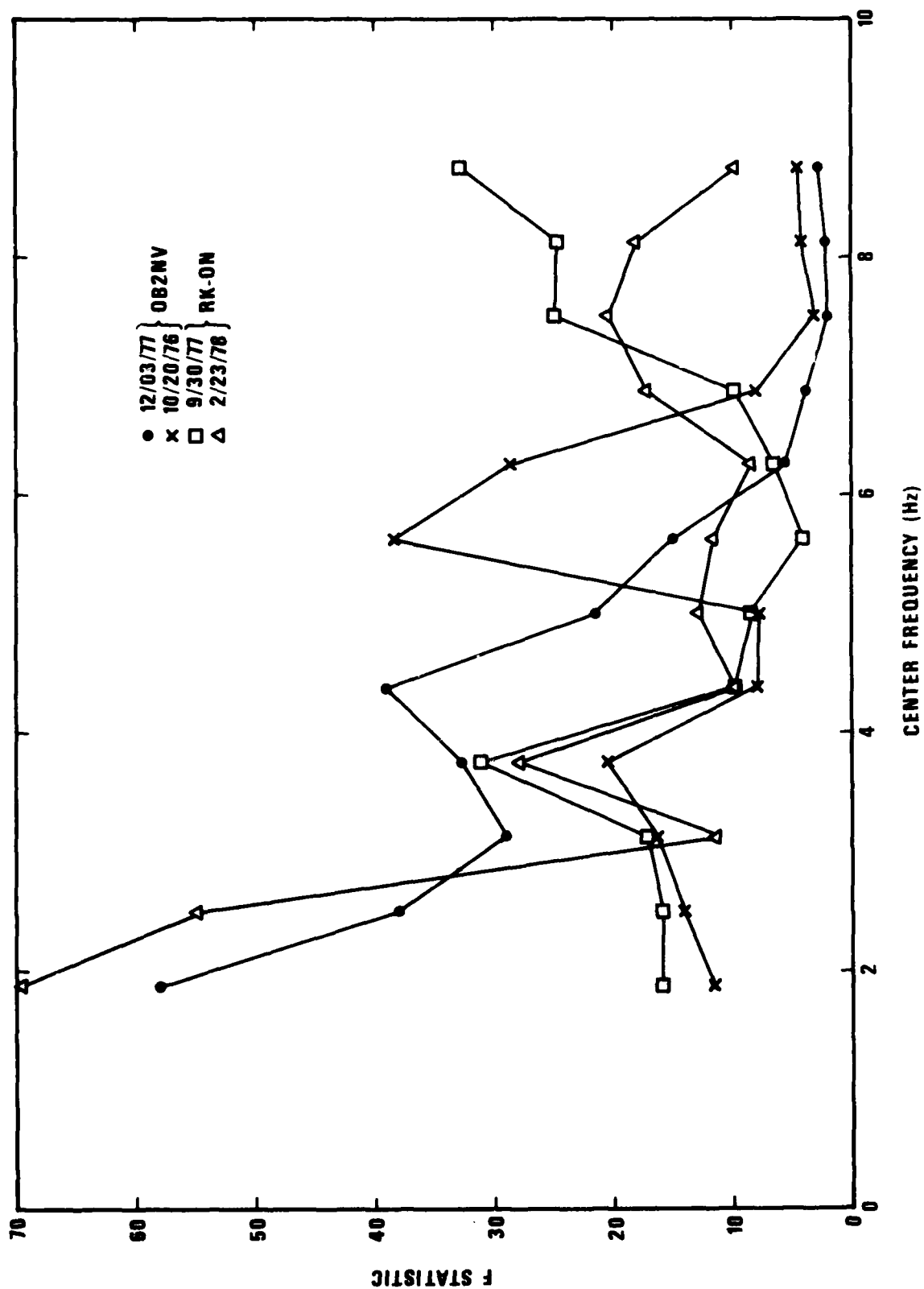
Figure 24. F-statistic versus frequency band used for P-wave processing.

P-type motion apparently persists for many seconds into these emergent arrivals though. Therefore, an experiment was programmed whereby the particle-motion processor was repeatedly run on the OB2NV and RK-ON signals of Tables II and IV using 50% overlapping 6.4 sec windows starting at the same P arrival times as used before and stopping at roughly 30 sec into the signal. The window which provided the best F-statistic in each case was used for the azimuth estimate, and the difference between this and the true azimuth is listed in Table XII. This table also lists the corresponding azimuth errors from Tables V and VIII where the first 1.6 sec only of P motion was used. As judged by the mean errors at the bottom, the procedure of looking for the best F window provides significantly better estimates of back azimuth at both stations. It is noteworthy, though, that the mean error is greater at OB2NV than at RK-ON for both procedures; because the overall S/N ratio quality of the two sets of signals is nearly equal, this result may indicate a more perturbed wavefield at OB2NV relative to RK-ON.

## Use of Longer Windows for Lg Motion

Although only 12.8 sec windows were used for $L_g$ processing to obtain the results of Tables IX and X, it is clear that $L_g$ motion persisted for much longer above the background noise level in most cases. A longer window of 51.2 sec was subsequently used, again starting at approximately the time of the maximum amplitude of $L_g$. Table XIII compares the results of using the two window lengths. It is seen that the longer windows generally provide better estimates and, in fact, decrease the mean error in azimuth to roughly one-half that of the shorter ones. However, it is noted that in cases where the F-statistic was low for the 12.8-sec window, e.g., event 14 at RK-ON or 37 at OB2NV, the longer window does not necessarily improve the result. Indeed, for cases where the S/N ratio is fairly low at the maximum of $L_g$ motion, it is expected that longer windows may often degrade the back-azimuth estimate simply because it incorporates more background noise in the processed signal. A decision regarding the optimum window length would be difficult to automate, especially when the signals are reported only by automated detection. In an interactive mode, however, a seismic analyst could easily set varying window lengths according to his perception of signal

## TABLE XII

Azimuth estimate errors of first 1.6 sec of P signal versus window
with highest F-statistic

### Absolute Errors (Abs. Value)

| | OB2NV | | | RKON | |
|---|---|---|---|---|---|
| Event | First 1.6 sec | Best F-Statistic (6.4 sec) window | Event | First 1.6 sec | Best F-Statistic (6.4 sec) window |
| 1 | 20° | 3° | 1 | 95° | 1° |
| 2 | 6° | 3° | 2 | 16° | 2° |
| 3 | 6° | 6° | 3 | 4° | 4° |
| 4 | 13° | 17° | 4 | 6° | 3° |
| 5 | 34° | 7° | 5 | 46° | 11° |
| 7 | 9° | 13° | 6 | 16° | 7° |
| 8 | 32° | 21° | 7 | 89° | 7° |
| 9 | 151° | 15° | 8 | 12° | 15° |
| 10 | 0° | 3° | 9 | 98° | 5° |
| 11 | 41° | 9° | 10 | 6° | 5° |
| 12 | 5° | 18° | 13 | 13° | 1° |
| 13 | 8° | 3° | 15 | 12° | 7° |
| 14 | 19° | 4° | 16 | 29° | 16° |
| 15 | 116° | 1° | 17 | 45° | 10° |
| 16 | 88° | 12° | 18 | 3° | 5° |
| 17 | 12° | 13° | 19 | 26° | 3° |
| 18 | 2° | 1° | 20 | 2° | 10° |
| 19 | 8° | 15° | 21 | 7° | 2° |
| 20 | 129° | 23° | 22 | 13° | 24° |
| 21 | 59° | 5° | 23 | 36° | 3° |
| 22 | 150° | - no P | 24 | 41° | 5° |
| 23 | 9° | 1° | 25 | 5° | 4° |
| 24 | 17° | 14° | 26 | 18° | 10° |
| 25 | 8° | 6° | 27 | 7° | 5° |
| 26 | 114° | 106° | 29 | 6° | 3° |
| 27 | 65° | 13° | 30 | 29° | 21° |
| 28 | 4° | 18° | 31 | 2° | 1° |
| 29 | 26° | 13° | | | |
| 30 | 4° | 21° | Mean Error | 25.1° | 7.0° |
| 31 | - no P | 29° | | | |
| 32 | 60° | - no P | | | |
| 33 | 9° | 5° | | | |
| 34 | 0° | 9° | | | |
| 35 | 108° | 46° | | | |
| 36 | - no P | 5° | | | |
| 37 | 54° | 28° | | | |
| Mean Error | 40.7° | 13.7° | | | |

TABLE XIII

Azimuth estimate errors for 51.2-sec $L_g$ windows versus
12.8-sec windows

Absolute Errors (Abs. Value)

| | OB2NV | | | RK-ON | |
|---|---|---|---|---|---|
| Event # | 12.8 sec | 51.2 sec | Event # | 12.8 sec | 51.2 sec |
| 8 | 19° | 20° | 1 | 2° | 17° |
| 9 | 52° | 31° | 2 | 66° | 7° |
| 10 | 0° | 6° | 3 | 7° | 4° |
| 34 | 12° | 24° | 4 | – | 1° |
| 11 | 68° | 14° | 5 | 2° | 7° |
| 12 | 20° | 21° | 6 | 1° | 0° |
| 13 | 34° | 27° | 7 | 45° | 17° |
| 14 | 9° | 5° | 8 | 8° | 4° |
| 15 | 5° | 5° | 9 | 6° | 7° |
| 16 | 12° | 6° | 10 | 2° | 0° |
| 17 | 25° | 24° | 11 | 0° | 1° |
| 35 | 24° | 12° | 12 | 54° | 26° |
| 18 | 117° | 1° | 13 | 5° | 4° |
| 19 | 57° | 22° | 14 | 11° | 38° |
| 20 | 26° | 31° | 15 | 3° | 2° |
| 21 | 4° | 5° | 16 | 9° | 2° |
| 22 | 8° | 7° | 17 | 13° | 7° |
| 23 | 12° | 21° | 18 | 1° | 2° |
| 24 | 15° | 6° | 19 | 9° | 1° |
| 25 | 2° | 29° | 20 | 6° | 4° |
| 26 | 46° | 54° | 21 | 0° | 12° |
| 36 | 1° | 4° | 22 | 48° | 24° |
| 27 | 3° | 7° | 23 | 4° | 1° |
| 37 | 62° | 55° | 24 | 0° | 1° |
| 28 | 0° | 1° | 25 | 5° | 1° |
| 29 | 5° | 3° | 26 | 2° | 0° |
| 30 | 11° | 23° | 27 | 55° | 3° |
| 31 | 107° | 12° | 28 | 14° | 1° |
| | | | 29 | 0° | 3° |
| | | | 30 | 63° | 10° |
| Mean Error | 27° | 17° | 31 | 0° | 2 |
| | | | Mean Error | 14.7° | 6.7° |

duration and according to perhaps some rudimentary estimate of epicentral distance from S-P or $L_g$-P time delays.

## REGIONAL PHASE IDENTIFICATION STRATEGY

Location programs which use regional phases Pn, Pg, and Lg have been developed at the SDAC (Chang and Racine, 1980; Rivers et al., 1981). Both arrival time and back azimuth information can be used in the new location algorithms; a complete location program incorporating these features is to be available within the RELS (Regional Location System) now under development at the SDAC. In order for these programs to generate meaningful results, it is necessary to make correct phase identification and to provide reasonably accurate back azimuth estimates. Trained seismic analysts can identify the various phases recorded from a regional event and could then run the particle-motion processors, as discussed above, to determine back azimuths. However, it is a goal to eventually do this in an automated manner so that, for instance, an automatic association program could function at a more complex level prior to analyst intervention in the data processing.

Ignoring the accuracy of back-azimuth estimates for the moment, consider just the problem of identifying phases when given a detection list formed by an ordinary power detector for instance. From the particle-motion results at OB2NV, which is perhaps only weakly representative of typical continental stations, it is apparent that discrimination of Pg from Pn phases will be difficult. Depending on the noise level and the event magnitude, either one or both of the phases may be detected. For Pg especially, the Pn coda and frequently emergent nature of the phase makes the start time given by an automatic detector unreliable. Given an isolated detection, it will be difficult, if not impossible, to classify it as Pn or Pg. Furthermore, teleseismic P wa must be considered also. Given two detections close in time though, a presumption of Pn followed by Pg may be warranted, and further diagnostics may be applied (e.g., frequency content which is not discussed in this report), to distinguish such occurrences from teleseismic P-pP, for instance. Further confidence in Pn or Pg identification will come through the particle-motion processor because both phases show the P-wave particle motion on real recordings.

Distinction of the regional Pn and Pg phases from teleseismic P phases can theoretically be made through the estimated incidence angle from the P particle-motion processor, but actual results as found in this study imply low confidence in such discrimination.

Now turning to Lg phases, one must keep in mind the erratic particle motion shown in Figures 8 and 9 for typical Lg arrivals. As an emergent phase, Lg will be detected at some point within the wavetrain depending on S/N ratio, if at all. Note that the application of the P-wave processor to a short window following the Lg detection time may fortuitously result in a P-wave identification if the detector was tripped at some point where Z*R was positive and the ellipticity ratio was within the range of that for regional or teleseismic P waves. Note that other characteristics of the Lg, duration and lower frequency, may not be sufficient to discriminate these phases. It may be that station-dependent phase characteristics can be used advantageously in helping to identify phases, but this topic is not pursued in this report.

In spite of all the nebulous situations discussed above, a strategy for phase identification given a detection list and access to the waveforms is proposed as follows:

1) Run the P-wave particle-motion algorithm on the first 6.4 sec of signal and subsequent overlapping 6.4 sec windows provided the S/N ratio is greater than that of the first window. Take the signal estimates from the window with the highest F-statistic. Accept the P-wave hypothesis provided the F statistic is high enough, the Lg F-statistic is less than the P one, and the estimated incidence angle is not too great.

2) If the P-wave hypothesis fails, examine the results of the Lg particle-motion algorithm on 12.8 sec of signal following the detection time and accept the Lg hypothesis if the F statistic

is high enough, the ratio of Love-to-Rayleigh motion is not too small, and the Rayleigh ellipticity is neither very large nor very small.

3)   Check the frequency content of signals to aid in discriminating regional from teleseismic phases and Lg waves from regional P waves.

4)   Examine particle-motion results for groupings of detections in time in order to associate Pn (and/or Pg) and Lg phases from a single event.

The next section of this report examines the outcome of testing parts 1 and 2 of the above strategy.  Parts 3 and 4 will require a more complex program and will be a topic for future research.

## POST-DETECTION PROCESSING AT THREE SRO SITES

This section describes the simulation of an on-line environment for the particle-motion processor. A detection log based on a simple power-type detector was formed and the particle-motion processing was performed on each detection above a certain threshold, producing an output log which augmented the detection log with signal characterization measures.

### Method

During the period 01 to 15 October 1980, three SRO sites, namely ANMO, BOCO, and BCAO, recorded 3-component, short-period data continuously. These stations provided a good data base, especially since ANMO and BOCO often record regional seismic phases. A detection log was created by operating on the vertical component of each station with a detection algorithm similar to that which has been used at the SDAC on LASA data. The recorded data is first filtered with a 0.8 to 1.8 Hz bandpass filter having 24 db/octave rolloffs. This data is then rectified and accumulated into 1.5 sec long STA (short-term average) values with two-thirds overlap of data in each STA. An LTA (long-term average) is maintained by updating with each new STA. The detection criterion is that 3 successive STA values exceed the LTA by a given factor, in this case 3.0.

With the detection logs formed in one pass over the data, a second pass was later made to process the signals in the detection windows. During this phase the P-wave algorithm was first applied to each detection, using again a 1.6 sec window commencing at the detection start time. Also during this phase, the Lg-wave algorithm was applied, but with a 12.8 sec window following the detection time. (The $L_g$ processing was bypassed if the P algorithm gave an F value exceeding 50, as defined by equation 1.) The output log of this processing provided these quantities: signal azimuth, incidence angle, ratio of transverse

-87-

to vertical energy, and F statistic for the P-wave processing; signal azimuth, ellipticity of the Rayleigh motion, ratio of Love-to-Rayleigh motion, and F-statistic for the Lg-wave processing.

## Results

Because of recording problems and a high noise level, the results for BOCO were too sparse to evaluate. The other two stations presented somewhat different results and are here discussed separately. All detected signals on which the particle-motion processors were run (S/N ≥ 3.0) were visually examined and notes made of the apparent wave type and other descriptive information.

The BCAO detections were of simpler nature than those at ANMO. Few regional phases were visually seen at BCAO, and no events on the NEIS list for the 15-day period were within regional distance to this station. Nearly all detections were of teleseismic P waves at BCAO, and of these, a large number were core phases with little apparent horizontal motion. Overall, arrivals were simple and generally easy to interpret at this station. A summary of the BCAO evaluation is given in Table XIV. Of 220 total detections, 107 had an F ≥ 6.0 for the P-wave particle-motion processor, a lower bound for considering the processing results to be meaningful. For those detections associated to NEIS events, by near coincidence of detection time and predicted P arrival time, the P-wave processor gave acceptable (< 20° error) back azimuths in nearly 70% of the cases and acceptable incidence angles (< 30°) in approximately 85% of the cases. Taking only those NEIS-associated arrivals having F ≥ 6.0, the acceptable azimuth estimates approached 75%. Note that most of those 12 cases with poor azimuth estimates were PKP core phases, whose horizontal-component motion is so small that the processor will be unable to provide good signal information even when the vertical component is large.

For almost all of those few i tances where detections at BCAO were visually classified as Lg motion, the Lg F-statistic exceeded 6.0 and the P F-statistic was less than 6.0. These detections cannot be

TABLE XIV

Detection and particle-motion processing results for BCAO –
01 through 15 October 1980

| | | |
|---|---|---|
| # | detections with S/N $\geq$ 3.0 | 220 |
| # | detections with P F $\geq$ 6.0 | 107 |
| | | |
| # | detections of NEIS events | 61 |
| | # with azimuth error < 20° | 41 |
| | # with azimuth error > 20° | 20 |
| | # teleseisms with incidence angle < 30° | 52 |
| | # teleseisms with incidence angle > 30° | 9 |
| | | |
| # | detections of NEIS events with F $\geq$ 6.0 | 44 |
| | # with azimuth error < 20° | 32 |
| | # with azimuth error > 20° | 12* |

* 10 of 12 were core phases

independently verified as true Lg phases; because they are not accompanied by earlier Pn or Pg detections, they may simply be noise excursions exceeding the S/N = 3 threshold.

The ANMO results are more interesting because of the many apparent regional phases seen during the visual examination of detections. It is noteworthy that ANMO P waves were generally less simple than those at BCAO and were contaminated by significant transverse motion even at the first cycle of motion. A summary of the ANMO evaluation is presented Table XV. First, note that only 28% of the ANMO detections had a P F-statistic $\geq$ 6.0, in contrast to BCAO where nearly half of the detections had such. For the 56 detections associated to NEIS events, the P-wave processor gave acceptable azimuth estimates in the minority of cases. Taking only the 26 NEIS-associated detections with F > 6.0, the azimuth is poorly estimated ( > 30° error) in one-half of the cases. The bottom of Table XV comprises the most important results and compares the machine phase identification to that of the human analyst. (In noting the phase type through visual analysis, only those detections which were reasonably identifiable were given a designation.) For those 70 detections designated as Lg, the machine results agreed in 46 cases, using the criteria that the Lg F-statistic exceeded 6.0 while the P F-statistic was below this value. (It is felt that most of these 70 "Lg" waves are not in fact Lg from true seismic events, but rather noise excursions which effectively appear as Lg-type signals.) For 17 detections designated as regional ' phases (Pn or Pg), the machine results agreed in 7 of the cases, using the criteria that the P F-statistic exceeded 6.0 and that it also exceeded the Lg F-statistic. A definitive evaluation of these latter results is impossible, due to the lack of a low threshold North American bulletin from which to predict regional arrivals at ANMO. However, because the visual designations are felt to be true, the machine algorithms appear to be somewhat inadequate. This must be tempered by the fact that the machine processing used here does not avail itself of all the signal characterization features which the human draws on such as frequency content, signal duration, and envelope shape, and that the machine

## TABLE XV

### Detection and particle-motion processing results for ANMO – 01 through 15 October 1980

| | |
|---|---|
| # detections with S/N $\geq$ 3.0 | 265 |
| # detections with P F $\geq$ 6.0 | 74 |
| | |
| # detections of NEIS events | 56 |
| # with azimuth error < 20° | 21 |
| # with azimuth error > 20° | 35 |
| # teleseisms with incidence angle > 30° | 19 |
| # teleseisms with incidence angle < 30° | 35 |
| # reg with incidence angle > 30° | 2 |
| # reg with incidence angle < 30° | 0 |
| | |
| # detections of NEIS events with F $\geq$ 6.0 | 26 |
| # with azimuth error < 20° | 13 |
| # with azimuth error > 20° | 13* |
| | |
| # detections designated as $L_g$ by visual analysis | 70 |
| # of "$L_g$" with $L_g$ F $\geq$ 6. and P F < 6.0 | 46 |
| # detections designated as $P_n$ or $P_g$ by visual analysis | 17 |
| # of "$P_n$" or "$P_g$" with P F $\geq$ 6.0 and $L_g$ F < P F | 7 |

* 5 of 13 were core phases

algorithms did not incorporate improved methods, such as longer Lg
windows and P windows farther into the signal.

Lastly, it is noteworthy that Lg phases from the 33 NEIS events at
regional distances from ANMO were undetected in all but two cases.
Clearly, since the Lg processing is initiated by a detection, a better
detection algorithm for Lg phases is first required for complete
regional phase information to be gained in a routine manner.

## CONCLUSIONS

Fitting a rectilinear particle-motion model to the first 1.6 sec of
recorded P waves allows the azimuth of the incoming signal to be
estimated to within $\pm$ 20° in the large majority of cases where the
F-statistic on the model fit exceeds 6.0.  Results for Pg waves are not
as good as for initial Pn and teleseismic P, probably due to the
inability to time the Pg signals well.  The estimation of incidence
angle is not reliable enough to permit routine separation of regional
from teleseismic signals with a sufficient degrees of confidence.
Neither high S/N ratio nor high F statistic insures good estimates of
the signal parameters; with the limited data base processed here, it is
unclear whether S/N or F should be taken as the indicator of the
reliability of the estimated parameters.

Back azimuth estimates from Lg waves are somewhat better than those
from P waves and would be preferable at equivalent signal amplitudes.
Because Lg amplitude usually exceeds P amplitude for events recorded at
regional distance, the Lg estimate of azimuth will most likely be
superior.

An examination of the accuracy of signal parameter estimates versus
the exact frequency band used revealed that any portion of the fre-
quency interval from 0 to 10 Hz yields equally good estimates.  Thus,
there is no characteristic frequency, at least for the two stations
studied here (RKON and OB2NV), for which crustal inhomogeneities at a
certain scale length may produce distorted arrivals at the surface.
Uniform bias of signal parameter estimates was established though, as
in the case of NTS signals processed at CPO and WH2YK.

A simulation of post-detection signal characterization using 15
days of continuous 3-component data at ANMO and BCAO yielded somewhat
disappointing results.  Simply subjecting detection windows to
particle-motion processing will not provide confident phase
identification except in cases of high S/N ratio arrivals.  Back

azimuth estimates are fairly reliable, though, provided the F-statistic exceeds 6.0. Use of a more complete particle-motion algorithm, i.e., using later-arriving signal, should improve the estimates. The particle-motion results would, however, be helpful after analyst review of signals because they provide reasonably accurate azimuth estimates, once phase type is established by the analyst. A larger data base of regional signals must be processed before the exact degree of utility for this processing can be determined. A truly automated signal characterization phase will need to implement further algorithms, such as computing spectral content, in order to improve performance.

In the final stage of implementing particle-motion processing into a seismic analysis system, some fine tuning will be beneficial. This need is shown by the bias in CPO incidence-angle estimates, bias in WH2YK azimuth estimates, differences in character of RKON and OB2NV Lg waves, and the distortion and complexity of ANMO P waves, among other phenomena.

Lastly, it is suggested that a radically different approach may be useful in signal characterization. This approach would be to combine detection and particle-motion processing by continuously estimating signal parameters using three components in the same manner that STA is computed continuously for power detectors. The new detector would then operate on the continuous output of the 3-component processor.

# REFERENCES

Blandford, R. R., D. Racine, and R. Romine (1981). Single channel seismic event detection, SDAC-TR-81-7, Teledyne Geotech, Alexandria, Virginia.

Bullen, K. E. (1963). An Introduction to the Theory of Seismology, Cambridge University Press, Cambridge, England.

Chang, A. C. and D. P. Racine (1980). Evaluation of location accuracy using $P_n$ and $P_g$ arrivals, SDAC-TR-79-4, Teledyne Geotech, Alexandria, Virginia.

Goncz, J. H. (1980). Present status and dynamic planning for automatic association programs, SDAC-TR-80-2, Teledyne Geotech, Alexandria, Virginia.

Rivers, D. W., J. A. Burnetti, and A. C. Chang (1981). Use of back azimuth measurements in seismic event location with regional data, VSC-TR-81-17, VELA Seismological Center, Alexandria, Virginia.

Shlien, S., and M. N. Toksoz (1973). Automatic event detection and location capabilities of large aperture seismic arrays, Bull. Seism. Soc. Am., 63, 1275-1288.

Smart, E. (1981). Regional phase processors, SDAC-TR-81-1, Teledyne Geotech, Alexandria, Virginia.

Smart, E. (1977). A three-component single-station, maximum-likelihood surface wave processor, SDAC-TR-77-14, Teledyne Geotech, Alexandria, Virginia.

Sodbinow, E. S., and G. A. Bollinger (1978). Seismic studies in central and eastern Tennessee, Bull. Seism. Soc. Am., 68, 1081-1094.

Sutton, G. H., W. Mitronovas, and P. W. Pomeroy (1967). Short-period seismic energy patterns from underground nuclear explosions and small-magnitude earthquakes, Bull. Seism. Soc. Am., 57, 249-267.

von Seggern, D. H. (1977). Methods of automating routine analysis tasks in preparing a global seismic bulletin, SDAC-TR-77-13, Teledyne Geotech, Alexandria, Virginia.

von Seggern, D. H. and R. R. Blandford (1972). Source time functions and spectra for underground nuclear explosions, Geophys. J., 31, 83-97.

von Seggern, D. H., A. C. Chang, and R. R. Baumstark (1978).